

学位論文 (要約)

**A geochemical study on trace element behavior in
sediments and soil formation on atolls, central Pacific**

(中部太平洋地域の環礁堆積物中の微量元素の挙動と
土壌化に関する地球化学的研究)

平成 30 年 2 月博士 (理学) 申請

東京大学大学院理学系研究科

地球惑星科学専攻

伊藤 理彩

**A geochemical study on trace element behavior in
sediments and soil formation on atolls, central Pacific**

by

Lisa ITO

Department of Earth and Planetary Science

Graduate School of Science

The University of Tokyo

submitted to the University of Tokyo

In Partial fulfillment of the requirements for the Degree of Doctor of Philosophy

February 23, 2018

Abstract

Majuro Atoll, one of atolls in the central Pacific and the main target area in this study, is isolated in term of the geography from other continents. The formation age was about 2000 years ago, and the human settlement started after the age. Therefore, Majuro Atoll has been subjected to lesser external effects on the soil formation as well as lesser anthropogenic influence than other developed countries with considerably longer human history and larger populations. Thus, this doctoral thesis focused on (i) the soil chemistry related to the soil formation in the atoll (Chapters 3 and 4) and (ii) environmental chemistry of various elements (Chapter 5) mainly based on the field survey of sediments and subsequent analyses of sediments such as the age, observation of foraminifera particles, and concentrations and speciation of various elements applied to their vertical profiles of the sediments. The novelties of this study are revealing the unknown but important process for the first time such as formation of an atoll, rapid soil formation process, and speciation of heavy metals in the area after the urbanization. More detailed descriptions of these studies are given below.

Soil acidification often occurs due to various factors such as NO_x and SO_x from anthropogenic combustion substances. In the process of rock weathering or nitrification, protons are also released which causes soil acidification. It is difficult to evaluate each factor independently in industrial countries, since the many factors have affected one another. On the other hand, it is relatively easy to discuss anthropogenic impacts and natural effects independently in the case of atoll, since atoll sediments are composed of bio-clastic sand such as foraminifera and coral that are made of calcium carbonate (CaCO_3), which exhibits simpler composition compared with other areas with more

heterogeneous geology. Here, I investigated the degrees of acidity in Majuro Atoll, one of the atolls of Marshall Islands. In Majuro Atoll, human residence has lasted for about 2000 years, which is the longest history among atolls around the world. However, the traditional life style in the atoll has changed and more industrial products such as motor vehicles have been used after 20th century.

In this study, I focused on factors which have a possibility to change surface environment of reef islands in atoll in terms of both artificial and natural factors. I evaluated the correlation between the elements contained in the sediment and sediment pH at different depths. I also examined the mechanism to acidify the sediment.

Samples were taken at different depths of the sediments in inland area, ocean side, and lagoon side of each island which was named as Laura, Calalen, Jelto, Delap in Majuro Atoll and Kebjeltak in Arno Atoll. All the surface layers are black-colored and well-vegetated. The grain size is medium to fine sand.

Concentration of major elements such as calcium (Ca) and magnesium (Mg) was examined by XRF. Concentrations of inorganic ions (NO_3^- , SO_4^{2-} , and NH_4^+) were measured by ion chromatography and absorption spectrophotometry, respectively. Concentration of organic acid was calculated by pH titration. Mineral composition of foraminifera, which is the main component of the sediment, was examined by XRD. Porosity of foraminifera was calculated using X-ray micro-Computed Tomography (μ -CT) coupled with Image processing. Stable isotopes of nitrogen (^{14}N and ^{15}N) and triple oxygen isotopes (^{16}O , ^{17}O , and ^{18}O) in nitrate contained in the sediment were measured by the denitrifier method to identify the origin of the nitrate. ^{13}C solid state Nuclear Magnetic Resonance (NMR) spectroscopy were used to identify the organic matter which was concentrated in the upper layer.

As a result, sediment pH decreased near the surface layer and the concentration of Mg decreased. Mg-calcite fraction to total CaCO_3 (calcite + magnesian calcite (Mg-calcite)) of foraminifera also decreased near the surface. In contrast, the porosity of foraminifera, concentrations of NO_3^- , NH_4^+ , TOC, and organic acid increased in the upper layer, whereas concentration of SO_4^{2-} fluctuated and especially became higher in the lower layer which is close to the water-table. Therefore, SO_4^{2-} may be originated from seawater, which did not induce acidification of the sediment. According to NMR analysis, organic matter enriched in the upper layer was identified as fulvic acid. Both the concentrations of nitrate and organic acid as fulvic acid had high correlation with sediment pH in the range from pH 7.5 to 8.2. Therefore, it is considered that both acid substances contribute to the acidification and dissolution of foraminifera test in the upper layer. From the analysis of the stable isotopes, the average of $\Delta^{17}\text{O}$ was close to 0‰ over all the areas, which suggested that nitrate was produced by bacterial activities. Therefore, it is concluded that highly concentrated nitrate produced during the excess nitrification and subsequent release of proton during the process should be one of the factors to acidify the sediments on Majuro Atoll. As a result of ^{14}C dating, which should reflect the initial age of vegetation, it is revealed that first humus was produced only 100 to 200 years after the island formation and soil formation. In general, it takes more than 1500 years before surface of elevated coral began to be weathered. This fact suggested that it took less than 1/10 period of time for the formation of soil in Atoll. For the factors for this promotion of soil formation, following reasons are considered. i) increased NO_3^- worked as nutrients for plants and contributed to the development of vegetation. ii) The production of organic matter including plants contributed to the increase of humus. iii) Soil acidification has

promoted chemical weathering of the sediment, and active nitrogen cycle and formation of humic substances.

The elements that were came out of the island (external elements) and the one which released from the island (internal elements) were also quantified in this study. The sedimentary depth profiles of elements showed that various elements were enriched in the upper layers of the islands of Majuro Atoll including heavy metals such as zinc (Zn) and copper (Cu). Carbon-14 dating revealed that the sedimentation of the upper layer was completed before 1670 and 542 cal BP in Laura and Calalen, respectively. The enriched elements could be categorized by their origins: (a) terrestrial elements transported as dust (aluminum (Al) and rare earth elements (REEs)), (b) anthropogenic elements (Zn and Cu), and (c) elements supplied by seabirds (phosphorus (P)). The total amount of Al supplied to sediments for ca. 2000 years was similar to those estimated from (i) total (dry + wet) depositions of Al in aeolian dust and (ii) Al in deep-sea sediments in the Central Pacific. These results suggested that Al in Majuro Atoll was of airborne origin. The enrichment factors (EFs) of the elements normalized to Al concentration of continental crust showed that REEs were also transported as dust. The EFs of Zn and Cu were greater than 21.1 and 4.99, respectively, suggesting that Zn and Cu were mainly of anthropogenic origin. The speciation analysis of Zn and Cu by K-edge X-ray absorption near-edge structure (XANES) showed the presence of Zn–Cu alloys originated from industrial products. It was also revealed that Zn was enriched in the surface due to anthropogenic emission after urbanization on Majuro Atoll and fixed by carbonate and phosphate at the upper layer, which inhibits migration of Zn into the deeper layer and its release to the groundwater and costal water. Hence, the fixation of heavy metals at the surface prevents their exposure to aquatic organisms and residents via fresh groundwater in the island.

Table of content

Chapter 1. General Introduction.....	1
---	----------

Chapter 2. Sampling area

2.1. Sampling site.....	21
2.2. Sampling.....	23
2.2.1. Sampling in 2008.....	25
2.2.2. Sampling in 2016.....	26
2.3. Sample description.....	29
2.4. Characteristics of vegetation.....	31
2.5. Anthropogenic modification.....	32

Chapter 3. Influence of acidification on carbonate sediments of Majuro Atoll, Marshall Islands

3.1. Introduction.....	35
3.2. Details of the sample.....	37
3.3. Methods.....	38
3.3.1. X-ray Fluorescence (XRF)	38
3.3.2. Ion chromatography (IC)	39
3.3.3. Total Organic Carbon (TOC)	40
3.3.4. X-ray diffraction (XRD)	40
3.3.5. Soil pH.....	41
3.3.6. X-ray μ -Computed Tomography (CT).....	42

3.3.7. Mg K-edge XANES.....	45
3.4. Results and Discussion.....	45
3.4.1. Soil pH and concentration of inorganic matters.....	45
3.4.2. Porosity of <i>Calcarina</i> spp.....	47
3.4.3. Different pattern of XRD.....	48
3.4.4. Selective dissolution of Mg-calcite observed by SEM.....	53
3.4.5. Chemical species of Mg.....	56
3.4.6. Correlation between soil pH, porosity, and Mg-calcite.....	56
3.4.7. Estimation of dissolution amount of calcite by rainwater and nitrate.....	60
3.5. Conclusions.....	65

Chapter 4. Relationship of sediment acidification and nitrification on Majuro Atoll, Marshall Islands

4.1. Introduction.....	67
4.2. Study area and Materials.....	71
4.3. Methods.....	74
4.3.1. Quantify of organic acid.....	74
4.3.2. Quantify of inorganic ions.....	75
4.3.3. Total organic carbon (TOC) and Nuclear Magnetic Resonance (NMR) spectroscopy.....	76
4.3.4. Stable isotope signatures ($\delta^{15}\text{N}$, $\delta^{18}\text{O}$, $\Delta^{17}\text{O}$).....	78
4.3.5. Radiocarbon (^{14}C) dating for humus.....	80
4.4. Results.....	85
4.4.1. Inorganic anions in the sediments.....	85

4.4.1.1 Concentration of NO_3^- , SO_4^{2-} , and NH_4^+	85
4.4.1.2. Stable isotope of NO_3^-	87
4.4.2. Organic matter in the sediments.....	88
4.4.2.1. Concentration of organic acid (OA).....	88
4.4.2.2. Concentration of TOC in the soil.....	89
4.4.2.3. Nuclear Magnetic Resonance (NMR) spectroscopy.....	90
4.4.3. Dates of Humus.....	93
4.5. Discussion.....	94
4.5.1 Soil pH and threshold of dissolution of Mg in sediments.....	94
4.5.2. Factor to lower pH value of sediments.....	95
4.5.3. Origin of NO_3^-	99
4.5.4. Origin of nitrogen.....	100
4.5.5. Relationship between soil acidification and soil formation.....	103
4.5.5.1. Nitrogen cycle.....	103
4.5.5.2. A possible role of nitrification on the acidification.....	106
4.5.6. Timing of soil formation.....	110
4.6. Conclusions.....	112

Chapter 5. Origin and migration of trace elements in the surface sediments of Majuro Atoll, Marshall Islands

5.1. Introduction.....	115
5.2. Site description and samples.....	117
5.3. Methods.....	120
5.3.1. Inductively coupled plasma mass spectrometry (ICPMS) for trace elements.....	120

5.3.2. Extracting experiments.....	121
5.3.3. X-ray Fluorescence (XRF) for major elements.....	122
5.3.4 X-ray absorption near-edge structure (XANES).....	122
5.3.5. Radiocarbon (^{14}C) dating.....	124
5.4. Results and Discussion.....	125
5.4.1. Depth profile of elements.....	125
5.4.2. Classification of elements on the basis of EF.....	128
5.4.3. Crustal origin: Al.....	134
5.4.4. Crustal origin: REE.....	135
5.4.5. Crustal origin: Fe.....	138
5.4.6. Non-crustal origin: P.....	139
5.4.7. Non-crustal origin: S.....	145
5.4.8. Non-crustal origin: As.....	146
5.4.9. Non-crustal origin: Zn and Cu.....	147
5.4.10. Source of Zn.....	156
5.4.11. Conservation of groundwater by the fixation of Zn at the surface.....	160
5.5. Conclusions.....	163
6. General conclusions.....	165
6.1. Soil acidification in atoll.....	166
6.2. Origin of materials in atoll.....	168
6.3. Novelities and significant points of this study.....	170
Acknowledgements	171
References	173

Chapter 1.

General Introduction

1. General introduction

There are many coral reef islands in the world. The types of coral reef are divided into 3 groups, fringing reef, barrier reef, and atoll. In the case of atolls, carbonate platforms have grown on sinking volcanic edifices (Darwin, 1842) (Fig. 1-1) and comprised an annular reef rim surrounding a central lagoon (Woodroffe et al., 1999) (Fig. 1-1) and now, about 500 atolls are present around the world. Yasukochi et al. (2014) showed the location of atolls scattered around the world (Fig. 1-2). Most of them are located in the Pacific Ocean near the equator, circum-tropical climate zone (e.g., Fujita et al., 2009).

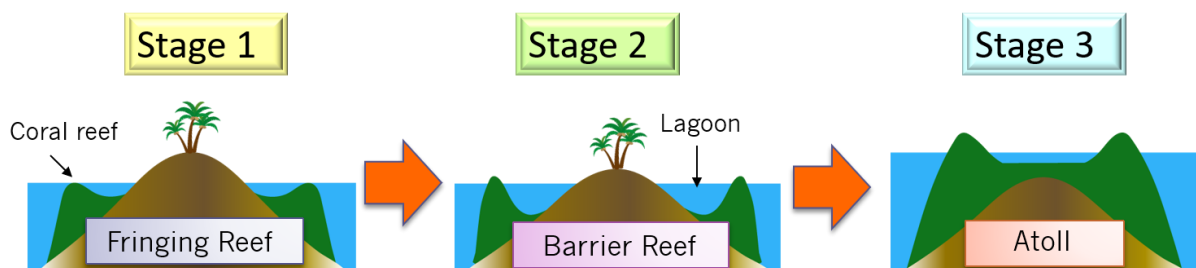


Fig. 1-1. Developing stage of coral reef islands.

インターネット公表に関する使用承認申請中
につき、本図については、非公開。

Fig. 1-2. Atolls in the world (Yasukochi et al., 2014).

Sea level fluctuations in the Holocene triggered the formation of reef island. (Dickinson, 2003). When the sea level rises, corals also move up to the sea surface, because they are capable of carrying out zooxanthellae in their body. Since the zooxanthellae perform photosynthesis, corals continue to grow upward near the sea

surface so that they can be exposed to more sunlight. As the sea level rise stopped and became stabilized around 2000 BC, corals continue to grow in the lateral direction without upward growth. This period lasted for about 2000 years, and later, these corals became foundation of the coral reef islands (Fig. 1-3). After late Holocene hydro-isostatic drew down in tropical Pacific sea level, the cemented mid-Holocene paleoreef flats have been exposed above declining sea level and now they strand well above sea level (Dickinson, 2003, 2004; Fig. 1-3). The timing when the seawater surface at the time of high tide falls below the top of the coral is called "close-over date" and it is a very important date in the history of coral land forming. This close-over date has locality (Dickinson, 2009) (Table 1-1). The close-over date of Majuro Atoll is considered to be 700 AD.

インターネット公表に関する使用承認申請中
につき、本図については、非公開。

Fig. 1-3. Sea level change and reef island formation. Modified from Dickinson (2003).

Table 1-1. Highstand magnitude, tidal range, and cross over date.

インターネット公表に関する使用承認申請中
につき、本表については、非公開。

*Modified from Dickinson (2009).

When the reef flats emerged above the sea level, island was formed by a relative reduction in wave energy and enhanced foraminiferal supply (Yasukochi et al., 2014; Fig. 1-4). Also, the unconsolidated calcareous bio-clastic sands and gravels (Fig. 1-5) started to deposit on the reef flats (e.g., Perry et al., 2011).

インターネット公表に関する使用承認申請中
につき、本図については、非公開。

Fig. 1-4. Formation stage of reef island (Laura, Majuro Atoll) (Yasukochi et al., 2014).



Fig. 1-5. Calcareous bio-clastic materials which constitutes the sediment of coral reef islands. Foraminifera (*Calcarina* spp.) in the left picture and coral gravels and shells in the right picture.

Soon after the emergence of the core islet, the earliest islanders established habitations around 2,000 years B.P. years ago in Laura on Majuro Atoll, one of the atolls in Marshall Islands (Yamaguchi et al., 2005, 2009) (Details are written in Chapter 2). The inhabitants started to excavate agricultural pits for the cultivation of wet taro some centuries later. The current landscape of Laura would have been formed by around 1,000 years B.P (Yamaguchi et al., 2009). This pit agriculture makes use of the groundwater of freshwater lens, which exist in the underground (Fig.1-6). This water is also an important resource as the drinking water even at present. Freshwater lens is an aquifer which floats on the seawater and formed by the difference of the density between seawater and freshwater. Once the rain water is precipitated, it permeates into the deep underground, because the sediment is made of unconsolidated bio-clastic remains such as foraminifera and coral gravel. These sediments are porous and very coarse. Therefore, this sediment has the characteristic of high permeability of rainwater. However, this freshwater lens does not always exist under the sediment of coral reef. The size of the freshwater lens and water quality (salinity) depend on the local climate condition and annual precipitation (Fig. 1-7a).

インターネット公表に関する使用承認申請中
につき、本図については、非公開。

Fig. 1-6. Structure of freshwater lens. Werner et al. (2017).

For example, Majuro Atoll have freshwater lens of good quality because of the large amount of annual precipitation more than 3000 mm, which is the largest precipitation of atolls (Stoddart, 1992) (Fig. 1-7b). On the other hand, annual precipitation is rather small in Kiribati. Therefore, atoll in this area have poor quality of freshwater lens, although the land size is large enough which often causes the salt damage problem of agriculture and drinking water. Therefore, existence of freshwater lens with good quality is very important for living on atolls.

(a)

(b)

インターネット公表に関する使用承認申請中
につき、本図については、非公開。

modified from Stoddart (1992)

modified from www.nocs.cc.

Fig. 1-7. (a) Climate data of Majuro, (b) Comparison of annual precipitation of atolls.

The constituents of the atoll sediments are often studied, such as in terms of their components, grain size distribution, and rate of abrasion of foraminifera, which is the main component of the sediment. For example, sediment constituents in Majuro Atoll were studied by Ph.D. thesis of Yasukochi (2008), Graduation thesis of author (Ito, 2010), and Yasukochi et al. (2014). Especially, the characterization of the constituents, ages of

islands, and timing of human settlement after the islands formation were studied in the graduation thesis (Ito, 2010). Brief contents of the thesis were shown as follows.

- i) Radiocarbon (^{14}C) dating: Determined the age of (a) foraminifera in the lowest sedimentary layer which is considered to nearly equal to the initial deposition age of the island and (b) oldest charcoal which should be anthropogenic in each island.
- ii) Particle size analysis: Sand is divided into seven stages and classified according to particle size ($+4\phi$ to -2ϕ) where $\phi = -\log_2 D$ (unit of D: mm)
- iii) Residual Spine Ratio: Divide the spine ratio of *Calcarina* spp. into three levels (Fig. 1-8) based on Yamanouchi proposal (1988), and obtain the abrasion degree (Figs. 1-11, 1-12).

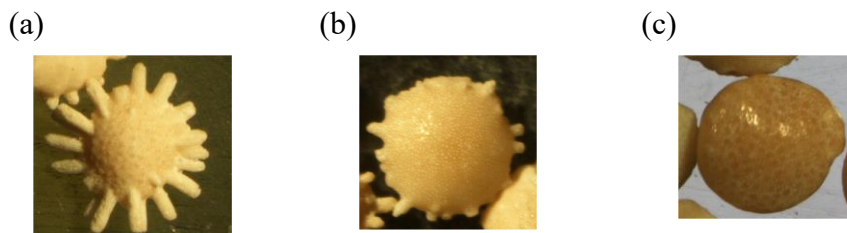


Fig. 1-8. Abrasion level of foraminifera spine (Ito, 2010) based on the standard of Yamanouchi (1988). (a) The spine remained almost completely. (b) Some spines are removed. However, there still remains several spines even though some of them were broken. (c) No spine. Abrasion level is high. Gloss is sometimes observed on the surface of the foraminifera. Difference of abrasion state can be seen in Fig. 1-13.

Regarding to study i), results were shown in following Table 1-2. The sampling points of Laura and Calalen corresponded to Lr3-1 and KOL (Fig. 1-9) and the lowest sedimentary layers corresponded to L6 and C6 (under the L5 and C5 layers of Chapter 3) in this study (Details in Chapter 3). However, there was a problem that applied ΔR value

used for calibration of *Calcarina* in my graduation thesis was found out to be rather older by the subsequent study (Kayanne et al., 2011). Therefore, the new ΔR value was applied in this thesis. From the dating results shown in Table 1-2 below, it was revealed that i) Despite the same atoll, there are differences in the formation age (about 1000 years) between three islands, Laura, Calalen, and Jelto. ii) Age gap between foraminifera (*Calcarina* spp.) and carbide was around 400- 500 years in all the islands. These results showed that difference between the age of initial formation stage of the islands and the trace of the first human activities were almost the same on every island, suggesting that humans have arrived within a short period of time after the island was formed.

Table 1-2. Gap between ^{14}C age of *Calcarina* (sediment) and carbide (Ito, 2010).

本表については、5 年以内に雑誌等で刊行予定のため、非公開。

*For the calibration of foraminifera (*Calcarina*) age, Marine 04, $\Delta R=164 \pm 43$ was applied. Measurement of ^{14}C dating was entrusted to Paleo Labo Co., Ltd.

Regarding to sedimentology of Laura in Majuro Atoll, Yasukochi (2008) firstly revealed that the rate of abrasion in sediments in north parts and ocean side of the island is larger than those in the south, which suggested the closeness of the production site of foraminifera. Subsequently, the depth profiles of the grain size and rate of abrasion of the

foraminifera was made by my graduation thesis. It was found that the foraminifers in the upper layer were worn to a greater degree and the grain size was smaller than those in the lower layer and average degrees of abrasion was different between the islands as shown in Figs. 1-10 to 1-13.

インターネット公表に関する使用承認申請中
につき、本図については、非公開。

Fig. 1-9. The picture of Majuro Atoll, Marshall Island. Excavated point is shown in red dots. The names of the excavated sites are referred to in the following figures (Figs. 1-10 to 1-12) Modified from Yamaguchi et al. (2009).

本図については、5 年以内に雑誌等で刊行予定のため、非公開。

Fig. 1-10. The results of sediment size analysis. 100 g of the bulk samples from each sedimentary layer were used for this analysis. The names of the excavated sites are indicated in Fig. 1-9. The left side of this figure is ocean side and the right side is lagoon side (Ito, 2010). The blue line showed the altitude of the Laura island modified from Yasukochi (2008).

本図については、5 年以内に雑誌等で刊行予定のため、非公開。

Fig. 1-11. The results of ratio of the spine of foraminifera. 200 individuals of foraminifera were picked up from each layer and observed.

The name is corresponded to the graph of Fig. 1-9.

The left side of this figure is ocean side and the right side is lagoon side. (Ito, 2010). The blue line showed the altitude of the Laura island modified from Yasukochi (2008).

(a)

(b)

本図については、5年以内に雑誌等で刊行予定のため、非公開。

(c)

(d)

本図については、5年以内に雑誌等で刊行予定のため、非公開。

Fig. 1-12. (a), (b) The results of sediment size analysis. 100 g of the bulk samples were used for this analysis. (c), (d) The results of ratio of the spine of foraminifera. 200 individuals of foraminifera were picked up from each layer. The left and right figures show the results of Jelto and Calalen islands, respectively, which were shown in Chapter 2. The blue line showed the altitude of each island measured by level staff (Ito, 2010).

本図については、5年以内に雑誌等で刊行予定のため、非公開。

Fig. 1-13. Difference of abrasion state of two island, Jelto and Calalen.

Human settlement on such atolls was revealed to be shorter than that on other continents or islands by the previous studies (Yamaguchi, 2005, 2009; Ito, 2010). Although Majuro Atoll has one of the longest human history among other atolls, only approximately 2000 years have passed since islanders first settled on this atoll (Yamaguchi et al., 2005, 2009). Therefore, Majuro Atoll has been subject to lesser anthropogenic influence than other countries with considerably longer human history and larger populations. As a world history of Marshall Islands, firstly, Spanish discovered the lands and declared the possession in 17th century. However, the lands were not particularly exploited and left as they were. In 1885, Germany protected territory and coconut cultivation, copra production has begun. In 1914, Japan occupied during the First World War, and subsequently, US military occupied in the battle of Gilbert Marshall Islands in 1944. In the Second World War, Majuro was a military base. It was necessary to excavate aggregate for building runways, causeway, docks and houses (Xue, 2001). In 1986, Marshall Islands were independent from the United States as a freed coalition partner. After the war, the center of the society in the atoll moved from Laura to east end

of the atoll and population of Majuro Atoll has been rapidly increasing (Xue, 2001). Especially, this east area is called Darrit–Uliga–Delap (D.U.D) area, which is composed of 3 islets. The D.U.D area (Figs. 1-14a, b) has 70% of the total population of the Majuro Atoll (Spennemann, 1992). In contrast, about 6,500 people (30% of the total population) have lived in less urbanize area, such as Laura, Calalen (Fig. 1-14c), and Jelto which is located on the north side of Laura. Nowadays, more than 20,000 people are living on Majuro Atoll (Osawa et al., 2010).

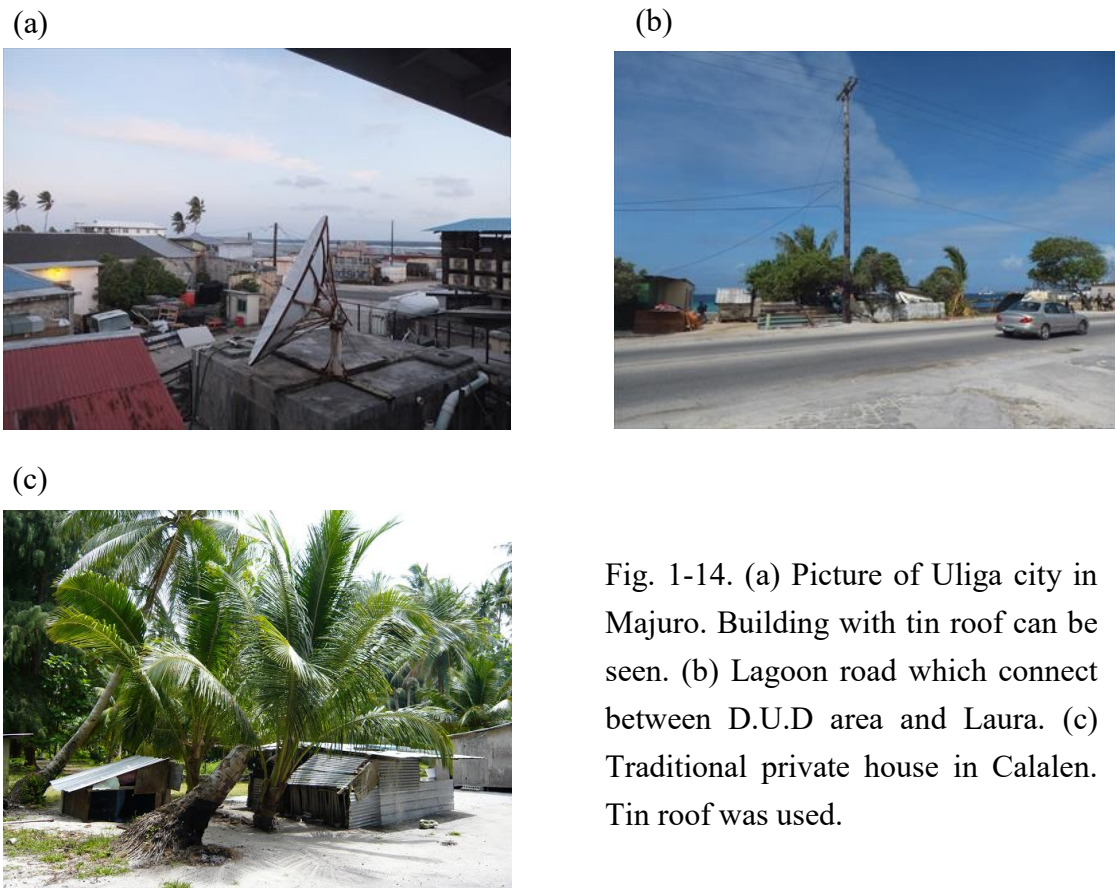


Fig. 1-14. (a) Picture of Uliga city in Majuro. Building with tin roof can be seen. (b) Lagoon road which connect between D.U.D area and Laura. (c) Traditional private house in Calalen. Tin roof was used.

The life styles in the reef islands have been dramatically changed with this urbanization. However, subsequent processes including anthropogenic effect is still not clear. As the sediments of atolls are composed of coarse bio-clastic sands and gravels

consisted of CaCO_3 (e.g., Kayanne et al., 2002), they are sensitive to environmental change such as ocean acidification caused by anthropogenic effects (e.g., Dias et al., 2010). Therefore, the materials which made from CaCO_3 are also potentially useful as indicators of environmental stress (e.g., Hallock. 2000; Collen et al., 2004). However, there should be another way to make use of this characteristics of the sediment. It may facilitate the identification of the anthropogenic sources of sediments in atolls. Thus, atoll is a suitable study site for investigating the influence of anthropogenic materials on the surface environment.

Some studies have investigated the environmental chemistry of atolls. Each previous study related to the theme of this study is described in each chapter. For example, Arimoto et al. (1985) investigated the concentrations of trace elements, such as aluminum (Al), scandium (Sc), manganese (Mn), iron (Fe), cobalt (Co), and thorium (Th), in dry and wet deposits in Enewetak Atoll in Marshall Islands. However, this study did not investigate the postdeposition processes of these elements. Furthermore, although some studies focused on several aspects of human life, such as agriculture and diet though, few studies have investigated environmental chemistry of trace elements in sediments. For example, Laird (1989), Deenik and Yost. (2006) studied sediments in Majuro Atoll and reported that the color of the upper sedimentary layer was darker than that of the lower layer. However, the samples in these studies were not collected from various depths by a systematically way. Therefore, the information of characterization of the initial deposition process of the trace elements and their subsequent migration in the vertical profile after the early stage of island formation to the present are lacking.

Furthermore, it is still not known the rapid soil formation mechanism in atolls. Black colored sediments were observed in the surface layer. However, the generation

process of this material has been unknown for a long time. In archaeology, these black colored layers were called “cultural layer” which implies that it has received anthropogenic influence such as cultivation, cooking food, or remains of green manure (e.g., Chikamori, 1995, 1996). In the contrast, white colored layers composed of calcareous bio-clastic sands were called “Natural layer”. However, it was considered that these black colored layers were not necessarily anthropogenic origin by following reasons.

i) These layers can be observed everywhere in the islands, even though the area or islands with no population. ii) Disturbances in succession of strata were not always observed around such layers. iii) If green manure was supplied to the surface of the sediment, there should remain that kind of layer at the top layer and also it is hardly possible to supply green manure all over the surface of the island. In practice, it was revealed that the matrix of this surface black layer was foraminifera by microscopic observation, of which the depth was 50-100 cm. Foraminifera tests in upper layers lost their original hardness and were covered with black materials (Fig. 1-15).

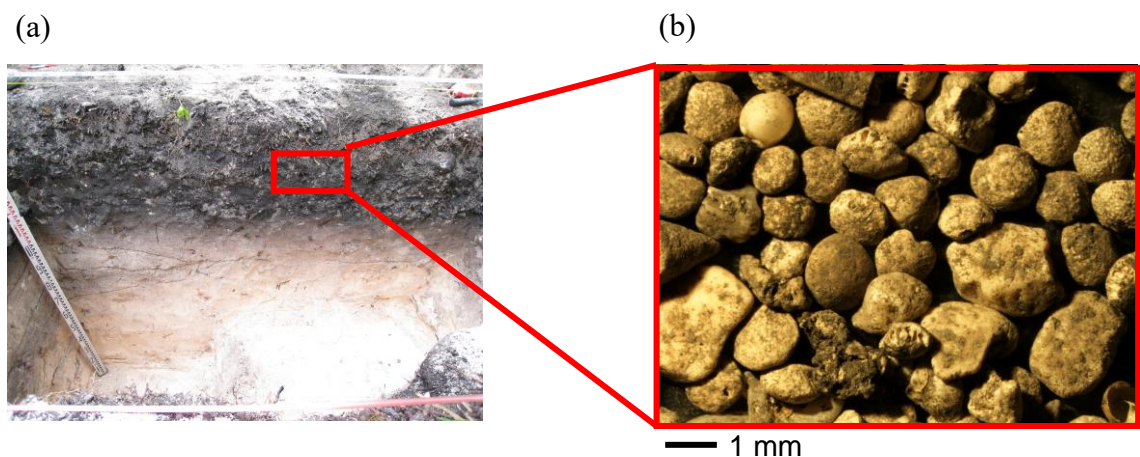


Fig. 1-15. (a) Sediment trench section of Calalen (KOL). (b) Microscopic image of the upper layer sediment.

However, it was still not known about the substance, source, and amount of these black materials (Fig. 1-16). There were also no quantitative chemical researches of the sediments on atolls; therefore, it is also unclear whether these materials were derived from natural source or anthropogenic factor. This layer which was called as “cultural layer” may have possibility to mislead the interpretation of prehistory in case that this black layer can be generated without anthropogenic influence.

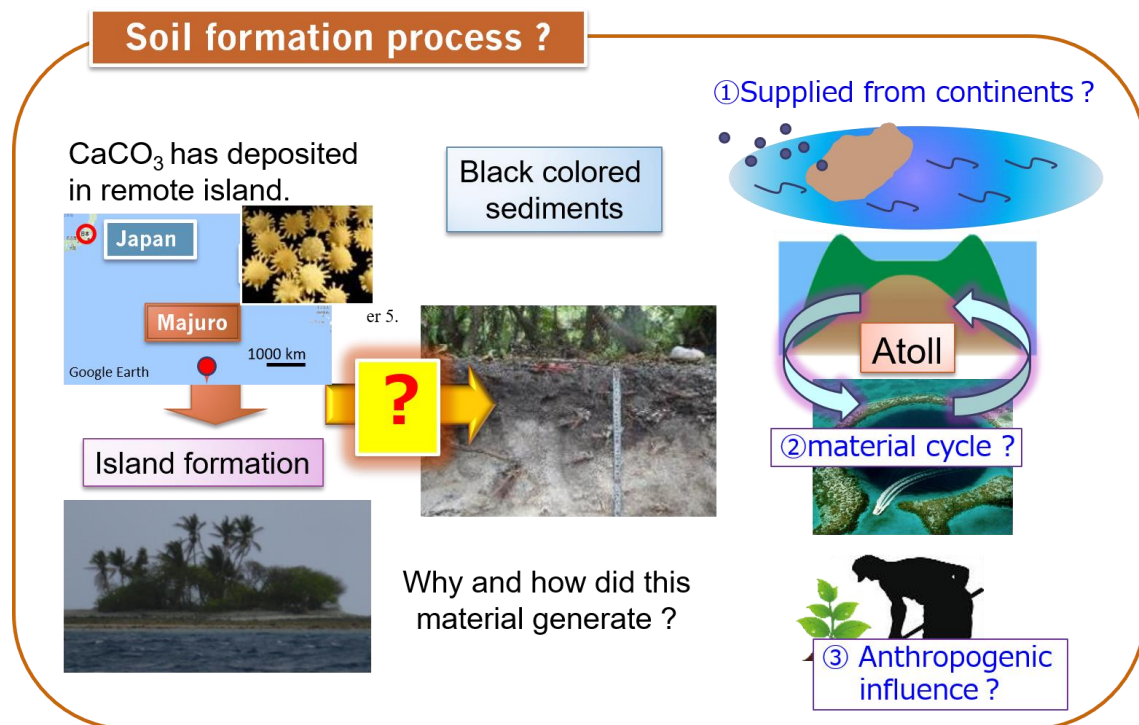


Fig. 1-16. Question on black colored sediments.

This thesis focused on i) Revealing the elements and chemical speciation which is concentrated in the sediment and identifying their origins. i) Reveal the degrees and influence of acidification of atoll sediments. ii) Reveal the characteristics of black sediments and factors which promoted the soilization of atoll. iii) Reveal the elements and their chemical speciation which is concentrated in the sediment and evaluating the

influence of urbanization on surface sediment quantitatively. The topic of i) and ii) were described in Chapters 3 (Ito et al., 2018a) and Chapter 4, respectively, while that of iii) in Chapter 5 (Ito et al., 2018b).

The novelties of this study is revealing the unknown but important process for the first time such as formation of an atoll, rapid soil formation process, and speciation of heavy metals in the area after the urbanization.

About the island formation, I revealed that sedimentation process occurred in a very short time scale in Laura from lowest part to the surface within 400 years. Similar process of the sedimentation within 400 years was also suggested in another island (Calalen) in the same atoll after 1000 years.

I also found that the soil formation rate of the atoll was faster compared to other coral islands which consist of elevated coral. Most of the atolls are located in the central Pacific Ocean which is far from other continents, where material supplies such as clay minerals were relatively small. For the reason of the rapid soil formation, I pointed out a possibility of activated nitrification as an important factor of the fast soil formation.

Finally, although conventional methods such as principal factor analysis have been employed for environmental problems in atoll, I have applied X-ray absorption fine structure (XAFS) spectroscopy with other conventional methods such as ICPMS, XRF, XRD, and SEM to the environmental chemistry studied to determine origins of various high-concentrated elements contained in atoll sediment and to discuss their behavior in the sediment. I found different vertical profiles of various elements and also found that the origin is different among various elements even though they were contained in the same spots. Especially, I suggested that Zn was incorporated into apatite which was secondarily generated on the surface of foraminifera. By this effect, I revealed that atoll

sediments have natural attenuation for heavy metals that prevent them from being released into the ground water (freshwater lens), which is important as a supplementary sources of drinking water for residents.

Chapter 2.

Sampling area

2. Sampling area

2.1. Sampling site

Majuro Atoll, an atoll in Marshall Islands, is located at latitude 7°05' N, longitude 171°23' E in the central Pacific, and Arno Atoll located 20 km east side of Majuro Atoll (Fig. 2-1). The atoll has an average annual temperature of approximately 27°C and receives an annual precipitation of approximately 3500 mm/year (Fujita et al., 2009). Majuro is one of Marshall Islands which located in the Central Pacific Ocean, which is northeast of Papua New Guinea. Majuro is shaped like an ellipse that extends west-east direction whose length is about 40 km.

Briefly, geological background of the Majuro Atoll is as follows. Holocene reef limestone was grown on atoll rims after eustatic sea-level rise which was over the surfaces of Last Interglacial (LIG) paleo reef. In Post-mid-Holocene, sea level was declined, and high-tide level became similar to the mid-Holocene low-tide level. This fostered the nucleation of stable atoll islands on resistant underpinning of emergent mid-Holocene paleoreef flats (Dickinson, 2009).

Among the islands of Majuro Atoll, Laura has the largest area and has one of the longest human residence history among all atolls in the world (Yamaguchi et al., 2005, 2009). Pit cultivation has been carried out in many areas in Laura where freshwater lens is available (Yamaguchi et al., 2005, 2009). In recent years, automobiles have been used in daily life as transportation to the Delap-Uliga-Djarrit (D-U-D) area, which is the central area of Majuro. By contrast, Calalen, which is located northeast of Laura, is an isolated island with a considerably smaller population than Laura (Spennemann, 1992).

(a)

インターネット公表に関する使用承認申請中
につき、本図については、非公開。

(b)

インターネット公表に関する使用承認申請中
につき、本図については、非公開。

Fig. 2-1. (a) Map of Marshall Islands. Majuro and Arno Atolls belong to Ratak chain (www.mappery.com/Marshall-Islands-Map-2). (b) Majuro (left) and Arno (right) Atolls with each island name studied in this work (earthobservatory.nasa.gov).

Samples were collected from the inland of the two islands, namely Laura and Calalen. The strata of the sediment layers were divided on the basis of the Munsell color system and sediment grain size.

In all the islands, the surface layers of the sediments are in black color (Fig. 2-2a), and this black-colored layer is thicker in Calalen than in Laura. On both islands, foraminifera tests in the upper sedimentary layer are covered with black materials (Fig. 2-2b).

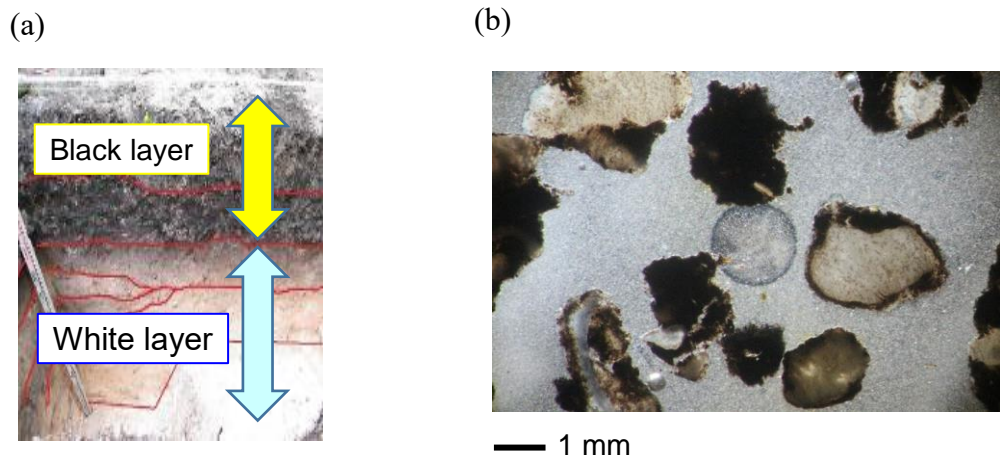


Fig. 2-2. (a) Sediment section. This is the section of Jelto. The red line shows the line of each sedimentary layers. picture(b) Thin section of sediment particles in upper layer observed by optical microscope. Picture shows surface layer of the Laura.

2.2. Sampling

Samples were collected from soil (sediment) profile in the soil trench excavated in $1 \times 1 \text{ m}^2$ area in the center of the five reef islands — Laura, Calalen, Jelto, and Delap (Fig. 2-3a) in Majuro Atoll, and Kebjeltak (Fig. 2-3b) in Arno Atoll at various depths with

different colors and grain sizes in August 2008 and February 2016. Manual-operated boring core sampler was also planned to use for the sampling of the sediments described below for the sediments deeper than 150 cm (Fig. 2-4a). However, since sand was unconsolidated with many coral gravels, the sampling was not successful. Therefore, this method was only applied for the sampling in the deeper layer in Delap (Fig. 2-4b).



Fig. 2-3. (a) Sampling point of Delap. (b) Sampling point of Kebjeltak (A1) in Arno Atoll.

Collection Methods

- (i) Dig a hole of 20×20 cm by a scup for 1 m and take a sample (100-200 g) for each sediment layer distinguished by color or size.
- (ii) Insert a plastic or metal tube (6.5 cm \times 6.5 cm) for 0.5~1 m in a dug hole. (Fig. 2-4)
- (iii) Pull up the tube.
- (iv) Knock the tube and take sample in the tube.

(a)

(b)

インターネット公表に関する使用承認申請中につき、本図については、非公開。



Fig. 2-4. (a) The method to collect sand sample (Adachi et al., 2010). (b) Picture of collecting a sample with this method in Delap.

2.2.1. Sampling in 2008

First sampling was carried out in August in 2008 in Laura, Calalen, and Jelto in Majuro Atoll. Samples from Laura and Calalen were used in the various studies in the whole thesis. The name of the sampling area is “Lr-3-1” in Laura (Fig. 2-5), and “KOL” in Calalen (Fig. 2-6).



Fig. 2-5. “Lr3-1” in Laura.

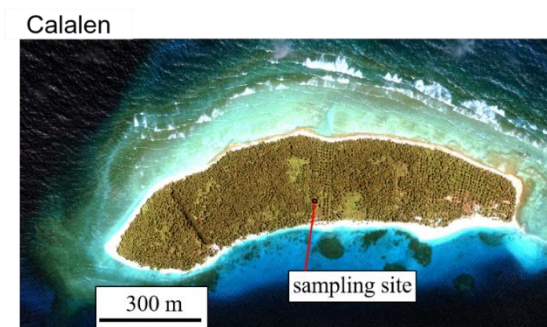


Fig. 2-6. “KOL” in Calalen.

2.2.2. Sampling in 2016

Second sampling was carried out in February in 2016 in the same islands of first sampling and Arno Atoll. Here, I describe details of the second sampling, which was carried out during my doctoral course.

Schedule

Our survey team took a boat to reach Calalen and Jelto in Majuro and Arno atolls, respectively. Living foraminifera was collected from north reef of each island. Fresh water sample was also taken from the trench or well of the sampling point. Red circle in each figure shows the sampling site.

In this study, samples named as “J.C” (Jelto) were used in Chapter 3. Groundwater sample from Freshwater lens, living foraminifera, and other sand samples were used in Chapter 5. All the sand samples were used in Chapter 4.

Day 1 (Feb/6/2016)

Area: **D.U.D (red circled area)** (Fig. 2-7)

- Make a reservation of a rental car
- Meeting with boat owner
- Take sand samples from D.U.D (Fig. 2-7)
=> sample was collected in Delap (DEL)
- Some samples were collected in a method shown in Fig. 2-4.



Fig. 2-7. D.U.D area.

Day 2 (Feb/7/2016)

Area: **Kebjeltak (Arno Atoll)** (Fig. 2-8)

- Charter a boat
Take sand samples from
- Cause way (A1, lower part in Fig. 2-8)
- Center area (A2, middle in Fig. 2-8)



Fig. 2-8. Kebjeltak.

※ Since there is no means of transportation in Arno Atoll, it is needed to move on foot.
It takes about 1 h from A1 to A2.

Day 3 (Feb/8/2016)

Area: **Calalen** (Fig. 2-9)

- Charter a boat
Take sand samples from
- Ocean side (C.O (Calalen-O), upper in Fig. 2-9)
- Lagoon side (C.L (Calalen-L), middle in Fig. 2-9)

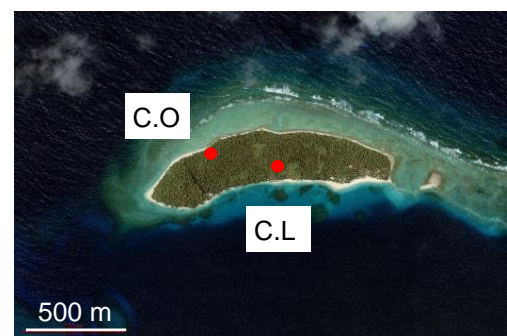


Fig. 2-9. Calalen

Day 4 (Feb/9/2016)

- Area: **Laura** (Fig. 2-10)
- Rent a car
Take sand samples from
 - Center part (L.C (Laura-C)) (middle in Fig. 2-10)
 - Ocean side (L.O (Laura-O)) (left in Fig. 2-10)
 - Lagoon side (L.L (Laura-L)) (right in Fig. 2-10)



Fig. 2-10. Laura

Day 5 (Feb/10/2016)

Area: **Jelto** (Fig. 2-11)

- Charter a boat
Take sand samples from
 - Ocean side (J.O (Jelto-O))
 - Center area (J.C (Jelto-C))
 - north reef flat of Laura

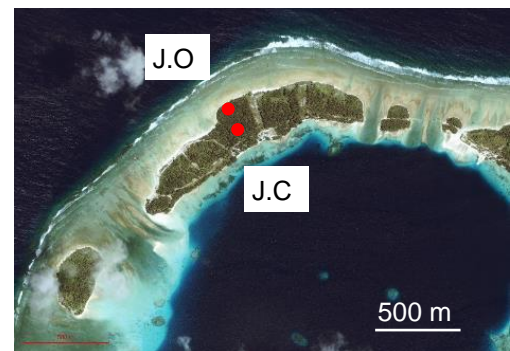


Fig. 2-11. Jelto

※Fig. 2-7 to 2-11: IKONOS,
except for Fig. 2-8: Google Earth

Notification

- It is needed to anchorage in Rong rong, the right east island, and switch to a smaller boat to go to Jelto.
- It is needed to ride a boat from Jelto at low tide, and anchorage a boat at the middle way, and walk in the sea, since the water depth becomes shallower because of the coral reef to go and do sampling at north flat of Laura.

2.3. Sample description

The grain size of the first layer (L1) and second layer (L2) layers in Laura and first layer (C1) layer in Calalen is classified as fine to medium sand (125–500 μm) (Figs. 2-12 and 3-1). *Calcarina*. spp, a large benthic foraminifera that inhabits algal turf on shallow reef flats, is the dominant species of foraminifera in these islands (Yamano et al., 2000). Deep sedimentary layers exhibit unconsolidated bio-clastic sand that consists of foraminifera, coral, and calcareous algae. Medium to coarse sands (0.5–2.0 mm) dominate the 3rd- 5th layer (L3–L5) and 2nd-5th layer (C2–C5) in Laura and Calalen, respectively. Large coral gravel is present in deep sediment layers (L5) (Figs. 2-12 and 3-1). The color of the sediment lightens and becomes whitish yellow with increasing depth. Fresh foraminifera tests were also collected in the coastal area of Majuro Atoll for comparison.

The sediment samples were taken from five islands, Laura (Lr3-1, L.O, L.C, and L.L), Calalen (KOL, C.O, and C.L), Jelto (J.C and J.O), Delap (DEL), and Kebjeltak (A1 and A2) (Figs. 2-5 to 2-11). Sampling points that are named as Lr3-1, L.C, KOL, J.C, and DEL are in the inland area, L.O, C.O, J.O, and A2 are in ocean side, L.L, C.L are in lagoon side, and A1 is causeway. Samples were taken in a depth range of 0-270 cm (Fig. 2-12). All the surface layers of the samples were black-colored sediments and well-vegetated. The grain size was medium to fine sand. The black-colored layer was thicker in Calalen compared to in Laura (Fig. 2-12).

本図については、5 年以内に雑誌等で刊行予定のため、非公開。

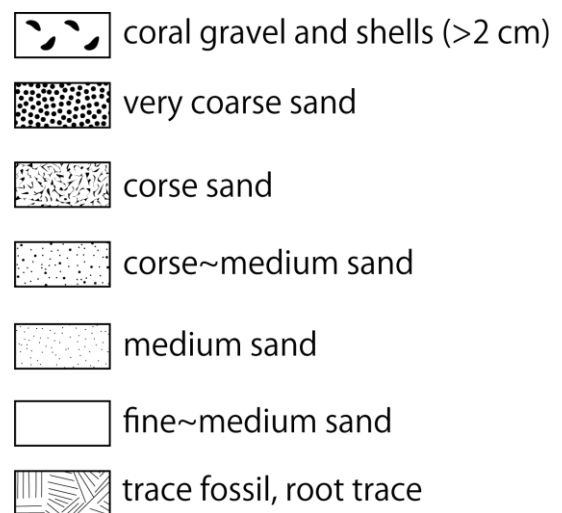


Fig. 2-12. Stratigraphic column of the sediment layers.

2.4. Characteristics of vegetation

In the survey view of 2008, palm trees were often observed. Plants such as breadfruits and *Cyrtosperma* spp. were also found in Laura. However, plants brought by people have also increased naturally, and there are many *Cyrtosperma* spp. in abandoned fields. In addition, *Casuarina*, nitrogen-fixing plants were also observed in Calalen. Normally, it is said that species of plants are originally limited in atolls. For instance, only 44 species were found in Arno atoll (Hatheway, 1953).

The urban and nonurban vegetation of a Pacific atoll has rapidly changed since 1944 (Sabath, 1977). In the case of Majuro Atoll, the nonurban areas are covered with coconut groves mixed with smaller breadfruits groves, which were probably planted in the late 1800s. Urbanization has changed indigenous and aboriginally introduced plant communities by replacing forested areas with open yards. Therefore, the indigenous vascular flora is limited in distribution and relative abundance on the *Cocos*- and *Artocarpus*- dominated islands (Sabath, 1977). In Majuro Atoll, *Guettarda*, *Scaevola*, *Tournefortia*, *Calophyllum* and *Pandanus* was distributed at both lagoon and ocean shores across all the islands, which also serve a function as salt-spray protection (Sabath, 1977).

2.5. Anthropogenic modification

In Laura, it is reported that habitation started as early as 2000 years ago and for the first 100 years, the inhabitants started excavating agricultural pits for the cultivation of wet taro, probably *Cyrtosperma* spp. (Yamaguchi et al., 2009). Around 1800-1600 yr BP, agricultural pits were excavated within the earliest habitation area and then moved to the lagoon side to make use of the groundwater in freshwater lens, which was located slightly deeper to the lagoon side. Subsequently, the habitation area expanded more lagoon ward around 1300-1000 yr BP, however, the back space of the ocean ridge was not habitation area, but temporary fishing camping area (Yamaguchi et al., 2009). Later than 1000 yr BP, people developed new agricultural pits in front of their habitation area, which was still limited to the lagoon side to central area of the island (Yamaguchi et al., 2009).

Although, there had been a continuous land connection between Laura and Delap (Spennemann, 1993), on 30 June 1905, the strong typhoon washed over the narrow parts of the long island from Delap to Laura. By this event, Majuro lost two tracts of land on its southern coast, apparently close to Delap (Spennemann, 1992).

Evident impacts of human activities on coastal environments has begun in the Second World War and greatly expanded after the War (Xue, 2001). In the Second World War, Majuro was a military base and excavation was carried out to gather the large amount of aggregate for building runways, causeway, docks and houses. In 1944 and the early 1970s, the continuous land from Djarrit to Laura has formed (Xue, 2001). Subsequently in the late 1970s and early 1980, a large Majuro Wharf constructed as a result of reclaimed land with excavated berths on both sides of the dock on the reef flat, on the eastern end of south rim; therefore, the most parts of the ocean shore from the

western end of Delap to the airport are artificial (Xue, 2001). For procuring aggregate in low costs, excavation was mostly carried out on the lagoon coast of the east atoll, which induces the erosion not only on this coast but also the coast of the east section of south rim and Laura, which suffered erosion in the last three decades since it lost sufficient sediment supply from south (Xue, 2001). However, dredging sites are still located on the edge of the lagoon reef flat and are connected to shore with breakwater from Darrit to the east part of Rairok (Xue, 2001).

Chapter 3.

Influence of acidification on carbonate sediments of Majuro Atoll, Marshall Islands

3. Influence of acidification on carbonate sediments of Majuro Atoll, Marshall Islands

3.1. Introduction

Acidification of soil is occurring all around the world (e.g., Galloway, 2001; Wallace, 1994). The cause of acidification can be both anthropogenic and natural factors. For example, acidification by anthropogenic factors such as acid deposition has been serious problems in developed countries such as Europe (Paces, 1985; Alcamo et al., 1987) and USA (Likens and Butler, 1981; Warby et al., 2009). However, the number of researches on environmental chemistry of the atolls including acidification are still limited, although there are more than 500 atolls such as Marshall Islands, Kiribati, and Tuvalu etc. in the world (Fujita et al., 2009; Yasukochi et al., 2014), where over tens of thousands of people live.

If soil acidification occurs on the atolls, it is possible that the amount of sediments decreases, since the component of the sediments are composed mainly of calcium carbonate (CaCO_3) (Perry et al., 2011; Yasukochi et al., 2014). The mineralogical characteristics of the sediments makes it more sensitive to acidification compared with other types of soil. If a large amount of acidic substances is provided, buffering effect of the acidification, namely, neutralization potential by CaCO_3 becomes weak, which eventually leads to decrease of total sediment mass of the reef island. According to previous studies on soil investigation conducted on Airik, Arno, Majuro, Mili, and Taroa Atolls in the Marshall Islands (Laird, 1989), the measurement method was not well-established, and the number of samples examined was very limited. Although these results are often cited in subsequent studies (Spennemann and Franke, 1995; Deenik and

Yost, 2006; Donnegan et al., 2011), it is difficult to evaluate whether acidification actually occurs or not on the atolls.

In this study, soil pH, concentrations of calcium (Ca) and magnesium (Mg), and porosity of foraminifera (*Calcarina* spp.) in Majuro Atoll were examined. For the calculation of porosity, X-ray μ -CT was used. It has been used in biological and medical sciences, but not widely used in environmental chemistry despite its applicability to quantitative analysis of microstructures of various minerals. This research showed the potential of X-ray μ -CT in environmental chemistry. In the conventional method to determine the porosities of microorganisms (Tetard et al., 2017) observation of cross-section slices have been used. However, the number of cross-section slices are much less compared with those acquired by X-ray μ -CT. Therefore, the conventional method using cross-section slices overlooks voids that can be detected by X-ray μ -CT. Moreover, X-ray μ -CT is a non-destructive method, which is superior to the cross-section method. This atoll is one of Marshall Islands and is located at latitude 7°05'N, longitude 171°23'E in the central Pacific. The average annual temperature is approximately 27°C, and the annual precipitation is approximately 3,500 mm (Fujita et al., 2009). In this chapter, I focused on three reef islands, Laura, Calalen, and Jelto (Fig. 3-1). Regarding the age of initial deposition of Laura, Yasukochi et al. (2014) mentioned that Laura island was formed around 2000 cal BP. Ages of sediments for other islands are also considered to be 2000 cal BP or younger, since Majuro Atoll was formed as a result of sea level fluctuations in Holocene (Dickinson, 2003). Right after Laura was formed, first islanders have settled down on this reef island (Yamaguchi et al., 2005, 2009). Therefore, Laura has one of the longest human histories among whole atolls over the world. The atoll has the characteristic as follows: (i) sediments consist of CaCO₃. (ii) urbanization has proceeded

within recent 100 years ago. Therefore, supplies of various industrial products are still limited compared to other developed countries. Thus, it should be easier to identify the factors that change the environment in the atoll during the initial stage of urbanization. In this study, the influence of acidification on the carbonate sediments was studied based on the chemical and mineralogical compositions and porosity of carbonate particles in the sediments.

3.2. Details of the sample

Samples were collected from center of the three reef islands (Laura and Calalen in August 2008; Jelto in February 2016) at various depths with different colors and grain sizes (Fig. 3-1; Table 3-1, 5-1). Laura has populated villages where automobiles have been used. On the other hand, Calalen and Jelto are isolated small islands where fewer people has lived (Spennemann, 1992). All the reef islands were well-vegetated and all the surface layers were black-colored. Each *Calcarina* spp. particle was covered with black-colored coating in the upper layer. Among them, *Calcarina* spp., larger benthic foraminifera which inhabit in algal turf on the shallow exposed-reef flat (Yamano et al., 2000) were the dominant species (Yasukochi et al., 2014). The sediments of the lower layer were unconsolidated bio-clastic sand consisting of foraminifera, coral, and calcareous algae in yellow or white color (Fig. 3-1). In Jelto, much more gravels or sand with coarse grain size were found compared to the other islands. Larger gravels (> 2 cm in diameter) were also found in the lower sedimentary layer in Laura.

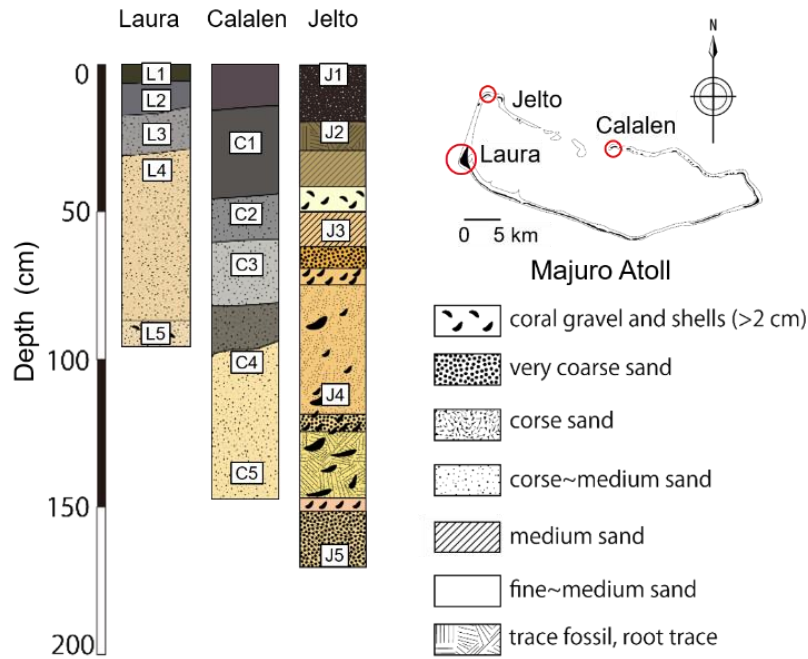


Fig. 3-1. Stratigraphic column of the sediment and location of study areas of Majuro Atoll.

3.3. Methods

3.3.1. X-ray Fluorescence (XRF)

To examine concentrations of Ca and Mg, X-ray fluorescence (XRF) analysis was carried out. Samples were firstly dried and sieved (< 2 mm).

Samples were homogenized by hand-grinding in an agate mortar and dried more than 4 h. Flux ($\text{Li}_2\text{B}_4\text{O}_7$) is also dried at 110°C for 24 h for dehydration. A five-step thermal treatment was performed for the samples in a muffle furnace (Fig. 3-2a) to remove organic matters and carbonate in the sample (0 - 100°C : more than 10 min, 100 - 500°C : 30 min, 500 - 800°C : 30min, 800 - 1000°C : 30 min, 1000°C : 6h). A flux and sample were mixed at the ratio of 10:1 (4 g : 0.4 g). A bead (Fig. 3-2b) and fuse sampler (TK-4100: Tokyo Kagaku Co., Ltd. Japan) was used for heating and mixing the sample and flux at 1200°C for 7 min and 10 sec. XRF spectrometer (PW4400/40: PANalytical Co.,

Ltd. Japan) (Fig. 3-2c) was used for the measurements (X-ray tube: Rh; voltage: 32 kV; current: 125 mA).

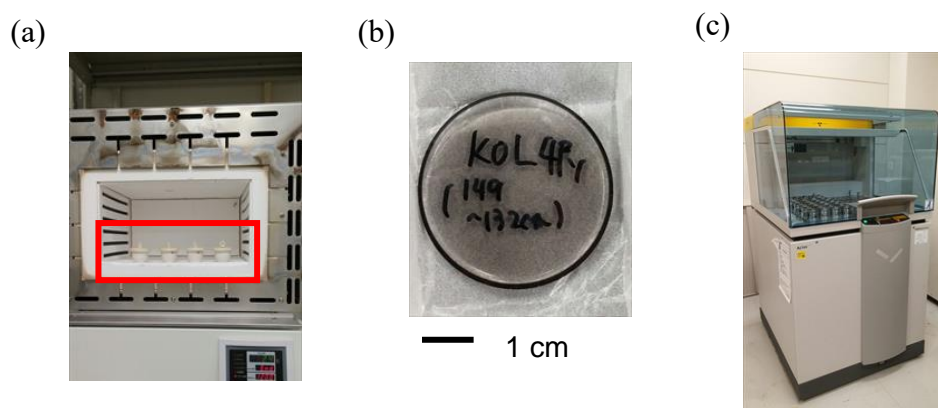


Fig. 3-2. (a) Sample were contained in the ceramic crucible (red square) and heated in a muffle furnace. (b) Bead (after the measurement). (c) XRF spectrometer (PW4400/40: PANalytical Co., Ltd. Japan)

For XRF analysis, calibration line was obtained by measuring 15 standard rocks (JA-1, JB-1b, JB-2, JB-3, JGb-1, JDo-1, JSI-1, JCh-1, JSd-1, JR-1, JR-2, JR-3, JG-2, JG-3, and JP-1; Imai et al., 1996). In particular, a certain amount of CaCO_3 (Wako Pure Chem. Ind., Ltd., Japan) was added to some of the standard rock samples to quantify Ca at higher concentration, because the samples contained high amounts of Ca.

The precision of the analysis was determined by the repeated analyses ($N=5$) of the same but independently-prepared sediment sample. The relative standard deviations of the analyses were 0.73% and 3.36% for Ca and Mg concentrations, respectively.

3.3.2. Ion chromatography

Ion chromatography (ICS-1100: Dionex Co., Ltd. Japan) (IC) was used to determine NO_3^- and SO_4^{2-} concentrations in the sediment and Mg^{2+} in *Calcarina*. For the extraction of NO_3^- and SO_4^{2-} , firstly, samples were mixed with ultra-pure water at the ratio

of 1: 8 (0.5 g : 4 g) and ultrasonic treatment was carried out for 30 min (Fig. 3-3). using 30% of acetic acid as the extractant. The solution was filtered with a 0.2 μm hydrophilic PTFE filter (ADVANTEC Co., Ltd. Japan). The precision was 4.79% determined by triplicate measurements of the same sample.

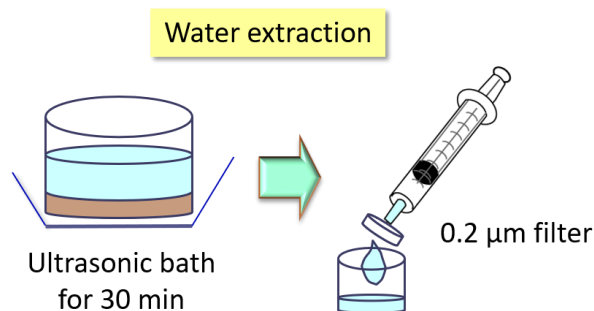


Fig. 3-3. Method of water extraction. This method is also applied to extract the solution of organic acid and absorption spectrophotometry.

3.3.3. Total Organic Carbon (TOC)

Total organic carbon (TOC) was measured by vario MICRO cube (Elementar, Co., Ltd., Germany) based on the oxidation of organic matter at 950°C (Fig. 3-4). 2 mg of - organic carbon was used for the TOC measurements. Before the measurement, inorganic carbon was removed by 1 N HCl (Fig. 3-4). The precision of this analysis was 0.27%.

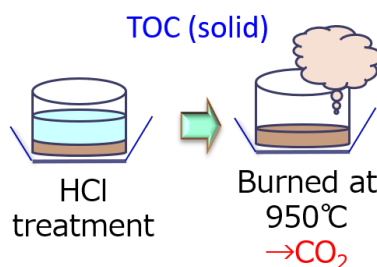


Fig. 3-4. Pre-treatment for TOC measurement.

3.3.4. X-ray diffraction (XRD)

The bulk samples contained bio-clastics such as fragments of coral and many kinds of foraminifera such as *Calcarina* spp., *Amphistegina* spp., Soritidae and others.

Chemical and mineral compositions differ depending on each species, even among the different genus of foraminifera. For example, Mg/Ca ratio of *Calcarina* spp. is about 4 times larger than that of *Amphistegina* spp. (Raja et al., 2007). Hence, I acquired XRD patterns of *Calcarina* spp. obtained by the homogenization of 20-30 individual *Calcarina* spp. particles. Unblemished adults *Calcarina* spp. were used for the measurements judging from their body size (around 1 mm). However, some or all spines were worn out. I acquired XRD patterns by a diffractometer (RINT2000: Rigaku Co., Ltd., Japan) with Cu K α_1 radiation. The measurements were carried out within the range from $2\theta = 10^\circ$ to 90° with 0.020° step and $4^\circ/\text{min}$ scanning rate (40 kV, 30 mA). Rietveld analysis (Rietveld, 1969) and whole-powder-pattern fitting (WPPF) method was used for the mineral composition analysis (PDXL2; Rigaku Co., Ltd., Japan). Here, the residual square sum R defined by Eqn. 1 is minimized by optimizing the least squares parameter p .

$$R(p) = \sum_i \frac{1}{\sigma(y_i)^2} [y_i - y_i^{\text{cal}}(p)]^2 \quad (1)$$

Here, y_i , $\sigma(y_i)$, and y_i^{cal} represented X-ray intensity against diffraction angle 2θ , intensity error (standard deviation), and calculated profile of X-ray diffraction. The difference of the fitting between the theoretical and measurement profiles is regarded as an analytical error, typically about 4% in this measurement.

3.3.5. Soil pH

Soil pH was measured for the sample mixed with fresh Milli-Q water (Millipore; $18.2 \text{ M}\Omega\cdot\text{cm}$ at 25°C) at a sediment : water ratio of 1 : 2.5 (weight/weight) (The Committee on Soil Reaction Measurements Second International Commission, 1930;

Islam and Weil, 2000). For soil pH measurement, Air-dried sediment sample and Milli-Q water were shaken together calmly for 1 min and left to settle for 30 min, which was repeated twice before measurement of the soil pH with a pH meter (LAQUA F-52: HORIBA Co., Ltd., Japan) (Luo et al., 2011). The pH value of each sediment sample at different layer was determined by measuring supernatant liquid after filtration by a membrane filter (pore size: 0.20 μm ; hydrophilic PTFE, Advantec, Japan).

3.3.6. X-ray μ -Computed Tomography (CT)

Projection X-ray μ -CT was measured at beamline BL37XU in SPring-8 (Hyogo, Japan) equipped with double crystal monochromator of Si (111) and two mirrors. The spatial resolution of μ -CT is 0.488 $\mu\text{m}/\text{pixel}$ (Figs. 3-5, 3-6a). The number of projections for each sample was 1800 for 180° rotations (Terada et al., 2016). Here, X-ray energy of 10 keV was used for the measurement. The dominant species of the foraminifera, *Calcarina* spp. (< 0.8 mm) at different layers was picked up and placed within a polyimide tube (inner-diameter: 0.8 mm) with α -cyanoacrylate adhesive (Fig. 3-6b). The tube containing a sample was placed perpendicularly on the motorized rotation stage for the projections of μ -CT measurements. Transmission X-ray images were obtained with a set of a beam monitor for X-rays and CMOS camera (Fig. 3-6c), which has 1920×1920 or 2048×2048 pixels for the measurement of Laura and Calalen samples and Jelto samples, respectively.

インターネット公表に関する使用承認申請中 につき、本図については、非公開。
--

Fig. 3-5. Whole structure of synchrotron radiation μ -CT method.

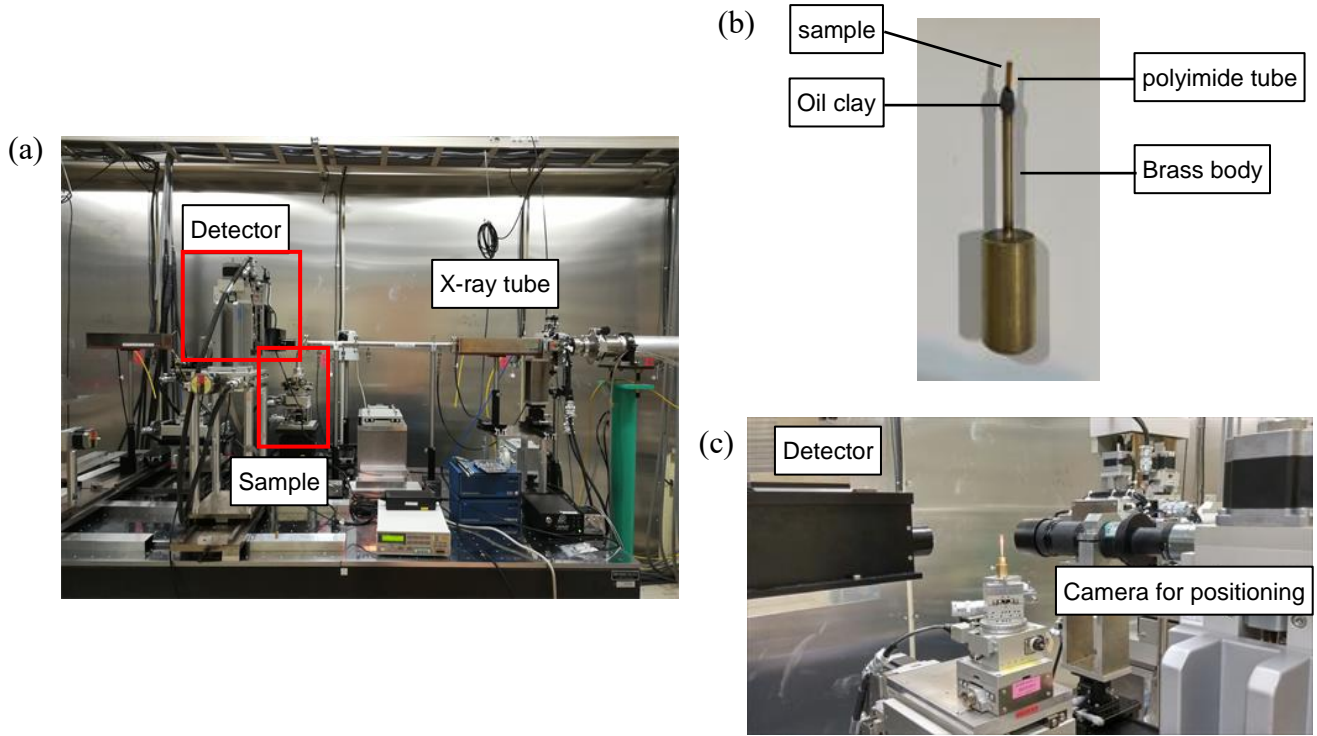


Fig. 3-6. (a) Equipment for μ -CT in hatch. (b) Equipment for fixing sample for measurement. Sample was contained in a polyimide tube. In order to accurately align the rotation axis, it is better that the length of the tube is shorter. The tube was fixed the joint with the brass body with oil clay. (c) Detector for μ -CT and camera for positioning of rotation axis.

The dark current data were prepared for reconstructing the images and for forming a sinogram. Subsequently, I reconstructed the images and converted them to 16-bit TIFF images. The reconstructions of the images were carried out on the basis of the Convolution Back-Projection (CBP) method (Huesman, 1977).

The porosity was calculated in all parts of the tests of *Calcarina* spp. by the sum of each slice of reconstructed μ -CT image (the number of slice (n) = 815-2047, depending on the size of *Calcarina* spp. test) using ImageJ (Rasband, 1997-2012). In each n th slice, area of matrix *Calcarina* spp. (= A_{mat}) and sum of areas of fine voids (= A_{void} ; size: 1-200 μm^2) were calculated (Fig. 3-7b).

The latter was defined here to avoid counting the original chamber and trace of pseudopod in *Calcarina* spp. test (Fig. 3-7a). I calculated the porosity of *Calcarina* spp. by the formula below in this study:

$$\text{Porosity (\%)} = [\Sigma A_{\text{void}}(n) / (\Sigma A_{\text{void}}(n) + \Sigma A_{\text{mat}}(n))] \times 100. \quad (2)$$

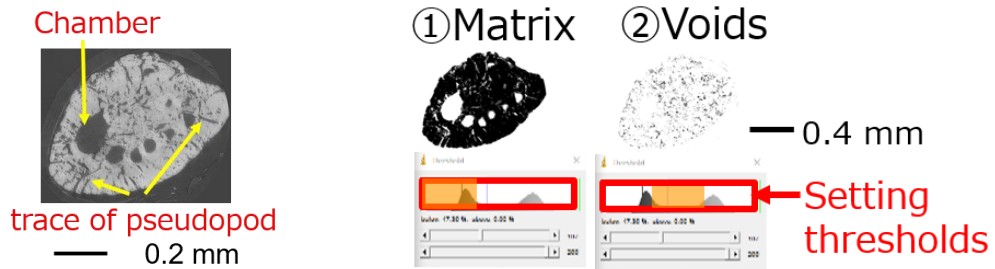


Fig. 3-7. (a) μ-CT reconstruction image. Chamber and trace of pseudopod of foraminifera. (b) matrix part and voids part which distinguish by the size and luminance of color in μ-CT reconstruction image by imageJ.

I measured 2-3 *Calcarina* spp. tests which had different colors (orange and whitish ones). The latter might have received bleaching effect from the seawater) and degree of abrasion of spines collected at the same depth. However, there was no significant difference among their porosities for the samples from the same depth. To examine the distributions of Ca and Mg in *Calcarina* spp. tests, scanning electron microscopy (SEM: JSM-7000F, JEOL Co., Ltd., Japan) equipped with an energy-dispersive spectroscopy (EDS) detector was used. Samples were prepared in polished cross-section (Fig. 3-8).



Fig. 3-8. Thin plate amounted the sample with resin, which was coated by carbon. Thin plate was set by carbon tape for SEM observation.

3.3.7. Mg K-edge XANES

Mg k-edge XANES measurements were applied to the bulk sample of Laura (L1-L5) to identify the chemical species. The measurements were carried out in Ritsumei University (SR center, BL-10). All the spectra were obtained by measured by fluorescence method.

3.4. Results and Discussion

3.4.1. Soil pH and concentration of inorganic matters

From the results of soil pH measurements, the sediment samples taken from three islands (Laura, Calalen, and Jelto) were characterized by high soil pH value around 8.2-8.5 at the depth below 100 cm. However, the soil pH decreased toward the upper layer (colored area in Fig. 3-9a), which was close to pH 7.5 in Laura, Calalen, and Jelto. Soil pH of most of the surface samples were lower than 8.0 above the depth of 20 cm.

Bulk XRF results showed that Ca concentration was constant within 34.9-36.6wt% through all the depths. In contrast, Mg concentration decreased from about 2.0% to 0.7% upward from 25 cm depth to the surface in Laura and Jelto (Fig. 3-9a). The Mg concentration also decreased from lower depth (68 cm) to the surface in Calalen. Magnesium should have been dissolved into the interstitial water, which can infiltrate into the groundwater (freshwater lens) in the atolls (Anthony et al., 1989) and finally discharged into seawater by the tidal movement (Underwood et al., 1992). If the plants remove Mg from the sediments, the same thing can be valid to K. However, its concentration was rather stable. (Table 3-1) On the other hand, TOC and NO_3^- concentration increased above 50 cm depth (Figs. 3-9a, 4-12a). The SO_4^{2-} concentration increased in the lower layer (below 100 cm depth) regardless of the soil pH (Fig. 4-12b).

Therefore, SO_4^{2-} should be present as a neutralized salt in the seawater that have permeated in the groundwater (below 150-200 cm depth) in the lower layer of the sediment (Hamlin and Anthony, 1987; Anthony et al., 1989). Since the size of sediment particle in Jelto is larger, the freshwater is more readily mixed with seawater compared with other two islands.

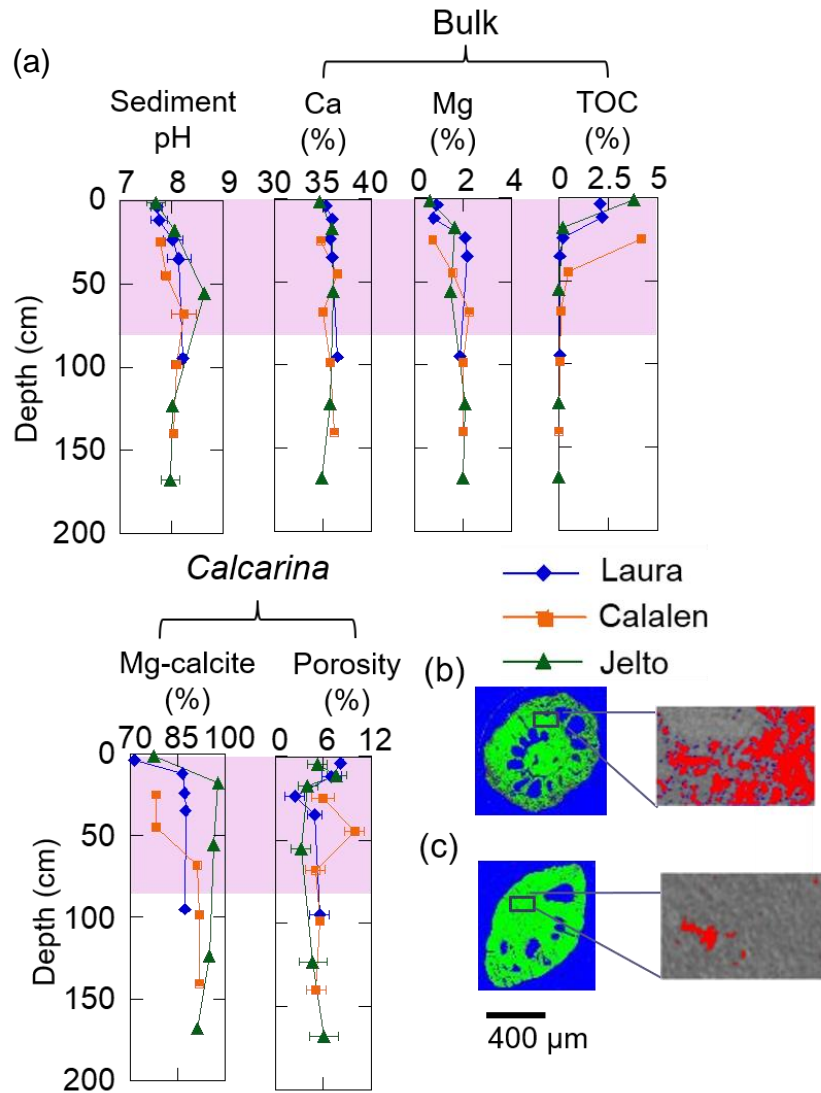


Fig. 3-9. (a) Depth profiles of soil pH, chemical composition of bulk soil/sediments, and magnesiumian calcite (Mg-calcite) fraction and porosity in *Calcarina* spp. particles. Colored areas indicate the ranges of the depths where large changes are observed in the analytical results. (b) and (c) are X-ray μ -CT images. Red areas show the voids that were taken into account in the calculation of porosity at the depths of (b) 12 cm and (c) 95 cm in Laura.

3.4.2. Porosity of *Calcarina* spp.

All the porosities of *Calcarina* spp. below 50 cm of the depth were lower than 5% in the three islands, where the soil pH values were above 8.0. However, the porosity was generally larger about 6-7% above 50 cm depth on the average (Fig. 3-9). The porosity increased toward surface between 24 and 12 cm depth, 68 and 45 cm depth, 18 and 11 cm depth in Laura, Calalen, and Jelto, respectively (Figs. 3-9). The porosity of fresh *Calcarina* spp. on the reef flat of Jelto was 0.21% (Fig. 3-10), which was a significantly lower value.

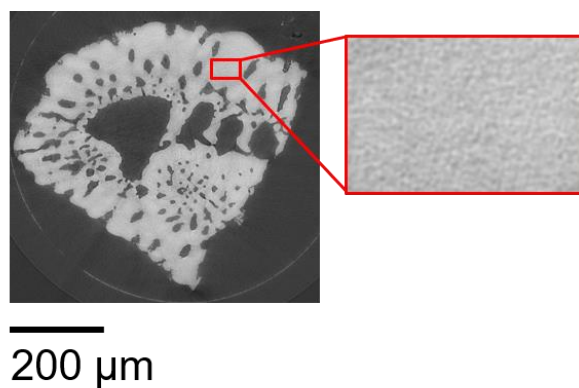


Fig. 3-10. X-ray μ -CT reconstructed image of fresh *Calcarina* spp. on the reef flat of west passage Jelto. The right is an enlarged picture for a part of the foraminiferal test, where small voids were not observed.

The depth profiles of both Mg concentration and magnesian calcite (Mg-calcite) fraction in the mineral composition of *Calcarina* spp. showed similar patterns, namely, the two parameters decreased toward the upper layer. Since Mg-calcite was originally contained in *Calcarina* spp., the depth profile of Mg concentration represented that of Mg-calcite contained in *Calcarina* spp., which dissolves more readily compared with calcite as shown in other studies (Busenberg and Plummer, 1989; He and Morse, 1993).

3.4.3. Different pattern of XRD

As a result of XRD pattern (Fig.3-11), the lattice parameter values of all *Calcarina* spp. in the samples were in agreement with calcite (CaCO_3 ; JCPDS #01-072-1650) which has the strongest peak at $2\theta = 29.52^\circ$, and Mg-calcite ($\text{Mg}_{0.129}\text{Ca}_{0.871}\text{CO}_3$; JCPDS #01-086-2336) at $2\theta = 29.76^\circ$. In order to confirm whether structural phase transitions occur due to pressure or temperature by grinding sample, measurements were carried out by halving and doubling the time for grinding the same sample. However, the results did not change by grinding time. As the depth became closer to the surface, Mg-calcite fraction to total carbonate minerals (= calcite + Mg-calcite) of *Calcarina* spp. decreased significantly from the depth around 20-25 cm. In the case of Calalen, the fraction decreased from the depth of 68 cm, which is lower depth than those in Laura and Jelto (Fig. 3-9a, Table 3-1). Magnesium content in *Calcarina* spp. based on Rietveld analysis was consistent with that in *Calcarina* spp. tests in the deeper layers measured by ion chromatography (Table 3-1). In the shallower depth, the two minerals were observed in the XRD patterns (Fig. 3-11a). This result shows the relative increase of calcite at the surface with decrease of Mg-calcite, which suggests that (i) calcite in the sample remains selectively due to its relatively larger stability against acidification compared with Mg-calcite (Andersson et al., 2008; Yamamoto et al., 2012) or (ii) re-precipitation of calcite after the dissolution of Mg-calcite. I considered that re-precipitation of calcite has occurred, which apparently reduces the porosity. In this case, the porosity does not increase as the decrease of Mg-calcite.

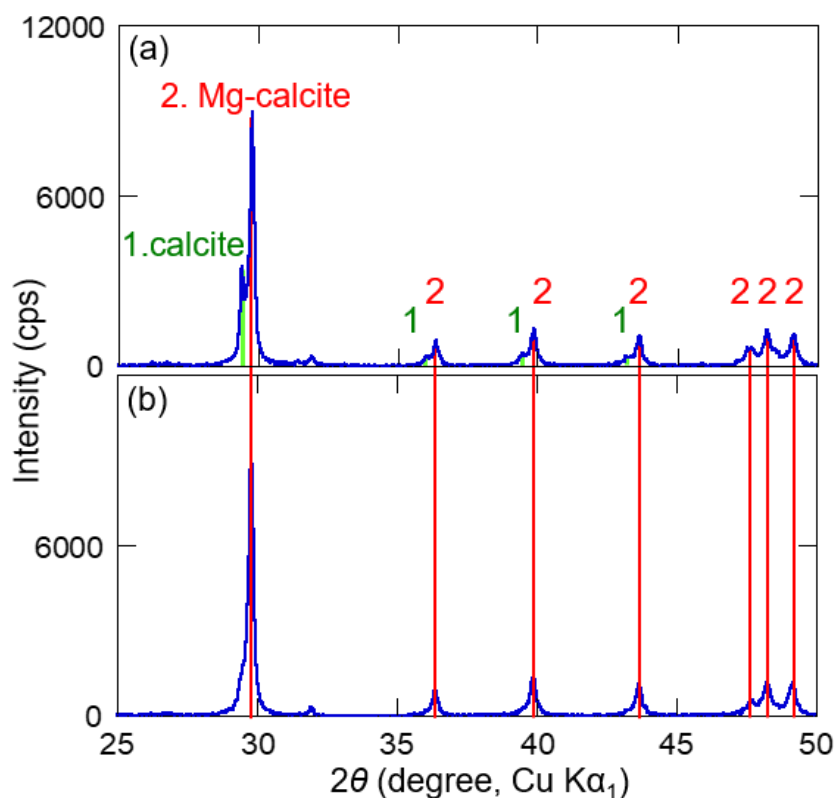


Fig. 3-11. XRD pattern of *Calcarina* spp. collected at the depths of (a) 4 cm and (b) 95 cm in Laura.

The XRD pattern was also taken in bulk sample. In bulk sample, not only *Calcarina* but also coral gravels are contained. Fig. 3-12 shows the mineral component at the different depth and Fig. 3-13 shows the XRD diffraction pattern of the bulk sample of the surface layer of Laura at the 4 cm depth (upper layer). Diffraction patterns of aragonite were observed from the bulk sample. Aragonite is normally contained in coral. Therefore, the patterns of aragonite should be derived from corals. On the other hand, Mg-calcite also decreased in the case of bulk sample. Especially, around 25 cm depth, the

ratio of Mg-calcite in the bulk in Calalen was much smaller than that of Laura, that the patterns of Mg-calcite hardly observed (Fig. 3-14). The possibility of this difference is that the species ratio of the foraminifera should be different, since the soil pH was almost the same between these sampling areas. Namely, more species with lower resistance to low soil pH may exist in the Calalen sample. As for the sediment as a whole, it is the same that Mg-calcite decreased in the upper layer. However, the ratio of Aragonite relatively increased. For that reason, the decrease of Mg-calcite in *Calcarina* should be the biggest factor, but it is also considered that coral fragile which is the major origin of aragonite may increase in upper sedimentary layer.

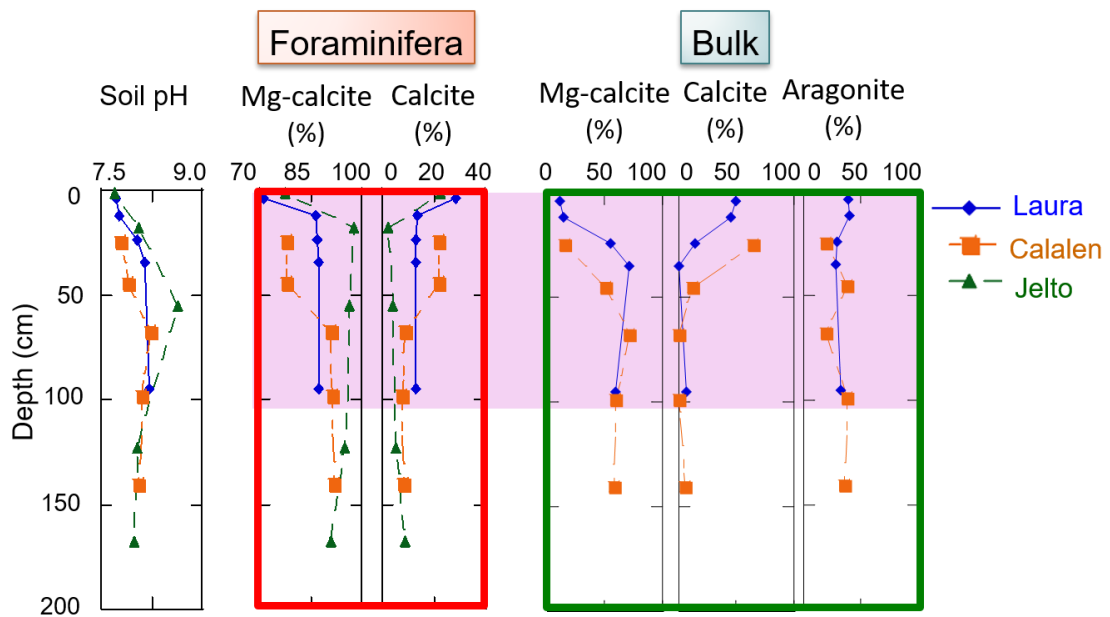


Fig. 3-12. Soil pH and mineral composition of foraminifera (red) and bulk sediments (green).

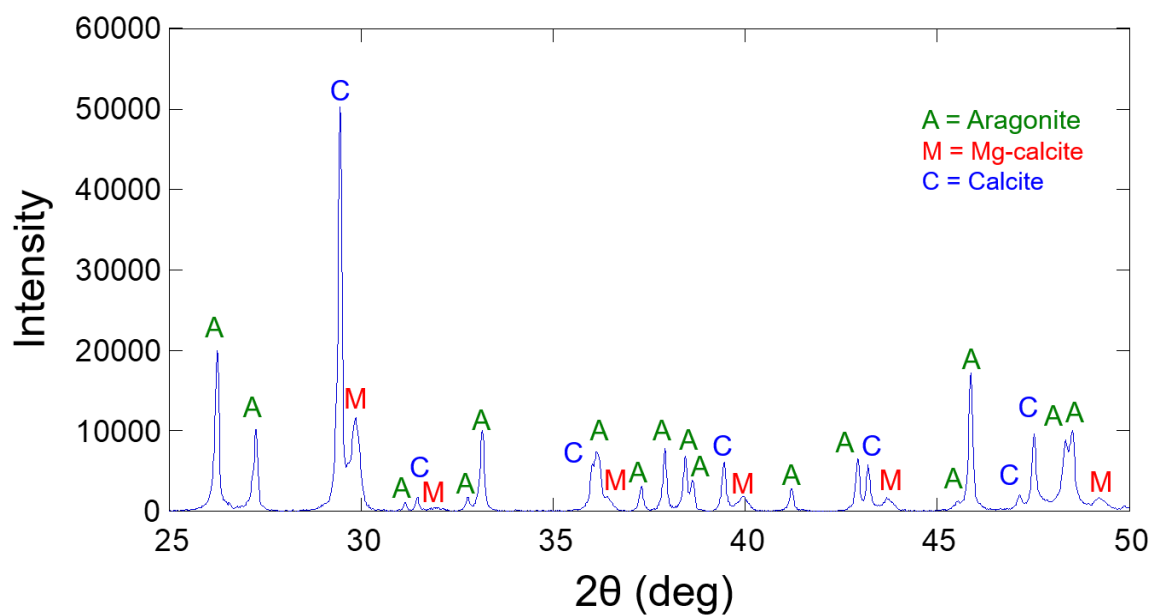


Fig. 3-13. XRD pattern of bulk sample collected at the depths of 4 cm in Laura.

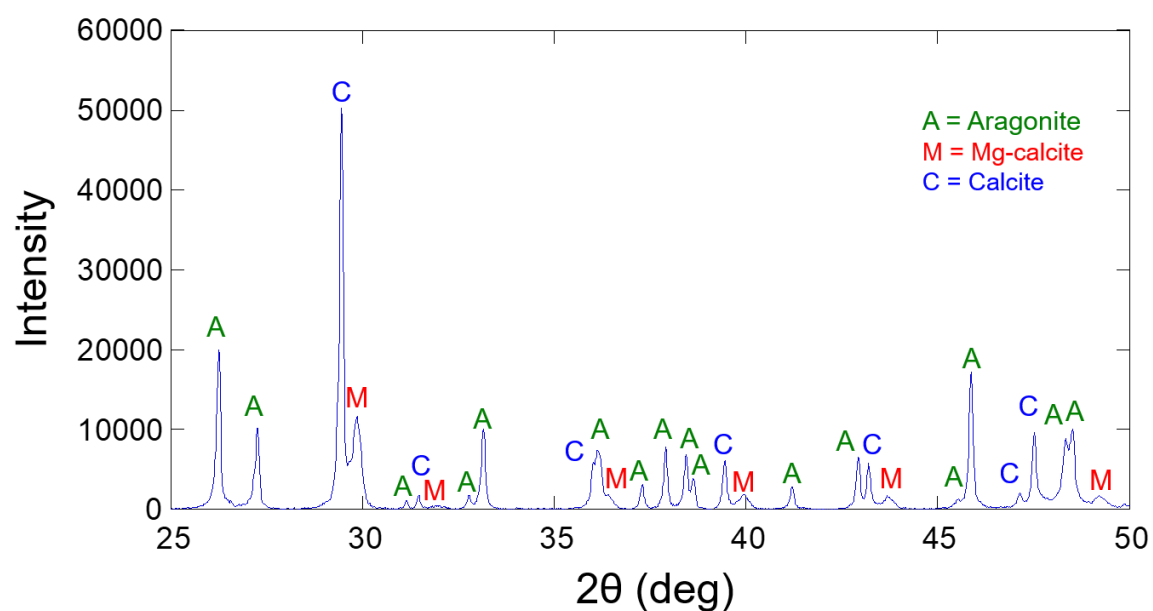


Fig. 3-14. XRD pattern of bulk sample collected at the depths of 25 cm in Calalen.

Table 3-1. Mean depth, soil pH, porosity, weight concentrations of Ca and Mg for the bulk sediments, and Mg-calcite fraction among total carbonate minerals (= calcite and Mg-calcite) in the foraminifera particles, estimated Mg ratio in *Calcarina* calculated by Rietveld analysis, and measured Mg content in *Calcarina* by ion chromatography.

Sample name	Depth (cm)	Soil pH	Ca (bulk) (wt%)	Mg (bulk) (wt%)	K (bulk) (wt%)	Mg-calcite (<i>Calcarina</i>) (%)	Mg in <i>Calcarina</i> calculated by Rietveld analysis (wt%)	Mg in <i>Calcarina</i> measured by ion chromatography (wt%)	Porosity (<i>Calcarina</i>) (%)
Laura-1 (L1)	4	7.72	35.4	0.930	0.007	71.3	2.28	2.09	7.54
Laura-2 (L2)	12	7.77	36.0	0.805	0.005	86.5	2.77	—	6.57
Laura-3 (L3)	24	8.03	35.8	2.10	0.006	87.0	2.78	2.76	2.44
Laura-4 (L4)	35	8.15	36.0	2.19	0.005	87.4	2.80	—	4.69
Laura-5 (L5)	95	8.22	36.6	1.88	0.006	87.3	2.79	2.62	5.28
Calalen-1 (C1)	25	7.79	34.9	0.767	0.007	78.0	2.50	2.41	5.22
Calalen-2 (C2)	45	7.89	36.5	1.58	0.007	78.0	2.50	—	8.70
Calalen-3 (C3)	68	8.24	35.1	2.29	0.007	91.1	2.92	2.78	4.83
Calalen-4 (C4)	99	8.11	35.8	2.01	0.012	91.7	2.93	—	3.27
Calalen-5 (C5)	141	8.06	36.2	2.00	0.010	91.9	2.94	3.13	4.86
Jelto-1 (J1)	2	7.70	34.9	0.767	0.005	77.4	2.48	2.40	4.41
Jelto-2 (J2)	18	8.07	36.5	1.58	0.004	97.8	3.13	—	3.95
Jelto-3 (J3)	56	8.65	35.1	2.29	0.004	96.4	3.08	3.01	3.68
Jelto-4 (J4)	124	8.03	35.8	2.01	0.008	94.9	3.04	—	4.48
Jelto-5 (J5)	168	7.99	36.2	2.00	0.008	91.0	2.91	3.08	4.63

3.4.4. Selective dissolution of Mg-calcite observed by SEM

In the SEM observation, many cracks and small voids were often observed in the tests of *Calcarina* spp. when the soil pH was lower than 8, but hardly observed above soil pH 8. Figs. 3-15a and 3-15b show the elemental mapping of Ca and Mg, respectively, in which Ca was distributed homogeneously, except for the rim of *Calcarina* spp. However, the Mg/Ca ratio in the mapping (Fig. 3-15c) became smaller in some parts of the center of *Calcarina* spp. (the area indicated by circles in Fig. 3-15c), where Ca intensity is still high. This result suggested selective dissolution of Mg-calcite and subsequent re-precipitation of calcite have occurred in the part shown in Fig. 3-17. Although Mg concentration is relatively low in enclosed areas, calcite was not found. Calcite was found from the edge of foraminifera (Fig. 3-17c) and inside edge of chamber (Fig. 3-17d-g) and trace of pseudopod (Fig. 3-17b), where Mg peak was not found by the spot analysis of SEM-EDS (Fig. 3-17h).

These results are consistent with the finding by the XRD patterns (Fig. 3-11). On the other hand, Fig. 3-16a and 3-16b show the elemental mapping of Ca and Mg of *Calcarina* spp. at 68 cm depth, respectively. Here, Ca and Mg were distributed homogeneously. Mg/Ca ratio in the mapping at 68 cm depth also showed homogeneous pattern (Fig. 3-16c), which suggested that selective dissolution of Mg did not occur.

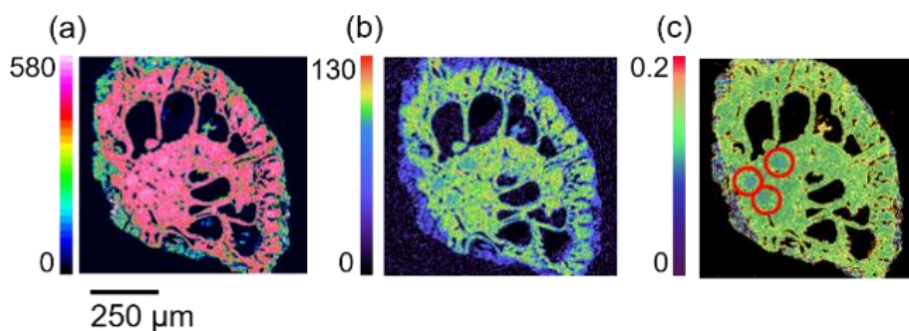


Fig. 3-15. SED-EDS mappings of the cross-section of *Calcarina* spp. collected at 12 cm depth in Laura. (a) Ca, (b) Mg, and (c) Mg/Ca ratio. Intensities are in arbitrary units.

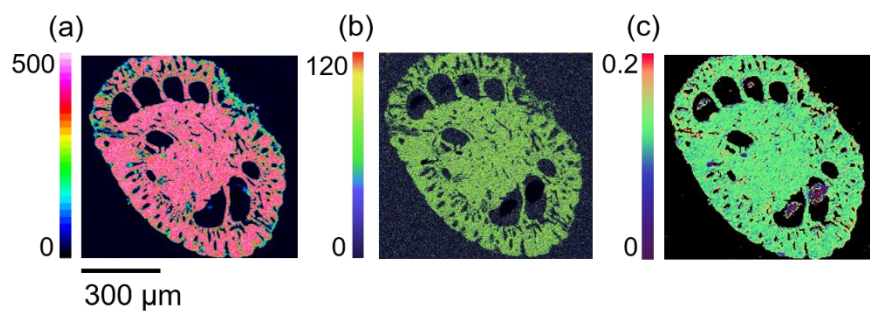
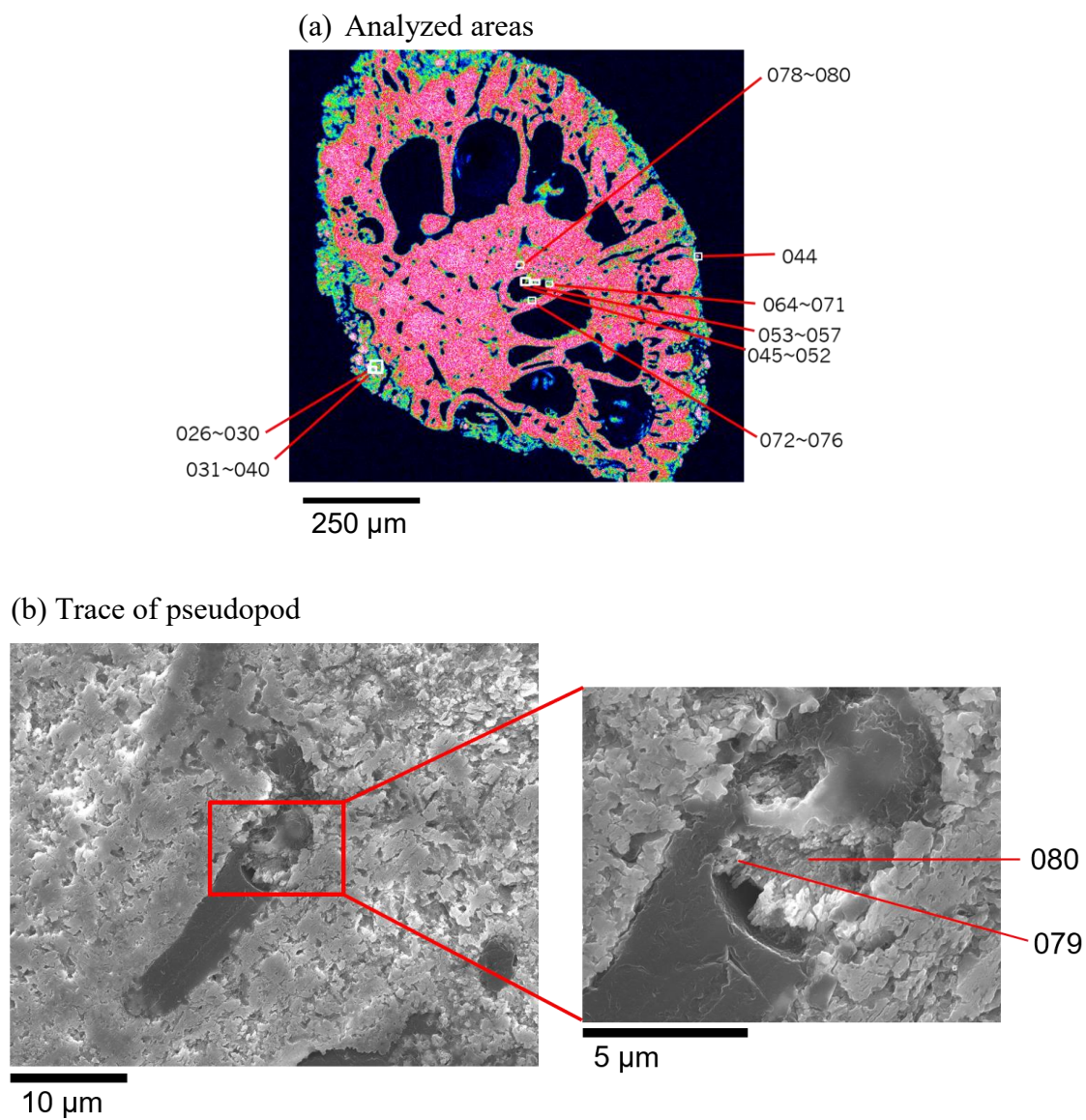


Fig. 3-16. SEM-EDS mapping of the cross-section of *Calcarina* spp. collected at 68 cm depth in Calalen. (a) Ca, (b) Mg, and (c) Mg/Ca ratio. Intensities are in arbitrary units.



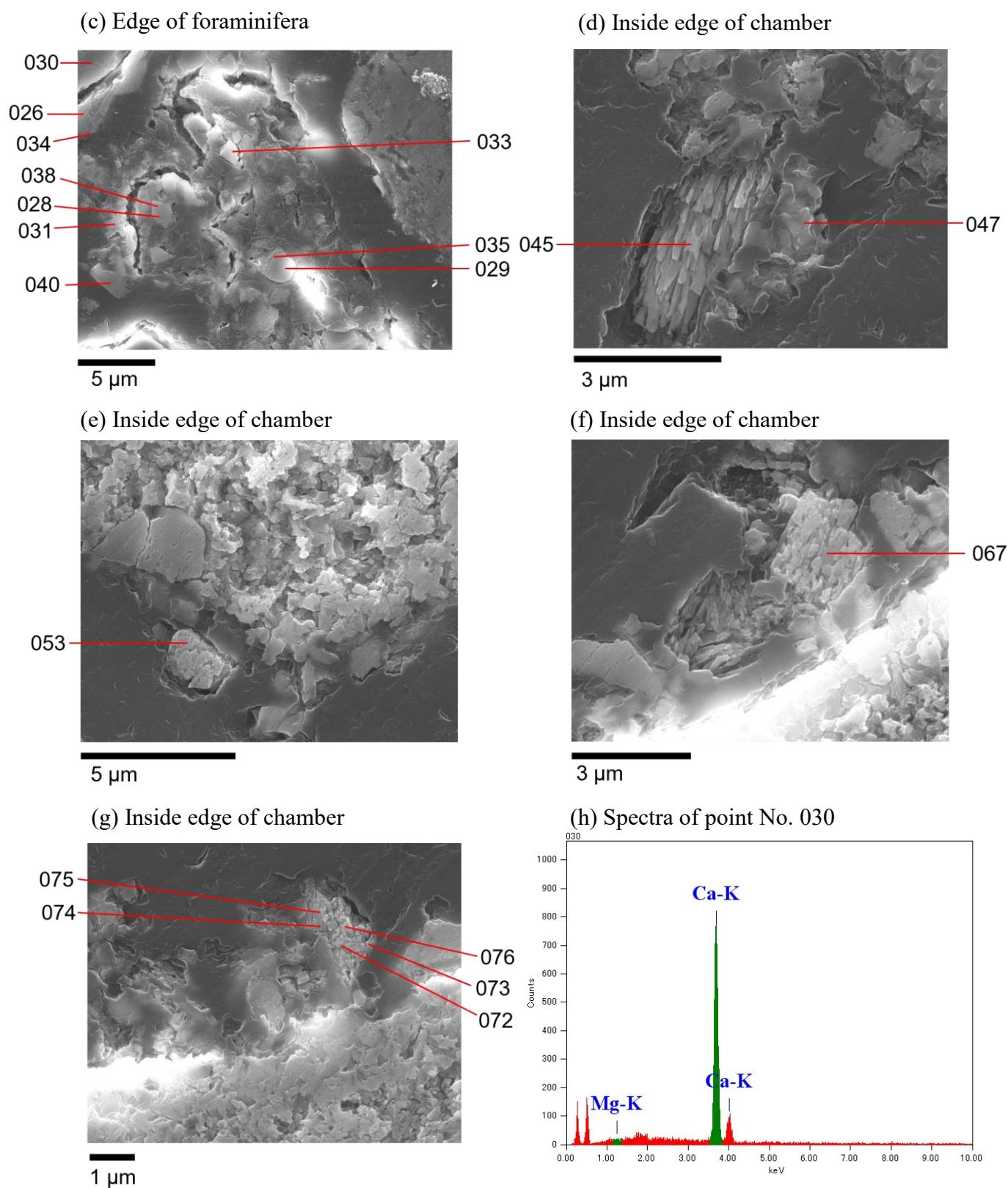


Fig. 3-17. (a) Areas of each spot where calcite was found by analyses of SEM-EDS. (b)~(g) SEM images of calcite. Numbers were corresponded to those in (a). (h) Spectra of the point (No. 030) which was found by SEM-EDS. Same spectra patterns were also obtained from other spots shown in (b)~(g).

3.4.5. Chemical species of Mg

As the results of Mg XANES, all the obtained spectra from Laura sample (Lr3-1) were similar (Fig. 3-18). Subsequently, they were identified as Mg which was coprecipitated in calcite. Calcite was main mineral component of foramiifera. Therefore, Mg in bulk sample were identified that they were originated from foraminifera.

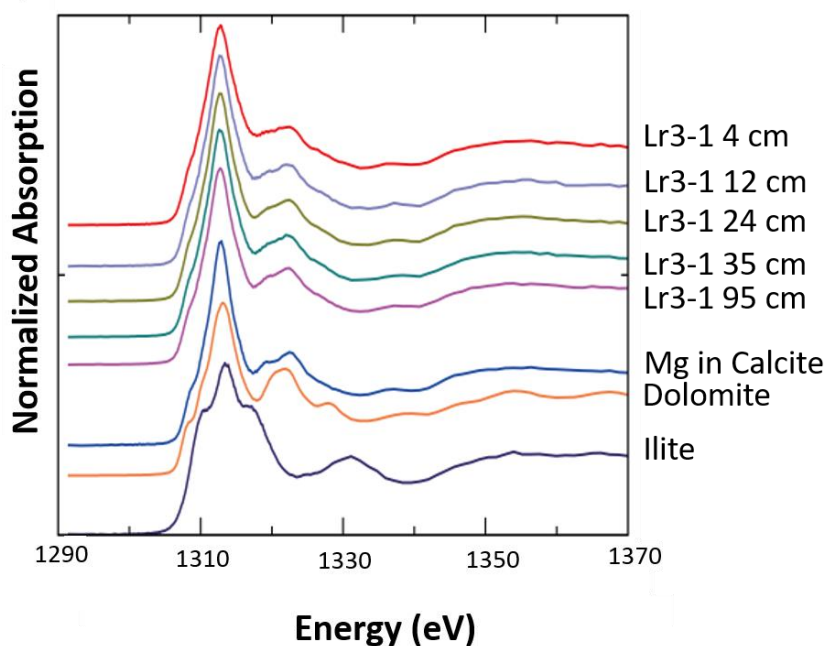


Fig. 3-18. Mg k-edge XANES spectra. The three spectra from the bottom showed reference spectra.

3.4.6. Correlation between soil pH, porosity, and Mg-calcite

The relationship between soil pH and the porosity of *Calcarina* spp was examined. Here, I added the porosity data of *Calcarina* spp. taken in ocean and lagoon side of three islands (Laura, Calalen, and Jelto) to the data in Fig. 3-19 as a function of soil pH. Along with the decrease of soil pH, the porosity of *Calcarina* spp. increased, which also suggests selective dissolution of Mg, or Mg-calcite, contained in the *Calcarina* spp. due to its lower stability to the acidification. However, this trend is not clear at pH below 7.8 (Fig. 3-19),

which is reflected in the decrease of the porosity near the surface of Calalen and Jelto. This result also indicates re-precipitation of calcite.

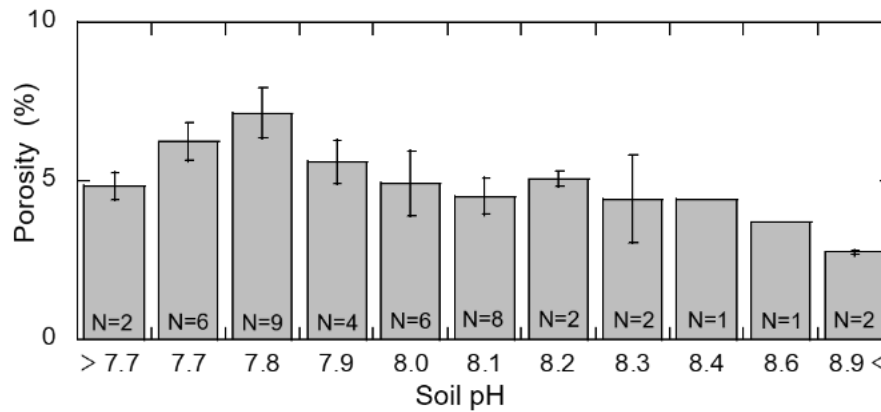


Fig. 3-19. Relationship between soil pH and porosity. For the samples at pH 8.4 and 8.6, error bars were not shown, since I have only one sample in the range.

The correlation coefficient (R) between soil pH and bulk Mg concentration was 0.90 (Fig. 3-20a), showing their high positive correlation. Figs. 3-20b and 3-20c showed the correlation of soil pH and porosity against Mg-calcite fraction to total carbonate minerals. High positive and negative correlations were observed between soil pH and the Mg-calcite fraction ($R = 0.72$) and the porosity and Mg-calcite fraction ($R = -0.62$). These results also revealed that the decrease of Mg-calcite fraction in *Calcarina* spp. is related to the lowering of the soil pH and the increase of the porosity of *Calcarina* spp., which means that the increase of porosity is caused by partial dissolution of *Calcarina* spp. tests. Considering all these results, Mg-calcite contained in *Calcarina* spp., which is relatively more sensitive to acidification (He and Morse, 1993; Andersson et al., 2008), have been dissolved due to the lowering of the soil pH. The data showed that the bio-clastics that contains Mg-calcite have lower durability for relatively lower soil pH value around 7.8

compared with original pH (= 8.2-8.5) of carbonate sediments below 100 cm depth, in which soil pH is relatively constant compared to the depth above 75 cm. The results of this study suggested that porosity of *Calcarina* spp. increases by approximately 6.3%, whereas about 27% of Mg-calcite in *Calcarina* spp. was dissolved with the decrease of soil pH from 8.2-8.5 to 7.7.

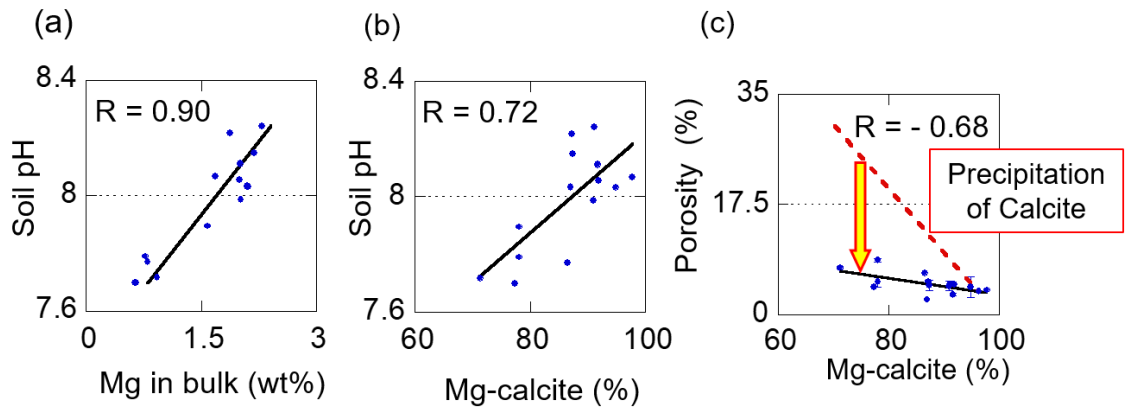


Fig. 3-20. Correlation between soil pH and Mg concentration (a); Correlations of Mg-calcite against (b) soil pH and (c) porosity of *Calcarina* spp. tests.

The correlation between Mg-calcite and porosity was worse compared with that between soil pH and Mg-calcite. This is presumably because re-precipitation of calcite occurred after the selective dissolution of Mg-calcite in the *Calcarina* spp. tests. When Mg-calcite ratio was reduced to 70% relative to total mineralogy (= Mg-calcite + calcite), measured porosity was around 10%, whereas theoretical value calculated from the decrease amount of Mg-calcite was around 30%. This difference between two values suggested the precipitation of calcite within the particle (Fig. 3-20c).

Dissolution rate of Mg-calcite has been studied in various studies (Wollast and Reinhard-Derie, 1977; Walter and Morse, 1985; Morse et al., 2007), suggesting that (i) the dissolution rate of Mg-calcite is faster than that of calcite and (ii) reprecipitation of

calcite during the dissolution of Mg-calcite was observed in the dissolution experiment (Wollast and Reinhard-Derie, 1977). The results of these studies are consistent with my finding. After reactions of Mg-calcite and calcite with acidic materials, there are certain amount of bicarbonate salt (e.g., NaHCO_3) in the soil, which can work as a buffer to control the soil pH.

Several reasons can be considered for the dissolution of Mg-calcite at $\Omega_{\text{calcite}} > 1$ (Ω : saturation index): (i) soil pH drops locally until Ω_{calcite} becomes 1 or less at the vicinity of plant roots (Hinsinger et al., 2003), (ii) stabilization of Mg^{2+} ion in the aqueous phase by the complexation with high concentrations of organic acid (Hinsinger et al., 2003), and (iii) continuous removal of water contained in the sediment by the rapid infiltration of rain water at surface sediments (Hamlin and Anthony, 1987).

Regarding (iii), one of the candidates dissolving the *Calcarina* is rain water. As it was mentioned in introduction, there are about 3000 mm of precipitation in Majuro per year. Thus, rain water at pH = 5.6 equilibrated with atmospheric CO_2 can also contribute to the lowering of the soil pH. The cause of the decreasing soil pH can be, on one hand, anthropogenic factors such as NO_x that are generated when fossil fuels are combusted (Hameed and Dignon, 1988; Dignon, 1992; Okazaki and Ando, 1997; Davis et al., 2001). Meanwhile, natural factors such as nitrification and organic acid should also contribute to the soil acidification. Regarding the organic acid, TOC increased near the surface layer; therefore, organic acid also possibility to have certain contribution to the soil acidification. Root respiration and microbial activities of soil organisms are also related to the acidification and subsequent dissolutions of carbonate. However, considering that sediments are very porous and dry except for the time of sudden shower in the tropics, the contribution of soil respiration should be very small, since most of CO_2 emitted from

the organisms in the soil may be released to the atmosphere. Regarding the factors of soil acidification, it is certain that NO_3^- and organic matter have been involved in the acidification based on their contents in their vertical profiles (Fig. 3-9, 4-12a), but contributions from rainwater also had considerable effect, which may be possible to dissolve 26 g/cm^2 of CaCO_3 as discussed in this Chapter 3. Also, ammonium vaporization should be one of the acidification factors. The contributions of nitrification, organic acid, and ammonium vaporization are discussed in Chapter 4.

3.4.7. Estimation of dissolution amount of calcite by rainwater and nitrate

As the result of bulk-XRD, Mg-calcite percentage of the total was about 70% in the lower layer (L4) (Table 3-2), which should be relatively unaffected by soil acidification. Therefore, I made an assumption that original rate of Mg-calcite was around 75%, though there should be certain variation from the real value. Therefore, “Estimated decreased amount of Mg-calcite” in Table 3-2 was calculated as follows:

$$\begin{aligned} & [\text{Estimated decreased amount of Mg-calcite}] \\ &= [75 \text{ wt\% of Mg-calcite to the total amount}] - [\text{Measured rate of Mg-calcite}] \quad (3) \end{aligned}$$

As a result of calculation, about 21.9 g of calcite should be dissolved in 2000 yr.

Table 3-2. Mg-calcite ratio in bulk sediment and concentration of NO₃⁻.

Sample name	Density (g/cm ³)	Weight (g/cm ²)	Mg-calcite (bulk) (%)	Estimated decreased amount of Mg-calcite (g/cm ²)	NO ₃ ⁻ (μmol/cm ²)	NO ₃ ⁻ (μmol/l)
Laura-1 (L1)	1.25	7.52	11.1	4.80	4.93	821
Laura-2 (L2)	1.20	13.2	14.0	8.05	11.4	1038
Laura-3 (L3)	1.30	18.2	54.7	3.69	2.24	160
Laura-4 (L4)	1.40	85.3	71.4	3.07	5.83	95.6
Laura-5 (L5)	1.27	14.0	59.5	2.17	0.98	89.0
Total				21.79		
Average					5.08	440

Subsequently, dissolution amount of calcite by rainwater was calculated as follows. The equilibrium distribution of solutes in aqueous carbonate solution in the atmosphere are expressed as follows (25°C, $P_{CO_2} = 10^{-3.5}$ atm; Stumm and Morgan, 1996).



Equilibrium constant is

$$K_{CO_2} = \frac{[H_2CO_3]}{P_{CO_2}[H_2O]} = 10^{-1.47} \quad (*[H_2O] = 1) \quad (5)$$

From the law of mass action,

$$[H_2CO_3] = K_{CO_2} P_{CO_2} \quad (6)$$

Here,



The equilibrium constant is

$$K_1 = \frac{[\text{HCO}_3^-][\text{H}^+]}{[\text{H}_2\text{CO}_3]} = 10^{-6.36} \quad (8)$$

About HCO_3^- , following equation is established.



The equilibrium constant is

$$K_2 = \frac{[\text{CO}_3^{2-}][\text{H}^+]}{[\text{HCO}_3^-]} = 10^{-10.33} \quad (10)$$

From the law of mass action,

$$[\text{HCO}_3^-] = \frac{K_1 K_{\text{CO}_2} P_{\text{CO}_2}}{[\text{H}^+]} \quad (11)$$

From (9),

$$[\text{CO}_3^{2-}] = \frac{[\text{HCO}_3^-] K_2}{[\text{H}^+]} \quad (12)$$

From (10) and (11),

$$[\text{CO}_3^{2-}] = \frac{K_1 K_2 K_{\text{CO}_2} P_{\text{CO}_2}}{[\text{H}^+]^2} \quad (13)$$

The solubility product of CaCO_3 (s) and the charge balance are expressed as follows:

$$[\text{Ca}^{2+}][\text{CO}_3^{2-}] = K_{s0} \quad (14)$$

where

$$K_{s0} = 10^{-8.48} \quad (\text{at } 25^\circ\text{C}) \quad (15)$$

From (12) and (13),

$$[\text{Ca}^{2+}] = \frac{K_{s0} [\text{H}^+]^2}{K_1 K_2 K_{\text{CO}_2} P_{\text{CO}_2}} \quad (16)$$

$$2[\text{Ca}^{2+}] + [\text{H}^+] = [\text{HCO}_3^-] + 2[\text{CO}_3^{2-}] + [\text{OH}^-] \quad (17)$$

Here,

$$K_w = [H^+][OH^-] = 10^{-14} \quad (18)$$

$$[OH^-] = \frac{K_w}{[H^+]} \quad (19)$$

Substituting (10), (12), (15), (18) to (16),

$$2 \frac{K_{s0}[H^+]^2}{K_1 K_2 K_{CO_2} P_{CO_2}} + [H^+] = \frac{K_1 K_{CO_2} P_{CO_2}}{[H^+]} + 2 \frac{K_1 K_2 K_{CO_2} P_{CO_2}}{[H^+]^2} + \frac{K_w}{[H^+]} \quad (20)$$

$$10^{13.47}[H^+]^4 + [H^+]^3 - 10^{-11.32}[H^+] - 10^{-14}[H^+] = 10^{-21.35} \quad (21)$$

As a result, following value was obtained.

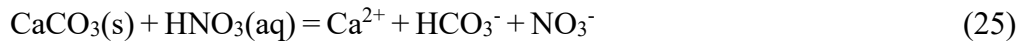
$$[H^+] = 10^{-8.26} \quad (\text{pH} = 8.2) \quad (22)$$

$$\text{As calculated in the same way, } [Ca^{2+}] = 10^{-3.35} \quad (23)$$

As annual mean precipitation in Majuro is about 3000 mm/yr. Therefore 600 L/cm² of rainwater is supplied per 2000 yr. Thus, the total amount of dissolved CaCO₃ in 2000 yr is

$$10^{-3.35} \times 600 \times 100 = 26.8 \text{ (g/cm}^2\text{)} \quad (24)$$

Third, amount of dissolved calcite by NO₃⁻ was calculated. The equation for dissolution of calcite by NO₃⁻ is expressed as follows:



From the equation above, one mole of CaCO₃(s) can be dissolved by one mole of HNO₃.

From L1 to L5, total NO₃⁻ concentration per unit area was 25.4 μmol/cm², which dissolves 25.4 μmol/cm² × 100 (molecular weight of CaCO₃) = 2.54 mg/cm². If I assume that (i)

nitrate ions is complete washed out from the sediment by one rain event and (ii) such rain event occurs about 50 times in a year, the dissolution of the calcite for 1000 years can be roughly 127 g/cm^2 .

Considering that the size of sediment particle was rather large ($\geq 1 \text{ mm}$), rainwater would have not stayed in underground for long time sufficient for the complete reaction between $\text{CaCO}_3(\text{s})$ and rainwater. Therefore, the actual dissolved amount of $\text{CaCO}_3(\text{s})$ should be much smaller than the calculations above. It is possible that dissolution rate of $\text{CaCO}_3(\text{s})$ by HNO_3 may be also overestimated. However, if HNO_3 was produced continuously by nitrification, the contribution rate of HNO_3 must be higher than rainwater.

3.5. Conclusions

The present results showed the acidification of surface environment of Majuro Atoll based on multiple approaches such as soil pH measurement, chemical and mineralogical composition analyses, and porosity of foraminifera test measured by X-ray μ -CT.

As the soil pH decreased, Mg concentration of the sediments decreased, and Mg-calcite fraction to total mineral which was contained in foraminifera also decreased. However, the porosity did not increase as much as the value estimated from the decrease of the Mg-calcite ratio in the foraminifera. This fact suggested that Mg-calcite contained in the foraminifera was selectively dissolved and calcite was reprecipitated. As factors of soil acidification which cause this dissolution of Mg-calcite in foraminifera, organic acid, nitrification, rainwater, and ammonia vaporization are considered.

This is also the first study to apply this non-destructive method to determine the micron scale porosity of microscopic marine organisms in natural environment based on a large number of slices ($n = 815-2047$) compared with conventional method using thin section (Tetard et al., 2017). This technique can also be applied to the estimation of dissolution rate of marine calcareous organisms related to ocean acidification.

Chapter 4.

Relationship of sediment acidification and nitrification on Majuro Atoll, Marshall Islands

第4章

本章については、5年以内に雑誌等で刊行予定のため、非公開。

Chapter 5.

Origin and migration of trace elements in the surface sediments of Majuro Atoll, Marshall Islands

5. Origin and migration of trace elements in the surface sediments of Majuro Atoll, Marshall Islands

5.1. Introduction

Majuro Atoll in Marshall Islands (Fig. 5-1) has one of the longest human histories among atolls in the world. Still, only approximately 2000 years have passed since islanders first settled on this atoll (Yamaguchi et al., 2005; Yamaguchi et al., 2009).

Some studies have investigated the environmental chemistry of atolls. Arimoto et al. (1985) investigated concentrations of trace elements in dry and wet deposits in Enewetak Atoll in Marshall Islands (Fig. 5-1). This study, however, did not investigate the postdeposition processes of these elements. Osawa et al. (2010) and Fujita et al. (2014) examined the anthropogenic impacts on atolls, but these studies were limited to the water area. Furthermore, few studies have actually investigated the influences of trace elements in sediments on several aspects of human life, such as agriculture and diet. Deenik and Yost (2006) examined the chemical properties of Marshall Islands, but the samples were not systematically collected from various depths. Thus, the initial deposition process of the trace elements and their subsequent migration in the vertical profile after the early stage of island formation to the present were still not well known.

Thus, this study aimed to quantify the total amount of supplied elements, subsequent postdeposition migration, and chemical interactions in the sediments. Especially, Zn has adverse impacts on some aquatic species, such as zooplankton and algae. The diversities and population of zooplankton and algae decrease upon exposure to high concentrations of Zn in water even below 0.05-0.1 mg/L (e.g., Greene et al., 1975; Carlson and Roush, 1985; Clements and Kiffney, 1995). Relative to mammalian

consumers, it is reported that Cu is exceedingly toxic to aquatic biota (e.g., Flemming and Trevors, 1989). Sublethal effects have been documented for many species of invertebrates exposed to 5 to 100 $\mu\text{g/L}$ Cu (Hodson et al., 1979). Therefore, migration of heavy metals such as Zn and Cu from the surface to deeper sediments is crucial for their exposure to aquatic organisms and even to the residents, since groundwater is the only natural source of freshwater when rain catchment storage is exhausted in Majuro Atoll (Presley, 2005; Koda et al., 2013; Bailey and Jenson, 2014). Thus, I primarily focused on Zn, which can be regarded as an anthropogenic element given its presence in numerous industrial products (Nakanishi et al., 2008).

Other elements, such as aluminum (Al), rare earth elements (REE), phosphorus (P), copper (Cu), and selenium (Se), were also studied. The enrichment factor (EF_M) of an element M (Kemp et al., 1976) was utilized to distinguish elemental sources on the assumption that terrigenous Al is supplied through airborne transport (Arimoto et al., 1985), which is related to the impact of natural and anthropogenic sources and the migration of elements within the sediment column.

The reason why I chose Majuro Atoll as a study field is that the atoll has been subject to lesser anthropogenic influence compared to developed countries that have considerably longer human history and larger populations. On the other hand, many atolls have been urbanized within 100 years. Thus, it should be easier to examine anthropogenic influences. Furthermore, the original sediments of atolls consist of bioclastic materials composed of calcium carbonate (CaCO_3) (e.g., Perry et al., 2011; Yasukochi et al., 2014). This characteristic also makes it possible to identify anthropogenic sources from the sediments. Thus, atoll is a suitable site for environmental chemistry. Furthermore, the outcome obtained from this study field on the atoll can be widely applicable to other

developing countries as an example of anthropogenic impacts at the early stage of urbanization.

5.2. Site description and samples

Majuro Atoll, an atoll in Marshall Islands, is located at latitude 7°05' N, longitude 171°23' E in the central Pacific (Fig. 5-1). The atoll has an average annual temperature of approximately 27°C and receives an annual precipitation of approximately 3500 mm/year (Fujita et al., 2009).

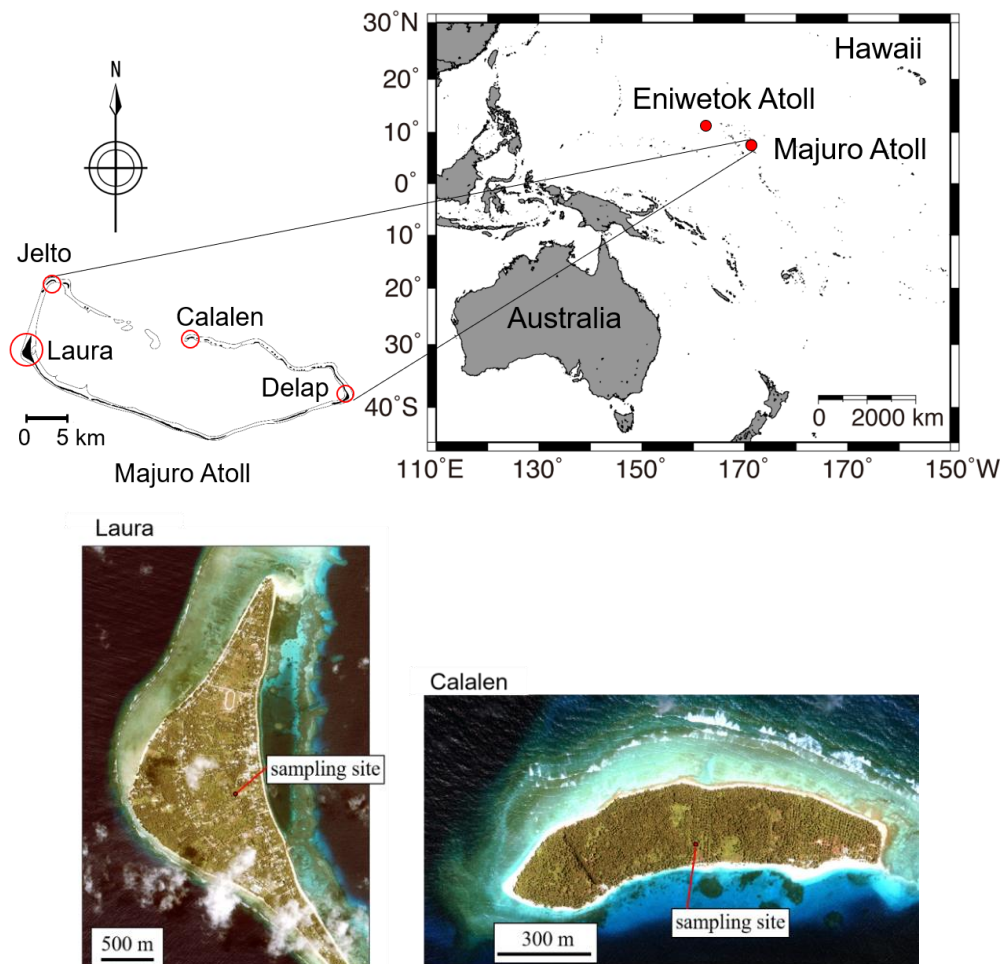


Fig. 5-1. Location of Majuro Atoll. Majuro is the capital city of Marshall Islands, which consists of 29 atolls and 5 islets. Majuro Atoll is located between Hawaii and Australia near the equator. Map and pictures of Delap, Jelto, Kebjeltak were shown in Chapter 2.

In this chapter, samples collected from five islands (Laura, Calalen, Jelto, Delap, and Kebjeltak) were used. Especially, two sampling sites in Laura (Lr3-1) (7.14661° N, 171.03606° E, 203.0 cm above sea level) and Calalen (KOL) (7.15836° N, 171.2109° E, 255.8 cm above sea level) were focused in this chapter (Fig. 5-1).

The strata of the sediment layers were divided on the basis of the Munsell color system and sediment grain size (Fig. 5-6a ; Table 5-1).

Table 5-1. Sample information.

Sample name	Sampling depth (cm)	Munsell color	Grain size
Laura-1 (L1)	4	10YR 3/1	fine~medium
Laura-2 (L2)	12	10YR 1.5/1	fine~medium
Laura-3 (L3)	24	10YR 6/1	coarse~medium
Laura-4 (L4)	35	10YR 9/2	coarse~medium
Laura-5 (L5)	95	10YR 9/1.5	coarse~medium
Calalen-0 (C0)	—	10YR 3/1	fine~medium
Calalen-1 (C1)	25	10YR 2/1	fine~medium
Calalen-2 (C2)	45	10YR 3/1	coarse~medium
Calalen-3 (C3)	68	10YR 6/2	coarse~medium
Calalen-4 (C4)	98.5	10YR 7/3	coarse~medium
Calalen-5 (C5)	140.5	10YR 7/3	coarse~medium

In Majuro, automobiles have been used in daily life in recent years. By contrast, Calalen, which is located northeast of Laura, is an isolated island with a considerably smaller population than Laura (Spennemann, 1992). In Majuro Atoll, census data for each island have not been taken continuously, but in 1988, for example, 1575 and 19 people lived on the Laura and Calalen, respectively (OPS, 1989).

Laura and Calalen are well vegetated at present. The surface layers of the sediments are in black color, and this black-colored layer is thicker in Calalen than in Laura (Fig. 5-6a). On both islands, foraminifera tests in the upper sedimentary layer are covered with black material. The color of C0, the top layer of Calalen section was blackish brown. Small gravels (ϕ : 1-3 cm) were contained in it. The sediment was loose, and viscosity was medium. Many palm roots were observed. Surface sediment in Laura also had a black-colored layer. However, their thickness was thinner than that in Calalen. The grain size of the L1 and L2 layers in Laura and C1 layer in Calalen is classified as fine to medium sand (125–500 μ m). *Calcarina* spp., a large -benthic foraminifera that inhabits algal turf on shallow reef flats, is the dominant species of foraminifera in these islands (Yamano et al., 2000). Deep sedimentary layers exhibit unconsolidated bio-clastic sand that consists of foraminifera, coral, and calcareous algae. Medium to coarse sands (0.5–2.0 mm) dominate the L3–L5 and C2–C5 layers in Laura and Calalen, respectively. Large coral gravel is present in deep sedimentary layers (L5). The color of the sediment lightens and becomes whitish yellow with increasing depth. Fresh foraminifera tests were also collected on the ocean reef flats of north part of Laura, Majuro Atoll for comparison. Furthermore, groundwater samples were collected from wells located near the sampling areas of Laura and Calalen.

5.3. Methods

5.3.1. Inductively coupled plasma mass spectrometry (ICPMS) for trace elements

The Al, Mg, P, Ca (calcium), titanium (Ti), manganese (Mn), iron (Fe), Cu, Zn, Se, REE, and Pb concentrations of the collected sediments and groundwater were quantified. Aluminum, Ti, Mn, Cu, Zn, Cu, Se, REE, As and Pb concentrations were measured using an inductively coupled plasma mass spectrometer (ICPMS; Agilent 7700cs, Agilent Technology, Japan) (Fig. 5-2c). Prior to measurement, samples were decomposed with HNO₃ (68%) at 180°C for 2 days. The absence of residual materials from the decomposed samples was confirmed, and the samples were then dried at 130°C (Fig. 5-2b). Subsequently, 2% HNO₃ was added to redissolve the sample. Selenium (⁷⁸Se) was measured through ICPMS using a reaction cell to decrease the background level of molecular ions (e.g., ³⁸Ar⁴⁰Ca). REE concentrations were measured by ICPMS after ion-exchange separation using AG 50W-X8 resin (200–400 mesh) to eliminate cations, including Ba and Ca (Takahashi et al., 2002) (Fig. 5-2a). Moreover, we also corrected interferences of ¹³⁵Ba¹⁶O, ¹⁴⁰Ce¹⁶O¹H, and ¹⁴¹Pr¹⁶O on ¹⁵¹Eu and ¹⁵⁷Gd following Takahashi et al. (2002).



Fig. 5-2. (a) Column processing for extracting REEs. (b) Evaporation to dryness of HNO₃ or HCl covering a PTFE sheet. (c) ICPMS (Agilent 7700cs).

5.3.2. Extracting experiments

The soil water cannot be readily collected, because the sediments at the surface are always unsaturated even after squall. Instead of soil water, I mixed sediment sample and water (0.0010 M CaCl_2) at the weight ratio of 1:5, 1:2, or 1:1. Concentration of each element leached into the water was measured by ICPMS following the method as mentioned above.

Certain Zn species such as Zn in CaCO_3 were selectively extracted with acetic acid (5 M; TAMAPURE-AA-100, Tama Chemicals Co., Ltd, Tokyo, Japan) at the ratio of 20 mL:0.1 g (acetic acid : sediment sample). After the inorganic components, such as CaCO_3 , of the sample were dissolved by the acetic acid, the solid and liquid phases were separated by filtration using a membrane filter (pore size: 0.20 μm ; hydrophilic PTFE (25HP202AN), Advantec, Japan). The filtered water was dried at 130°C and redissolved in 2% HNO_3 for ICPMS measurement. Solid phase was carried out the XANES measurement to identify its chemical species (Fig. 5-3).

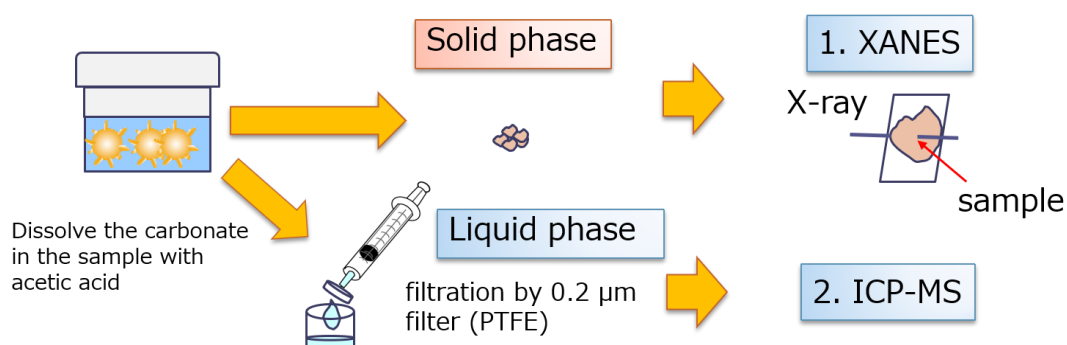


Fig. 5-3. Procedure of extracting experiment of acetic acid.

For ICPMS measurements, I measured the samples and geochemical reference samples (JB-2 for REE; JLs-1 or JCp-1 for other trace elements) under the same condition to confirm the uncertainty of the analytical value. The values of the reference samples

agreed with the recommended values within 2.81%, 1.73%, 5.25%, 22.1%, 4.55%, 16.4%, and 16.1% error for Al, Fe, Mn, Ti, Zn, Cu, and REE, respectively, except for Se and Pb for which recommended values were not given. The precision of the analysis was determined by repeated analysis (N=3) of the same sediment sample, which were typically less than 9%, except for deeper sediments with very low concentrations of the trace elements.

5.3.3. X-ray Fluorescence (XRF) for major elements

Magnesium, Ca, P, Fe, Si, Mn, Ti, Na, and K concentrations were measured through X-ray fluorescence analysis (XRF; PW4400/40: PANalytical Co., Ltd. Japan). A powdered sample was heated in a stepwise fashion from 100°C to 1000°C over five stages of heating. The sample and flux (lithium tetraborate) were mixed at the weight ratio of 1:10 and then used to prepare beads using a bead sampler (TK-4100: Tokyo Kagaku Co., Ltd. Japan). The intensity of the fluorescent X-rays irradiated by incident X-ray (Rh tube) was measured for quantitative analysis. Details were described in method of Chapter 3.

For XRF analysis, calibration line was acquired by measuring 15 standard rocks (Imai et al., 1996). The precision of the analysis was determined by repeated analysis (N=5) of the same sediment sample but independently prepared, which were 0.73%, 3.36%, 3.60%, and 0.06% for Ca, Mg, P, and Fe concentrations, respectively.

5.3.4 X-ray absorption near-edge structure (XANES)

Zinc, Cu, Fe, As, S, and Al species in the sediments were estimated through two X-ray absorption near-edge structure (XANES) methods: bulk XANES analysis using mm-size X-ray and μ -XRF-XANES analysis. Samples for the former analysis were

homogenized using an agate mortar prior to measurement through bulk analysis. Then, Zinc and As K-edge XANES were obtained using $1.0 \times 0.5 \text{ mm}^2$ beam at beamline 12C at Photon Factory (PF; Tsukuba, Japan). Al and S K-edge XANES were obtained at beamline 27SU at Spring-8. Al K-edge XANES was also obtained at beamline 10 in SR center of Ritsumeikan University. The samples were excited by monochromatized X-rays with a Si(111) double crystal monochromator. The details of the measurement are similar to those described by Takahashi et al. (2007).

Sediment particles were embedded in a high-purity resin (EpoFix Resin, Struers ApS, Denmark) and polished for the preparation of thin sections (Takahashi et al., 2007) for μ -XRF-XANES analysis. Zinc, Cu, and Fe K-edge XANES spectra at a local area in the sample were measured with $5 \times 5 \text{ }\mu\text{m}^2$ beam at beamline 4A in PF (Fig. 5-4). Details of the analysis at the beamline were described in Takahashi et al. (2011). Phosphorus K-edge XANES and S K edge XANES was also measured with $20 \times 20 \text{ }\mu\text{m}^2$ beam at beamline BL27SU in SPring-8, Japan. Details of the analysis at BL27SU were described in Ohashi et al. (2001).

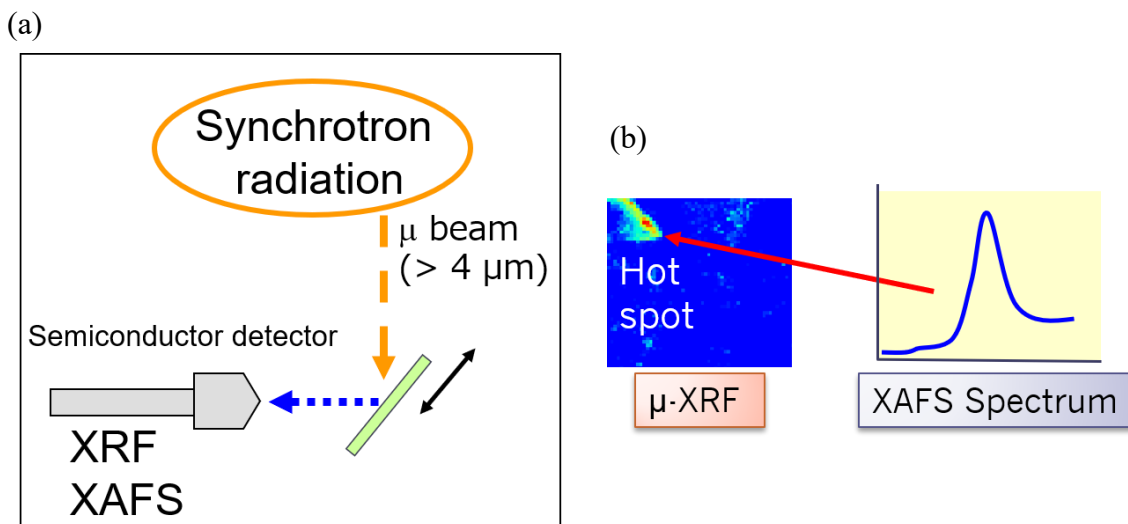


Fig. 5-4. (a) Structure of μ -XRF-XAFS. (b) Example of μ -XRF-XAFS. Searching the concentrated spot of target elements by μ -XRF mapping and obtain its coordinate. Subsequently, X-ray beam is radiated the spot and obtained XAFS spectra.

REX2000 software (Rigaku Co., Ltd., Japan) was used for the least-squares fitting of the XANES spectra with the linear combination of various reference materials. Zinc coprecipitated with apatite was synthesized by dropping 0.10 M K_2HPO_4 (Wako Pure Chem. Ind., Ltd, Osaka, Japan) in 0.10 M CaCl_2 (Wako) solutions in the presence of Zn^{2+} (0.1 mM) at pH 8.5–9.0 adjusted with a KOH solution. The resulting suspension was aged at 120°C for 7.5 h with stirring (Wakamura et al., 1997; Liu et al., 2003). Zinc adsorbed on apatite was synthesized by the adsorption of Zn^{2+} on hydroxyapatite (Wako). Zinc coprecipitated with calcite was synthesized by mixing 0.10 M CaCl_2 (Wako) and 0.10 M NaHCO_3 (Wako) solutions (e.g., Dittrich et al., 2003; Sugiura et al., 2014) in the presence of Zn^{2+} (0.1 mM) at pH 7.5–7.8.

5.3.5. Radiocarbon (^{14}C) dating for sediments

Radiocarbon (^{14}C) dating was conducted through CHRONOSHPERE compact accelerator mass spectrometry (AMS) at the University Museum, the University of Tokyo, on the basis of Bayesian age-depth models (OxCal ver. 4.3; Ramsey, 2013). *Calcarina* was dissolved in phosphoric acid for analysis. Carbon dioxide released upon dissolution was purified, graphitized, and then measured through AMS. Measured foraminifera was etched by 1M HCl and outermost test was removed to prevent the contamination. Etched foraminifera were picked up by tweezers sonicated with acetone after the observation of stereoscopic microscope in order to confirm whether impurities were removed completely. The detail procedure of purifying CO_2 was described in Chapter 4.3.5. However, one procedure was different. For extracting CO_2 from foraminifera, they were dissolved by phosphoric acid and heated at 60°C for 1 h in the sealed vacuumed bifurcated glass pipe, instead of burning with CuO as in the case of treatment of humic substances. IntCal 13

and Marine 13 (Reimer et al., 2013) were used for calibration. As for the local reservoir effect (ΔR), I applied $\Delta R = -35 \pm 25$ years (Kayanne et al., 2011) for the correction.

5.4. Results and Discussion

5.4.1. Depth profile of elements

^{14}C dates of foraminifera in the sediments of Laura ranged from 1670 cal BP to 2100 cal BP, which are similar to ^{14}C dates reported in Kayanne et al. (2011), whereas those in Calalen were from 542 cal BP to 730 cal BP (Fig. 5-5, Table 5-2).

Table 5-2. ^{14}C dating results of foraminifera in sediments.

Sample name	Delta ^{13}C (‰)	Conventional ^{14}C age (BP $\pm 1\sigma$)	Years cal BP (cal BP $\pm 1\sigma$)	Years cal BP (cal BP $\pm 2\sigma$)
Laura-1 (L1)	-4.2 \pm 0.6	2350 \pm 20	2036 - 1927	2100 - 1874
Laura-2 (L2)	-3.0 \pm 0.4	2242 \pm 19	1927 - 1839	1977 - 1801
Laura-3 (L3)	-4.4 \pm 0.4	2124 \pm 20	1813 - 1720	1862 - 1676
Laura-4 (L4)	-3.7 \pm 0.4	2123 \pm 27	1816 - 1718	1868 - 1668
Laura-5 (L5)	-4.4 \pm 0.5	2203 \pm 20	1889 - 1801	1933 - 1741
Calalen-1 (C1)	-9.7 \pm 0.5	1002 \pm 19	646 - 565	662 - 542
Calalen-2 (C2)	-5.6 \pm 0.5	1046 \pm 28	680 - 615	710 - 555
Calalen-3 (C3)	-3.6 \pm 0.4	1048 \pm 18	674 - 623	701 - 565
Calalen-4 (C4)	-3.8 \pm 0.5	1071 \pm 19	690 - 635	730 - 610
Calalen-5 (C5)	-4.7 \pm 0.5	1031 \pm 19	669 - 608	684 - 553

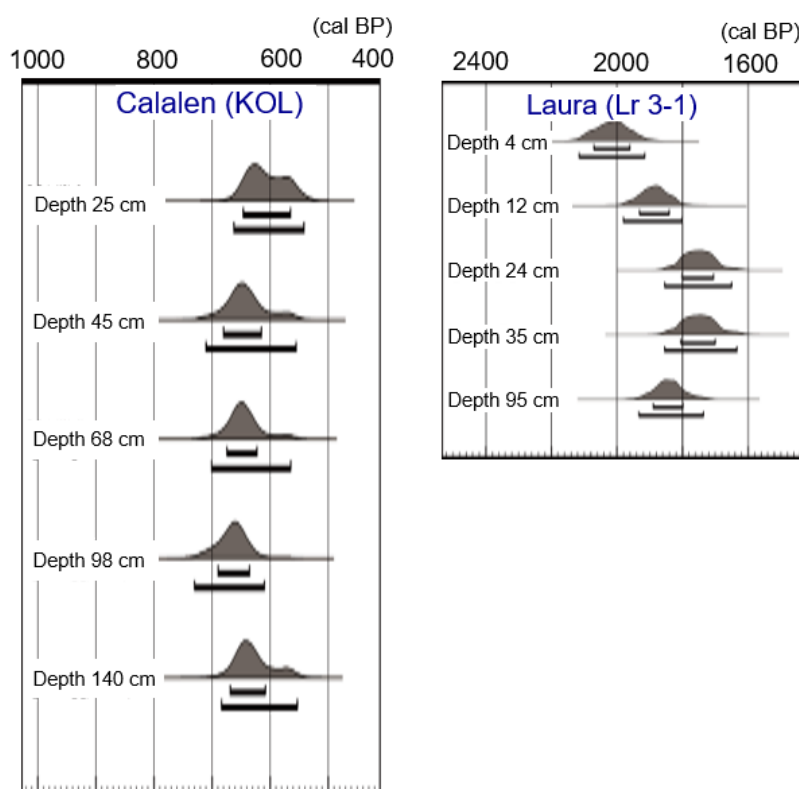
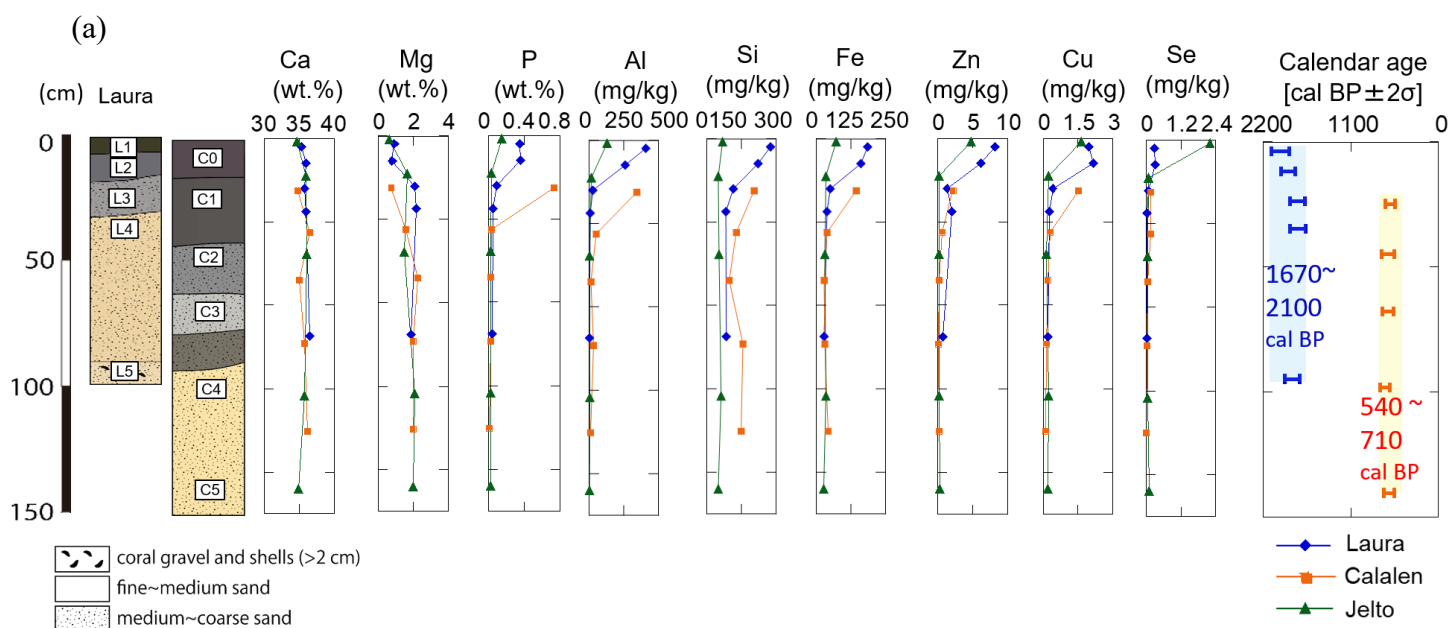


Fig. 5-5. Bayesian age depth model of ^{14}C from foraminifera (*Calcarina*). Each black shape showed the calibrated-age distribution of sediment age.

These results indicated that the sedimentation process was completed long before the emissions of elements from anthropogenic sources, which must have been provided by urbanization.

The depth profiles of various elements (major elements: Ca and Mg; trace elements: Al, Si, P, Fe, Cu, Zn, and Se) indicated that Ca concentration remained almost constant (Fig. 5-6). Magnesium content decreased near the surface layer, the details of which will be described elsewhere. On the other hand, the concentrations of Al, P, Fe, Cu, and Zn increased toward the surface in both islands. The concentration of Si, Na, and K were relatively constant except for that of Delap. In both islands, surface sediment (4–24 cm; Fig. 5-6, Table 5-3) had a high P concentration (Laura: 0.3–0.4 wt.%, Calalen: 0.7 wt.%, Jelto: 0.6 wt.%).



(b)

本図については、5年以内に雑誌等で刊行予定のため、非公開。

Fig. 5-6. (a) Stratigraphic column of sediment and depth profiles of various elements in the sediment column. The right graph shows the calendar age, which was estimated on the basis of the age-depth model, of foraminifera in the sediments. (b) Depth profile of major elements in Delap, Laura, Calalen, Jelto, and Kebjeltak (Arno). In surface data, lagoon side of each islands are also shown.

5.4.2. Classification of elements on the basis of EF

Al inventory was calculated by integrating total amount of Al in each sedimentary layer as shown in Fig. 5-6a. Density was measured in each layer by pycnometer. The average Al concentration and density were 410 mg/kg and 1.25 g/cm³ for the sediment from 0 to 6 cm depth in Laura, respectively. Thus, the calculation of the Al inventory was $410 \text{ (mg/kg)} \times 6 \text{ (cm)} \times 1.25 \text{ (g/cm}^3\text{)} = 7.67 \text{ mg/cm}^2 \text{ (for 2 kyr)}$.

According to Higgins et al. (1999), Al inventory in the central Pacific near Majuro Atoll (0-3.8°N, 159-163°E) was 2.68-16.5 mg/cm²/kyr. This result corresponds well to the value obtained in this study. Through back trajectory analysis, Duce et al. (1980) and Merrill et al. (1989) suggested that Al is transported as aeolian dust from Asia. Based on these data, I assume that most of Al originated from aeolian dust deposited on Majuro Atoll.

The results for Al allowed us to calculate EF_M of the elements in the surface layer (L1 and C1). Using the equation below, I normalized the concentration of each element (= M) to that of Al to obtain EF_M to estimate origin of the element (Kemp et al., 1976).

$$EF_M = (M/Al)_{\text{sample}} / (M/Al)_{\text{crust}}. \quad (45)$$

The (M/Al)_{sample} and (M/Al)_{crust} are the concentration ratios of M and Al in the sample and crust, respectively. The latter in upper continental crust was calculated in reference to Taylor and McLennan (1985).

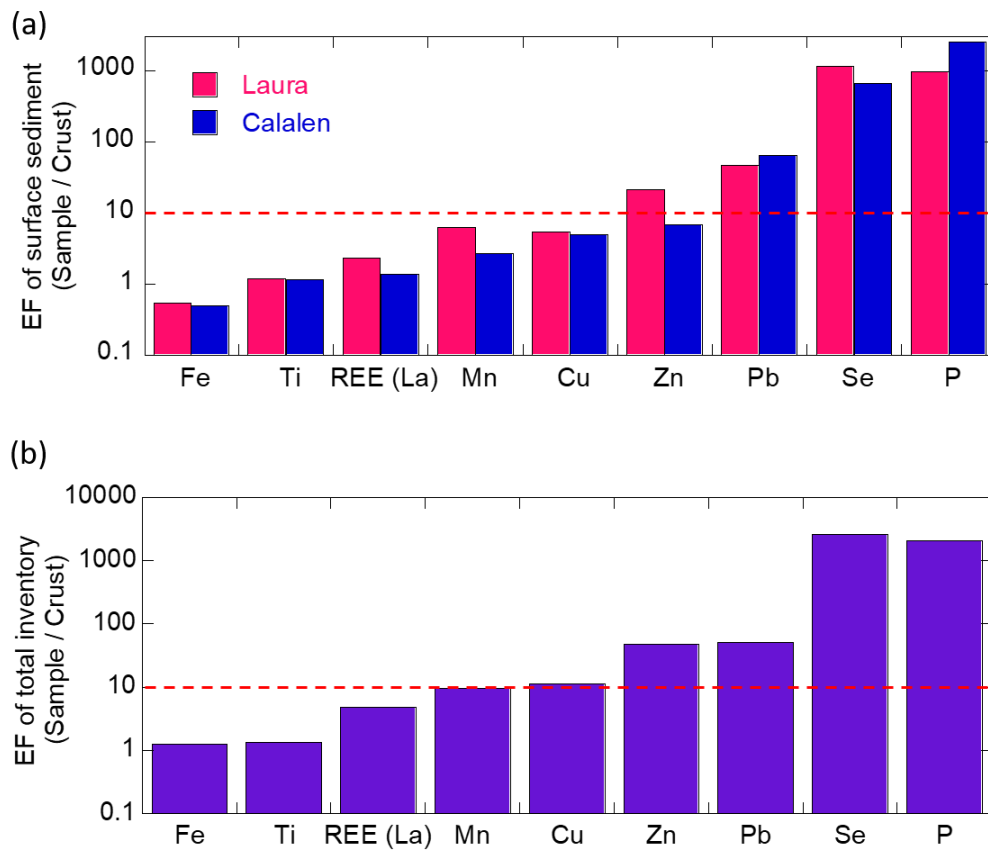


Fig. 5-7. (a) Enrichment factor (EF_M) of various elements (M) of Laura (pink rods) and Calalen (blue rods) in the surface layers. (b) Enrichment factor (EF_M) of total inventory (2 kyr).

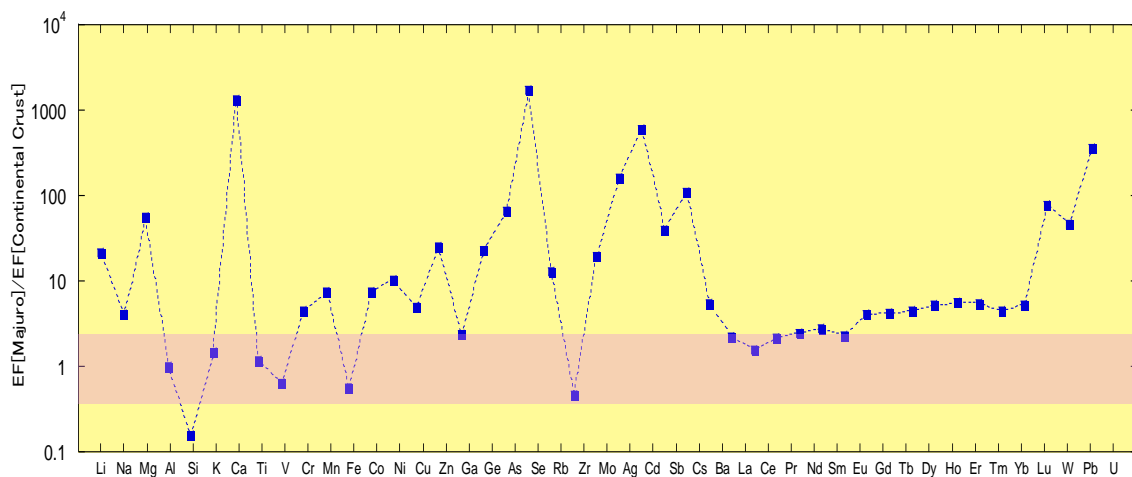


Fig. 5-8. Enrichment factor (EF_M) of all the elements in Laura. Pink shadow area showed the value around 1, which suggested that its origin was continental crust.

The EF values of P, Mn, Cu, Zn, Se, and Pb were over 10 or nearly 10 (Fig. 5-7a, Table 5-4), suggesting that their origins are non-crustal and likely anthropogenic (e.g., Kurisu et al., 2016). On the other hand, the EF values of Ti, Fe, and REE (La) were almost equal to 1, suggesting that they are of crustal origin. However, iron in Delap has a possibility that its origin is different from the other areas, such as Laura, because it has high concentration as much as 0.8% near the surface. This result suggested that the origin of Fe in Delap may be anthropogenic. I also showed the EF of total inventory of each element (Fig.5-7b, Table 5-4), which shows the almost same tendency of EF in surface sediment. EF of other elements were shown in Fig. 5-8.

According to the ^{14}C dating results, the deposition period of the Laura is about twice as long as that of Calaren. In spite of this fact, Al inventory of Calalen (= 16.2 mg/cm², given that C0 has the same Al concentration as C1) may be higher than that of Laura. This fact suggested that surface layer of Laura, which may correspond to L0, has been washed away at this point. In this case, total inventory of Al in Laura may be underestimated. However, the fact that the EF of the surface is similar to that based on the total inventory suggests that EF is not strongly affected by the possible wash out of the sediments due to similar depth profiles of Al and other elements. Thus, in the following sections, I provide discussion on the origin of each element on the basis of EF. (i) I discussed REE, which has an EF of approximately 1, as representative of trace elements supplied as aeolian dust from the continental crust, which was also discussed by the variation in REE pattern. (ii) I discussed the role of P, which has the highest EF (977 and 2480 in L1 and C1, respectively) (Fig. 5-7a, Table 5-4), as an element that fixes Zn

in the form of phosphate, which was confirmed by the P speciation analysis through XAFS and scanning electron microscopy (SEM) observation. (iii) I discussed Zn, which has an EF as high as 21.1 (Laura), as a representative anthropogenic element, which will be confirmed by speciation analysis using SEM, bulk XANES, and μ -XRF-XAFS analyses.

Table 5-3. Concentration of elements contained in the sediment and groundwater in Laura and Calalen.

Sample name	Sampling Depth (cm)	Ca (%)	Mg (%)	P (%)	Si (mg/kg)	Al (mg/kg)	Fe (mg/kg)	Mn (mg/kg)	Ti (mg/kg)	Zn (mg/kg)	Cu (mg/kg)	Pb (mg/kg)	Se (mg/kg)
fresh foraminifera	0	—	—	—	—	3.24	2.53	1.76	1.07	0.325	0.0862	0.0568	0.0369
Laura-1 (L1)	4	35.4	0.930	0.348	277	410	185	42.3	31.4	8.23	1.99	1.84	0.285
Laura-2 (L2)	12	36.0	0.805	0.362	222	262	162	33.4	15.8	6.18	2.18	1.07	0.319
Laura-3 (L3)	24	35.8	2.10	0.091	115	27.0	50.9	5.99	3.09	1.39	0.419	0.176	0.0881
Laura-4 (L4)	35	36.0	2.19	0.048	82.3	7.14	39.3	4.00	1.62	2.07	0.279	0.0738	0.0390
Laura-5 (L5)	95	36.6	1.88	0.040	85.1	2.45	27.6	2.65	1.22	0.773	0.198	0.0511	0.0251
groundwater (Laura)	300	—	—	—	—	2.71×10^{-3}	3.42×10^{-4}	5.83×10^{-6}	2.55×10^{-4}	4.99×10^{-5}	6.12×10^{-4}	N.D.	3.71×10^{-4}
Calalen-1 (C1)	25	34.9	0.767	0.742	204	345	145	15.6	25.2	2.23	1.53	2.14	0.162
Calalen-2 (C2)	45	36.5	1.58	0.034	128	49.6	39.0	3.19	2.58	0.639	0.304	0.0687	0.153
Calalen-3 (C3)	68	35.1	2.29	0.018	97.3	13.1	27.4	3.04	1.01	0.207	0.193	0.0394	0.0617
Calalen-4 (C4)	98.5	35.8	2.01	0.015	156	32.0	31.4	3.65	1.74	0.162	0.147	0.0433	0.0439
Calalen-5 (C5)	140.5	36.2	2.00	0.014	149	10.8	43.2	4.46	0.790	0.219	0.108	0.0397	0.0218
groundwater (Calalen)	230	—	—	—	—	1.02×10^{-3}	7.59×10^{-4}	9.40×10^{-7}	9.21×10^{-4}	1.54×10^{-4}	8.70×10^{-4}	8.58×10^{-6}	4.36×10^{-5}

N.D.: below detection limit.

Table 5-4. Enrichment factor and inventory of elements contained in the sediments and estimated ratio of local emission of each element.

Element	Surface EF of Laura	Surface EF of Calalen	Total inventory (Laura) (mg/cm ²)	Total inventory (Calalen) (mg/cm ²)	EF of total inventory of Majuro (2kyr)	EF of Enewetak Bulk Aerosol* ¹	Estimated ratio of local/total (%) ^{*2}
Al	1.00	1.00	7.67	16.2	1.00	1.0	—
P	977	2480	137	305	2060	—	—
Ti	1.19	1.14	0.656	1.14	1.33	—	—
Mn	6.20	2.72	1.25	2.17	9.75	0.96	85
Fe	0.538	0.498	8.19	10.6	1.27	0.86	N
Cu	5.45	4.96	0.0780	0.0808	11.4	3.2	41
Zn	21.1	6.77	0.357	0.122	48.9	14	34
Se	1170	666	0.0116	0.0141	2550	23000	N
Pb	47.2	65.1	0.0382	0.0868	52.3	40	15

*¹ Data from Duce et al. (1983).

*² Estimated ratio of each element supplied locally to total amount was calculated as follows:

$$\text{Ratio of local/total (\%)} = [(EF_{\text{Laura (surface)}} - EF_{\text{Enewetak}}) / EF_{\text{Laura}}] \times 100. \quad (46)$$

The ratio with a negative value was shown as N.

5.4.3. Crustal origin: Al

本章については、5年以内に雑誌等で刊行予定のため、非公開。

5.4.4. Crustal origin: REE

The REE patterns of Laura obtained through normalization to the REE pattern of shale (Post-Archean Australian average shale (PAAS); Taylor and McLennan, 1985) are shown in Fig. 5-10a. The shape of the REE pattern in the lower layer with a large negative Ce anomaly is similar to that of the surface seawater of the south Pacific (00°00.54'S, 149°57.34'E; Zhang and Nozaki, 1996), as shown in Fig. 5-10a. Akagi et al (2004) also showed that the shape of the REE pattern of a coral reef is similar to that of the surrounding seawater, though the absolute value is different (Akagi et al., 2004). This result strongly suggested that REE in the lower sediment was directly incorporated from that in seawater during growth of coral and foraminifera in seawater.

REE contents increased from the lower to upper sedimentary layers and the EF_{REE} of surface sediment was approximately 1. In addition, the degree of negative Ce anomaly decreased at depths shallower than 12 cm (Fig. 5-10a, Fig. 5-11). Furthermore, the light REE slightly increased at the upper sedimentary layer (Fig. 5-10b). These results suggested that terrigenous materials, which generally exhibits no Ce anomaly and relatively higher LREE/HREE ratio, were added to the surface sediments after the rapid sedimentation of $CaCO_3$ was almost over. All these results suggested that REE was of crustal origin which was transported as aeolian dust with Al and was added to surface sediments after the rapid deposition of the sediments to form the island. REE patterns of sediments at various depths normalized to that of chondrites were shown in Fig. 5-11. REE patterns of Calalen (Fig. 5-11b) was similar that of Laura (Fig. 5-11a). The REE pattern of sediment which was added to the surface sediment was estimated from the concentration of Ce as shown in Fig. 5-12. As a result of calculation, the pattern was that of continental crust (Fig. 5-12).

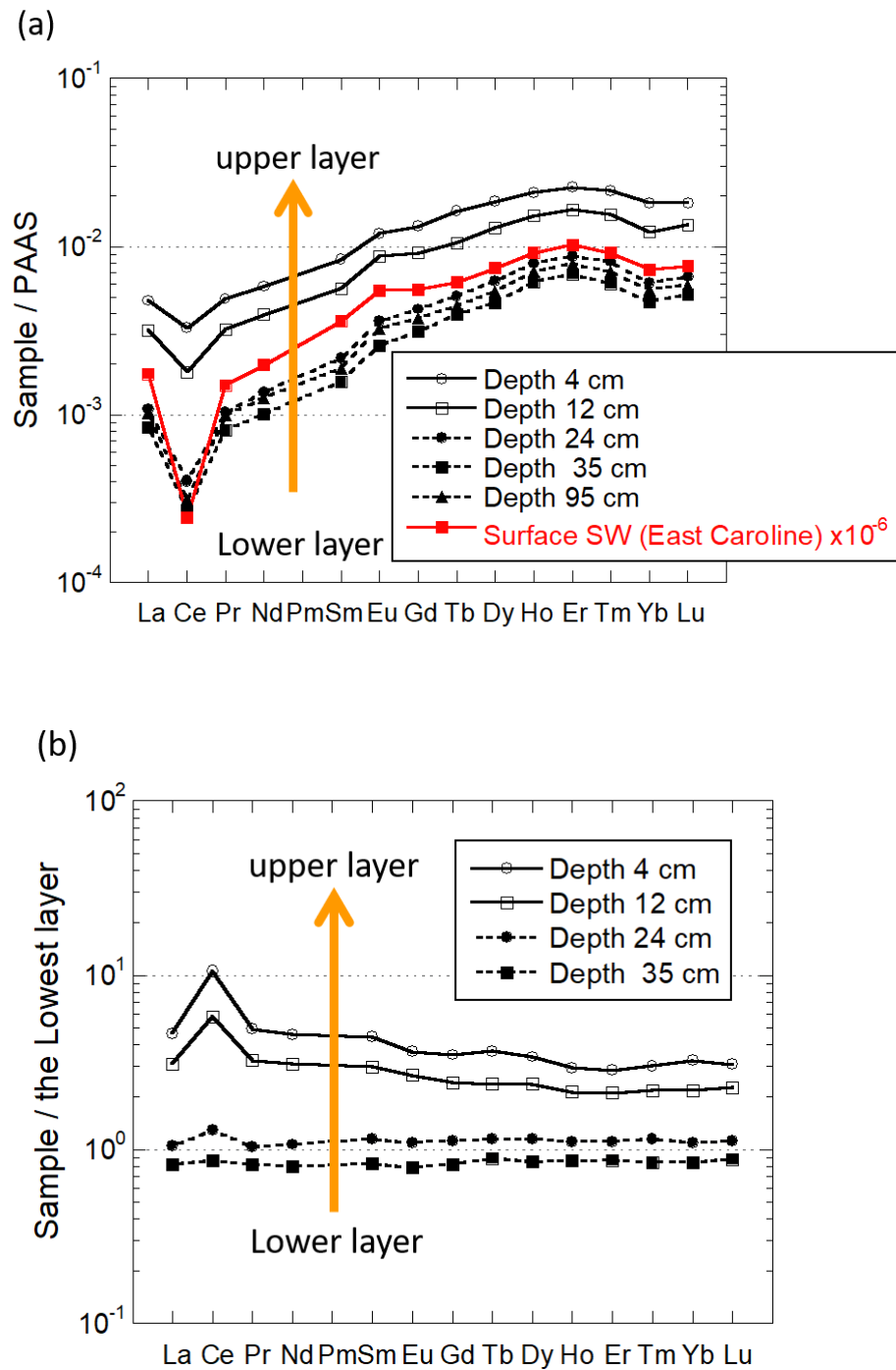


Fig. 5-10. (a) REE patterns of sediments at various depths normalized to that of Post-Archean Australian average shale (PAAS). The pattern of surface sea water in east Caroline (Zhang and Nozaki, 1996) is indicated by a red line. REE concentrations increased toward the upper layer. (b) REEs patterns normalized to that of the lowest layer (95 cm) in Laura. The light REE increased in the upper layer relative to that in the lower layer.

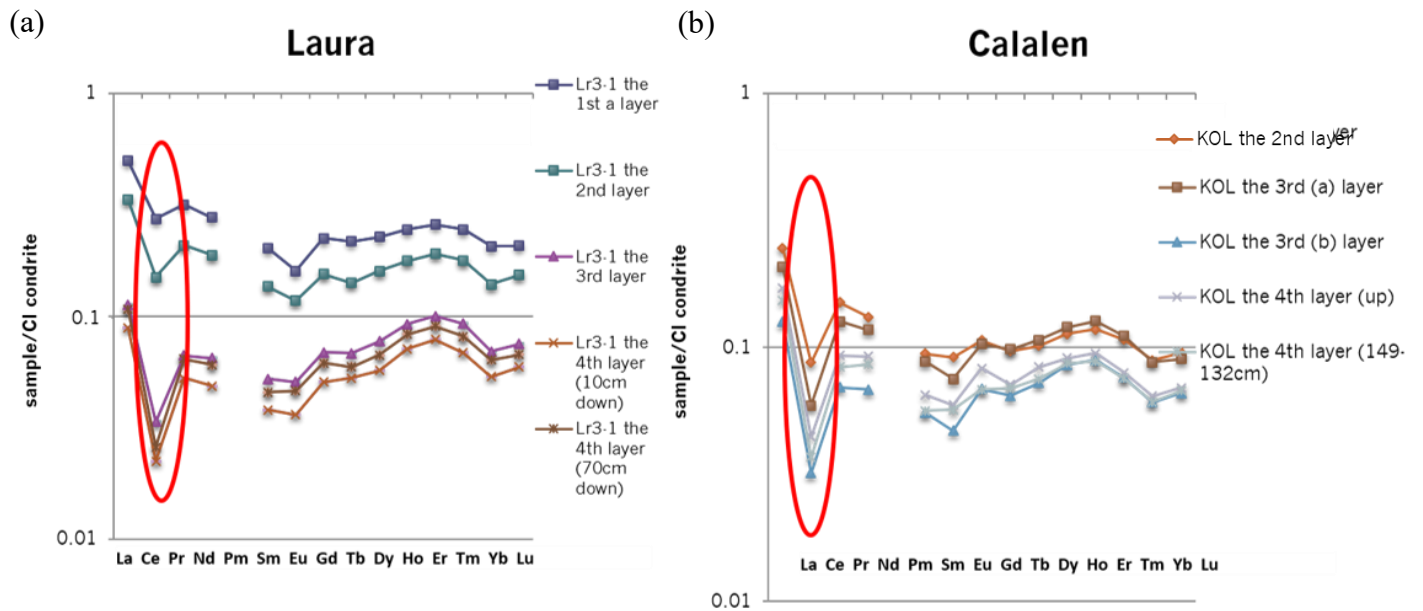


Fig. 5-11. REE patterns of sediments at various depths normalized to that of chondrites.

(a) Laura (Lr 3-1). (b) Calalen (KOL)

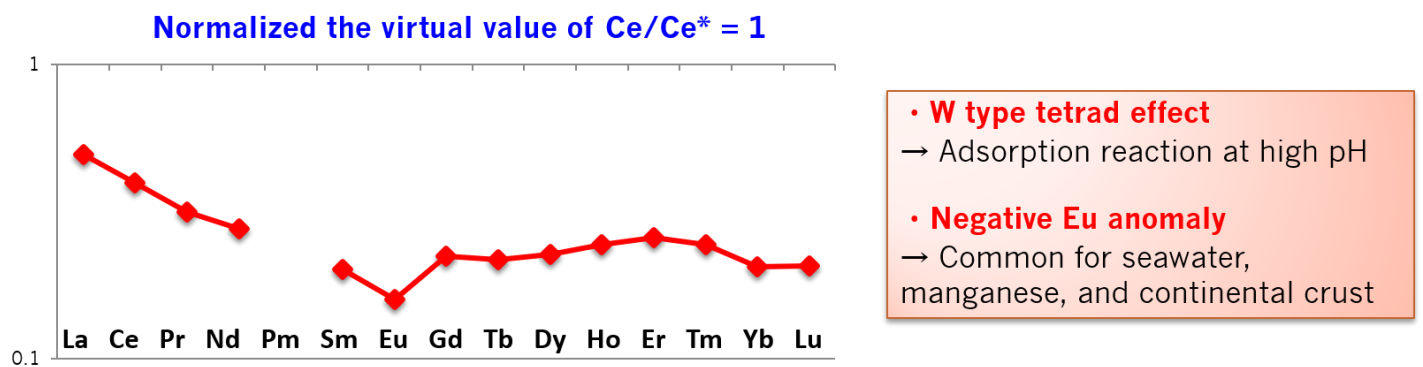


Fig. 5-12. A virtual REE pattern of sediment added to the surface layer of Laura.

5.4.5. Crustal origin: Fe

本章については、5年以内に雑誌等で刊行予定のため、非公開。

5.4.6. Non-crustal origin: P

Phosphorus concentration sharply increased at the depths of 25 and 50 cm toward the surface in Laura and Calalen, respectively. The highest P concentration in Laura and Calalen was 0.36 wt.% and 0.74 wt.%, respectively (Fig. 5-6a, Table 5-3). To identify the origin of P, foraminifera tests in the upper layer were observed through SEM (JSM-7000F, JEOL Co., Ltd., Japan or S-4500, Hitachi Co., Ltd., Japan) equipped with an energy-dispersive spectroscopy (EDS) detector.

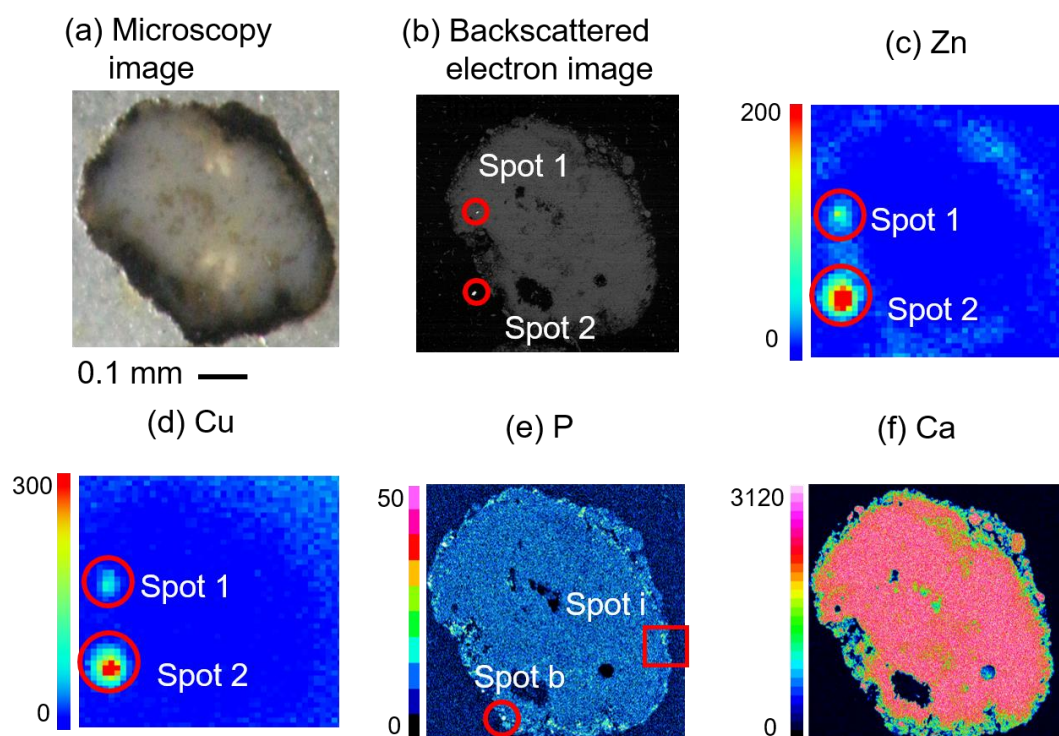


Fig. 5-14. Microscopic observations of a foraminifera particle. (a) Optical microscopy image. Foraminifera were coated by black-colored materials. (b) Backscattered electron image. (c) and (d) show the mappings of Zn and Cu that were extrapolated through μ -XRF measurement. (e) and (f) show the mappings of P and Ca that were taken by SEM.

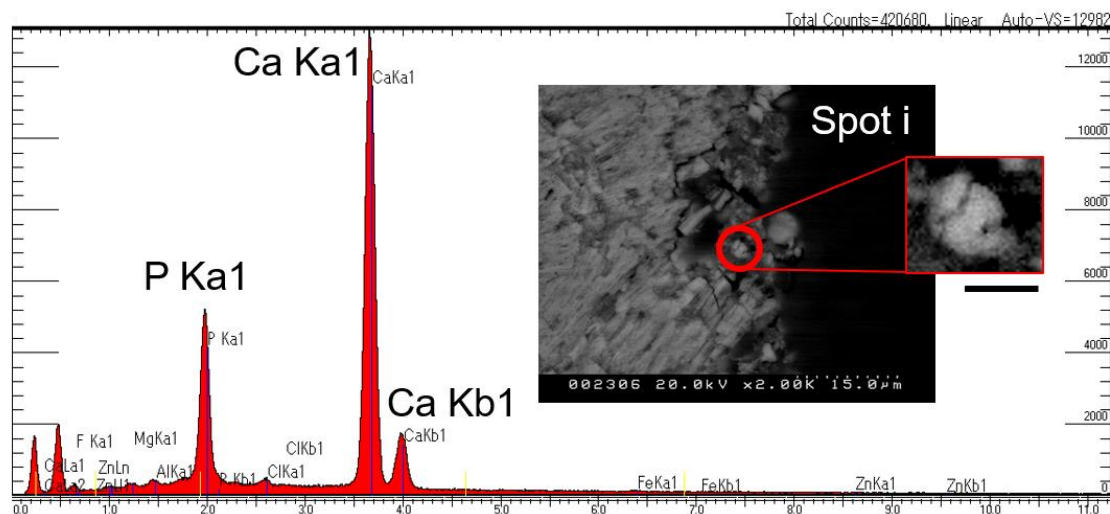


Fig. 5-15. Spectra and SEM images of Spot i.

Fig. 5-14f shows the distribution of Ca which was similar to the shape of foraminifera observed under optical microscope (Fig. 5-14a). Phosphorus in the foraminifera from the upper sedimentary layer were found at the edges of particles (Fig. 5-14e) and was coexisted with Ca. In addition, P was found in numerous spots in small soil aggregates (Fig. 5-16a and 5-16b). Each P hotspot was analyzed through SEM–EDS, which detected Ca and P signals in the particles (Figs. 5-15 and 5-16).

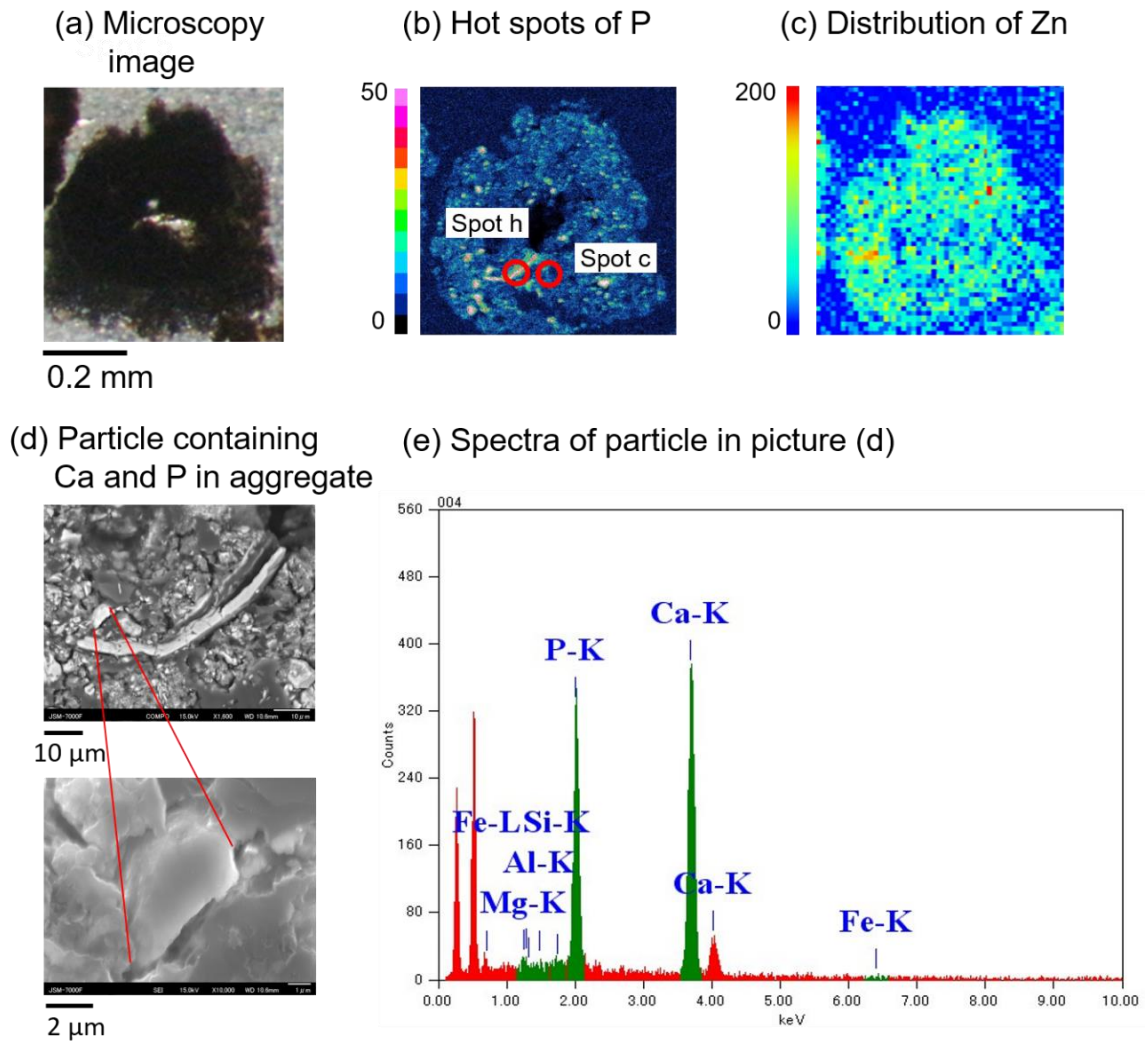


Fig. 5-16. Microscopic observations of an aggregate. (a) Optical microscopy image of an aggregate contained in the sediment of L1. (b) SEM-EDS image of P. Apatite particles can be observed in the aggregate. (c) Zn mapping by μ -XRF measurement. (d) Secondary electron image of P hotspots. (e) EDS spectra of the apatite particle shown in (d). Spots c and h correspond to the spots shown in Fig. 5-18.

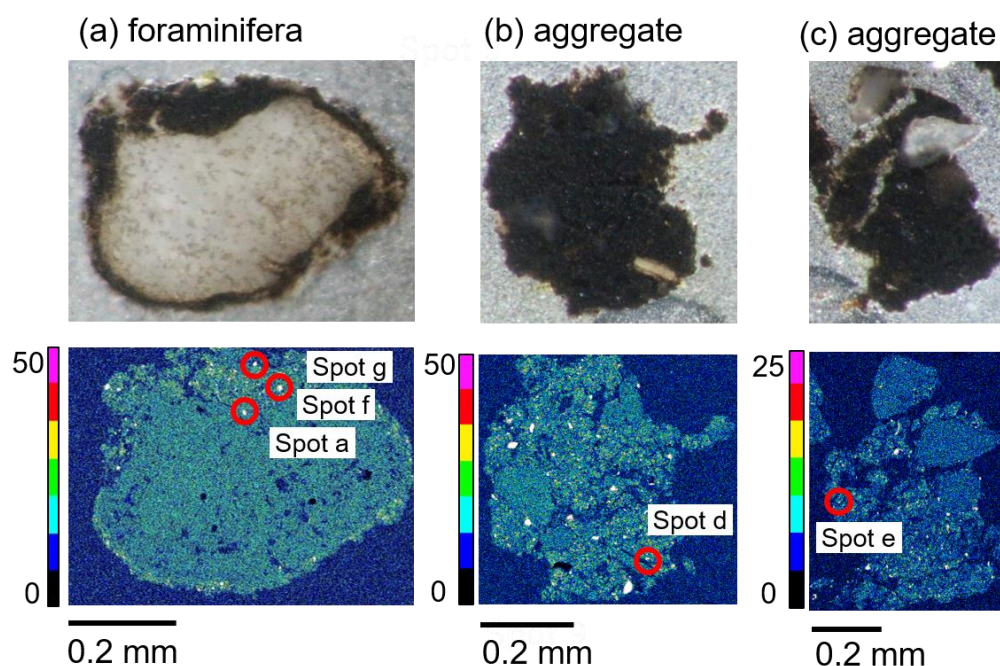


Fig. 5-17. Microscopic observations of (a) foraminifera, (b) and (c) aggregate contained in the sediment of L1. Upper and lower figures showed optical microscopy images and mappings of P by SEM, respectively. Spots a-g correspond to those shown in Fig. 5-18.

The P K-edge μ -XRF-XANES was measured for the detailed investigation of the chemical species. The XANES spectra were collected at various spots in foraminifera (spots a, b, f, and g) and soil particles (spots c, d, e, and h) as shown in Figs. 5-16 and 5-17. The hotspots of P were found (i) along the edges of foraminifera (Fig. 5-14e) and (ii) inside aggregates (Figs. 5-16b, 5-17b, and 5-17c). XANES spectra of the samples are shown in blue, whereas black dotted lines (Fig. 5-18a) indicate the fitting results for spots a–h. The spectra of five reference materials are also shown in the figure. The P K-edge XANES spectrum of P in local seabird feces showed a structure which was similar to the

spectra of the sediment samples or calcium phosphate. Mulder and Ellis (2010) also showed that seabird feces contain a large amount of P in the form of phosphate.

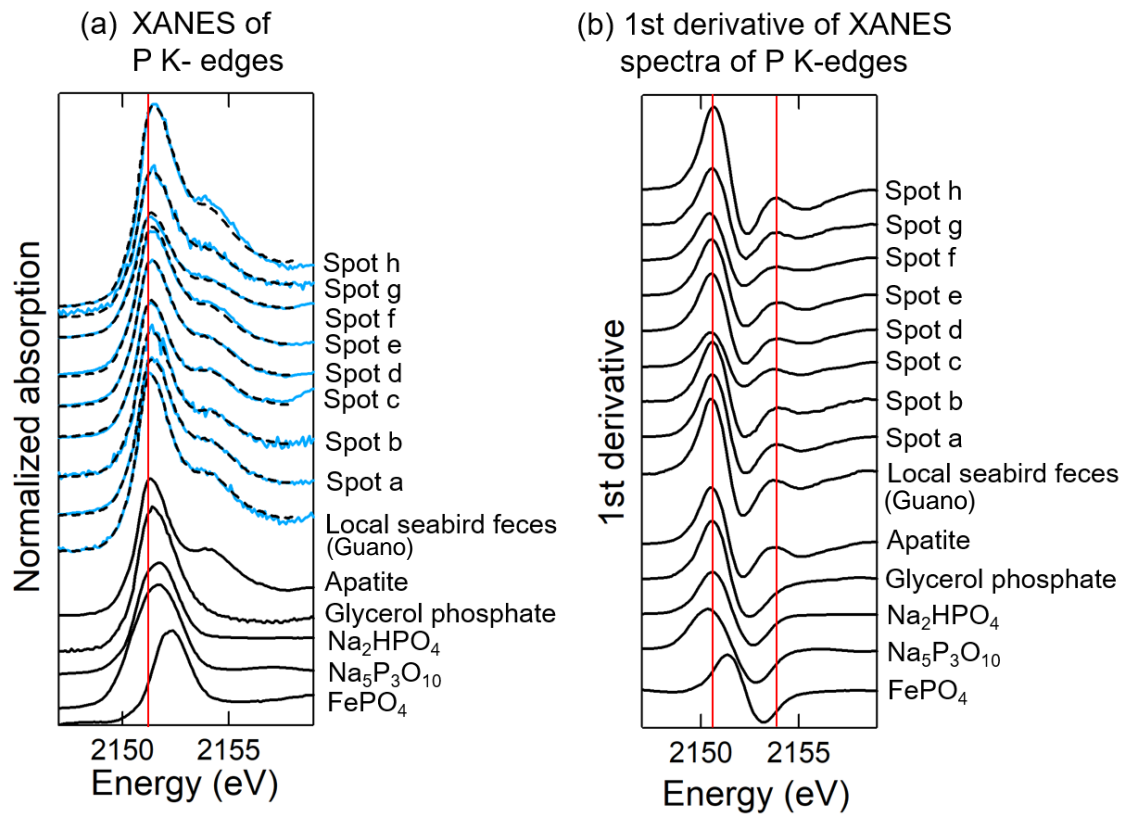


Fig. 5-18. (a) Phosphorus K-edge XANES spectra of P in foraminifera and local seabird feces. The XANES spectra in this figure were acquired for P-enriched spots in foraminifera or aggregates in the sediment. The shapes of XANES for the samples were similar to that of local seabird feces and apatite. (b) First derivative of XANES spectra at the P K-edge (a). Names of the spots corresponded to the spots shown in Figs. 5-16 and 5-17.

Fig. 5-18b shows the first derivative of each XANES spectrum at the P K-edge. The peak positions and shapes of the spectra were almost identical to those of the spectrum of local seabird feces. This result suggests that P detected in the edges of foraminifera or in soil aggregates originated from local seabird feces, which have been

suggested in various studies for origin of P in isolated islands (Aharon and Veeh, 1984; Piper et al., 1990; Liu et al., 2008; Xu et al., 2010). Thus, phosphorus in sediments is likely supplied by external sources, such as seabird feces (Fig. 5-19).

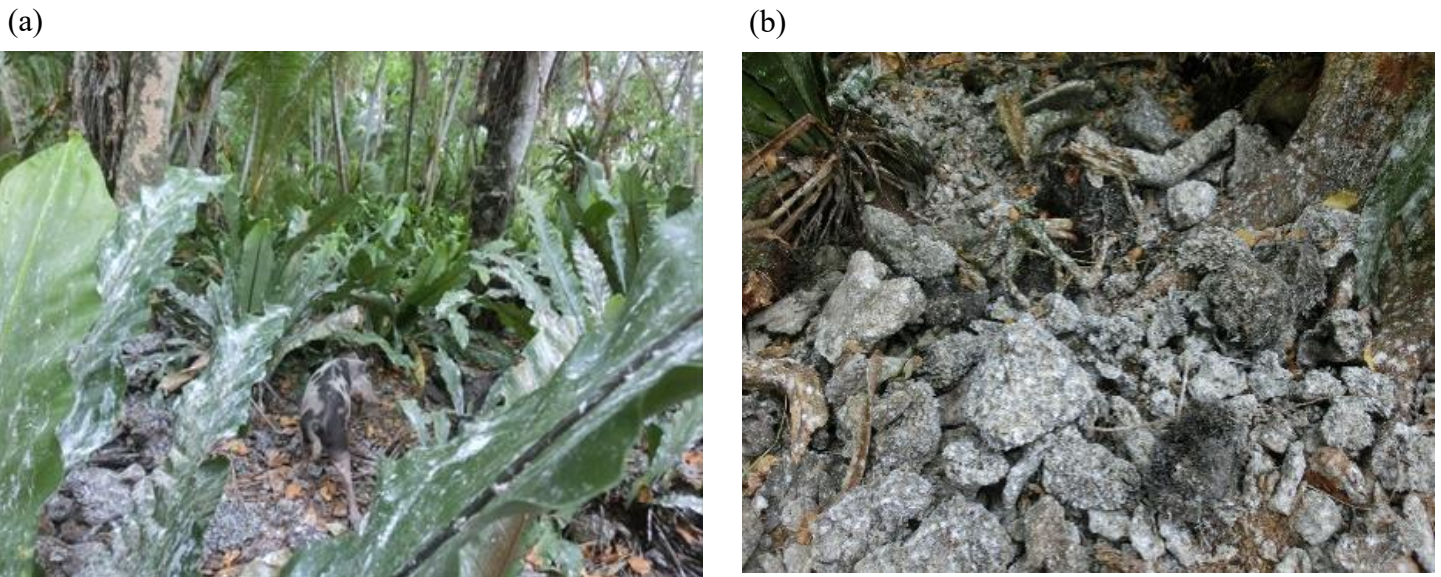


Fig. 5-19. (a) Seabird feces on the plants in Jelto. (b) Seabird feces on the coral gravels in Jelto.

Therefore, the vertical profile of P concentration is high at the surface and decreases toward deep layers. Considering the ^{14}C dating results, Laura was formed about 1000 years earlier than Calalen. However, urbanized ages of both islands were similar around 100 years ago in Majuro. Therefore, the durations after the start of the emission of anthropogenic materials were similar in both islands. Regarding the high P concentrations of Calalen, the contribution of seabird feces should be one possible factor. Another possibility is that surface sediment containing enriched P has been washed away in Laura. However, only by the present data, it is difficult to state the exact reason why P has been more concentrated in Calalen, and further study is needed to understand the fact.

5.4.7. Non-crustal origin: S

本章については、5年以内に雑誌等で刊行予定のため、非公開。

5.4.8. Non-crustal origin: As

本章については、5年以内に雑誌等で刊行予定のため、非公開。

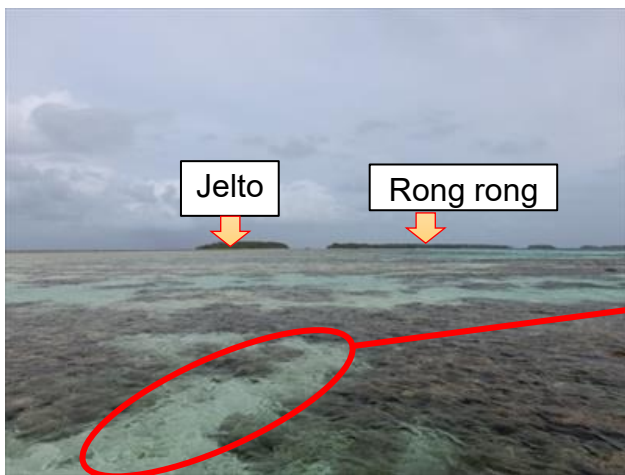
5.4.9. Non-crustal origin: Zn and Cu

As shown above, Zn concentration increased from the depth of 50 cm in the upper layer, particularly in Laura (highest concentration of Zn: 8.23 mg/kg; Fig. 5-6a, Table 5-3). In Laura, the surface EF_{Zn} was 21.1 (Fig. 5-7a, Table 5-4), suggesting that the sediments had a non-crustal Zn source.

(a)



(b)



(c)



Fig. 5-22. (a) Broad reef flat located on the north of Laura. (b) Enlarged photo of reef flat taken from Laura side, Jelto and Rong rong can be seen in north way. (c) Groups of Algae which is the habitats of living foraminifera.

On the other hand, below the depth of 95 cm, Zn concentration was low and is close to the low Zn concentration of living foraminifera test collected on the ocean reef flats of the north part of Laura (Fig. 5-22), which has much less anthropogenic influence compared with the populated area such as the Delap–Uliga–Djarrit (DUD) area in Majuro Atoll (e.g., Fujita et al., 2009; Osawa et al., 2010). The average concentration of Zn in 20-30 living foraminifera was 0.325 mg/kg (Table 5-3).

Similarly, in both islands, Cu concentration increased from the depth above 45 cm at the upper layer, and the highest concentration of Cu was 2.18 mg/kg in the L2 layer (Fig. 5-6a, Table 5-3). The EF_{Cu} at the surface in Laura and Calalen was 5.45 and 4.96 (Fig. 5-7a, Table 5-4), suggesting that Cu is also of non-crustal origin. On the other hand, Cu concentrations were low in the sediment of each lowest layer (0.198 mg/kg and 0.108 mg/kg in L5 and C5, respectively) (Fig. 5-6a, Table 5-3). These results suggested that anthropogenic Cu was not incorporated in the carbonate sediments in the deeper depth. To confirm this, I also measured the Cu concentration of living foraminifera (= 0.0862 mg/kg). This value was similar to that of the lowest sedimentary layers in both islands, showing that Cu originally contained in the sediment sample should be low. This fact also suggested that Cu was not initially present in the carbonate sediments. Similar results were also obtained for Calalen for Zn and Cu, as shown in Table 5-3.

From the results of ^{14}C -dates, sedimentation of the surface sediments was completed well before the urbanization of Majuro Atoll. Considering the absence of the major natural emission sources of Zn and Cu, such as volcanic eruption and forest fires (Nriagu, 1979, 1989), and the higher Zn and Cu concentrations of surface sediments than those of sea salt spray (Nriagu, 1979, 1989), Zn and Cu should have been added as anthropogenic components. The voids of foraminifera are connected to the outside.

Therefore, some other particles such as Zn and Cu debris can be easily trapped inside of the foraminifera.

Micro-XRF analysis showed that Zn-enriched spots were mainly observed (i) at the edges of foraminifera (Spot 1; Fig. 5-14, Spot 3; Fig. 5-23) and (ii) in pores within foraminifera (Spots 4 and 5; Figs. 5-23, 5-24). In addition, Zn-enriched particles were also found as isolated particles outside of foraminifera (Spot 2; Fig. 5-14).

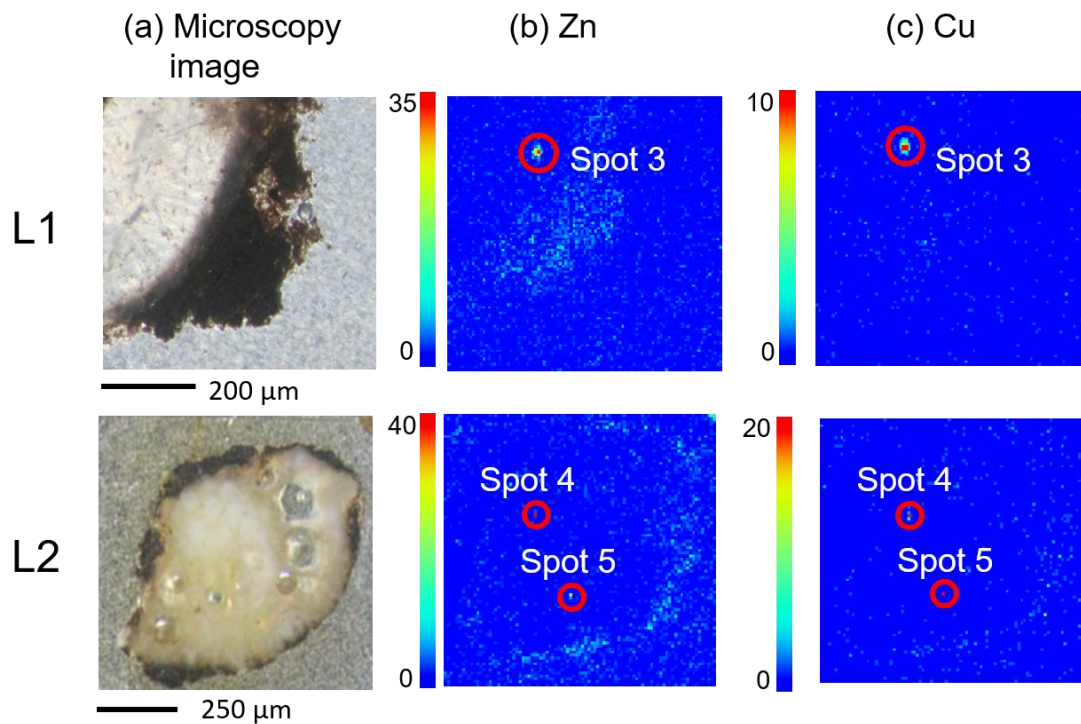


Fig. 5-23. Microscopic observations of foraminifera particles. (a) Optical microscopy images. XRF mappings of Zn (b) and Cu (c). Zn hot spots contained high amounts of Cu, which were observed inside of each foraminifera.

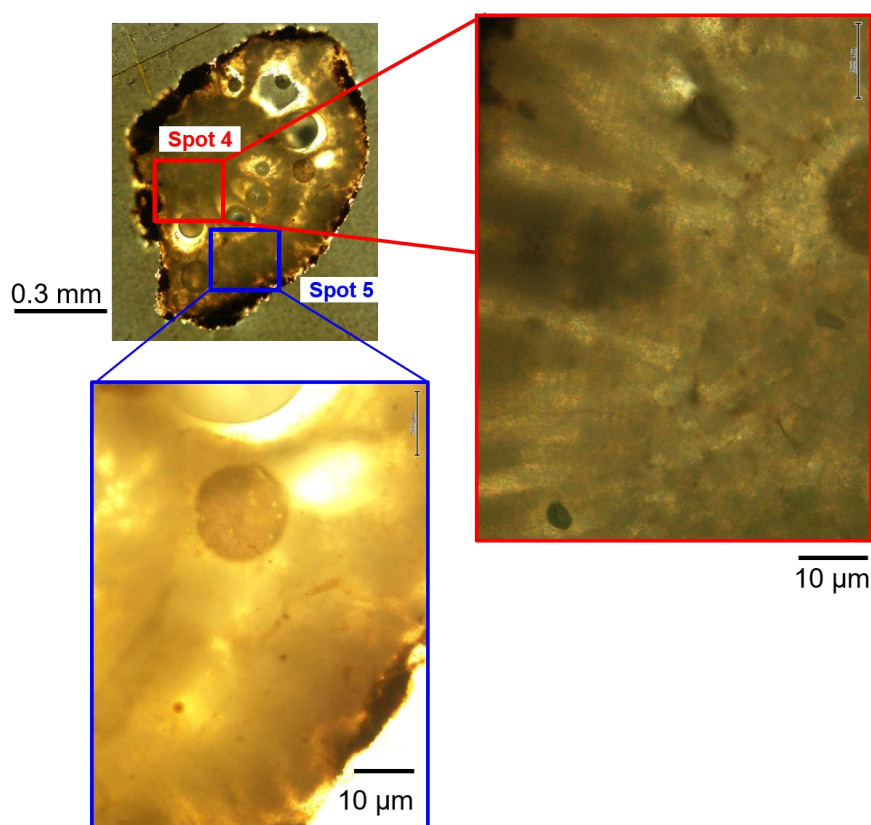


Fig. 5-24. Polarized microscope images of thin section of foraminifera which correspond to Fig. 5-23, L2. Spot 4 and Spot 5 are enlarged, where the particles which contained Zn and Cu were found.

Fig. 5-25a shows the Zn K-edge XANES spectra of various standard Zn materials that were used for least-squares fitting (LSF). Fig. 5-25b shows the spectra of bulk sediment samples collected using the mm-size X-ray beam (bulk analysis). Here, the spectra of original samples are shown in blue and that of residual samples after extraction with 5 M acetic acid are shown in purple (Fig. 5-25b). Fig. 5-25c shows the μ -XANES spectra at Zn-enriched spots in the sediments. The spectra of Zn hotspots in sediment in layers L1, L2, and L3 layers are shown in purple, blue, and green, respectively. The spectra of Zn standard materials and results of LSF results are shown in black and dotted black in Fig. 5-25b, c, respectively.

The results of bulk Zn K-edge XANES suggested that the dominant Zn species in the bulk sediments were Zn coprecipitated with calcite and apatite, which are insoluble in water (Figs. 5-25b, e). The speciation results are reasonable considering the high carbonate and phosphate concentrations of the sediments. It was also reported that carbonate and phosphate stabilize Zn in lake sediments (Lake DePue, IL, USA; Webb et al., 2000; Gaillard et al., 2001). In addition, the samples contained water-soluble species, such as ZnCl_2 and $\text{Zn}(\text{NO}_3)_2 \cdot 6\text{H}_2\text{O}$. In the upper layer (sampling depths: 4 and 12 cm for L1 and L2, respectively), $63 \pm 4\%$ and $33 \pm 3\%$ of Zn remained, whereas $45 \pm 1\%$ of Zn remained in the middle layer (L3; sampling depth: 24 cm) (Fig. 5-25d). As expected, water-soluble chemical species were absent from the three samples after extraction experiment whose aim was to focus on the discussion of incorporation of Zn into various phases except for calcite, which is originally contained in foraminifera test. In the experiment, Zn coprecipitated with calcite was dissolved by acetic acid (Fig. 5-25b, e).

Consequently, the main Zn species found after extraction were Zn coprecipitated with and adsorbed on apatite, as identified through XAFS analysis (Fig. 5-25e). These results suggested that approximately 50% of Zn existed as water-insoluble Zn in apatite. The coprecipitation of Zn in apatite has hindered the migration of Zn into deeper layers.

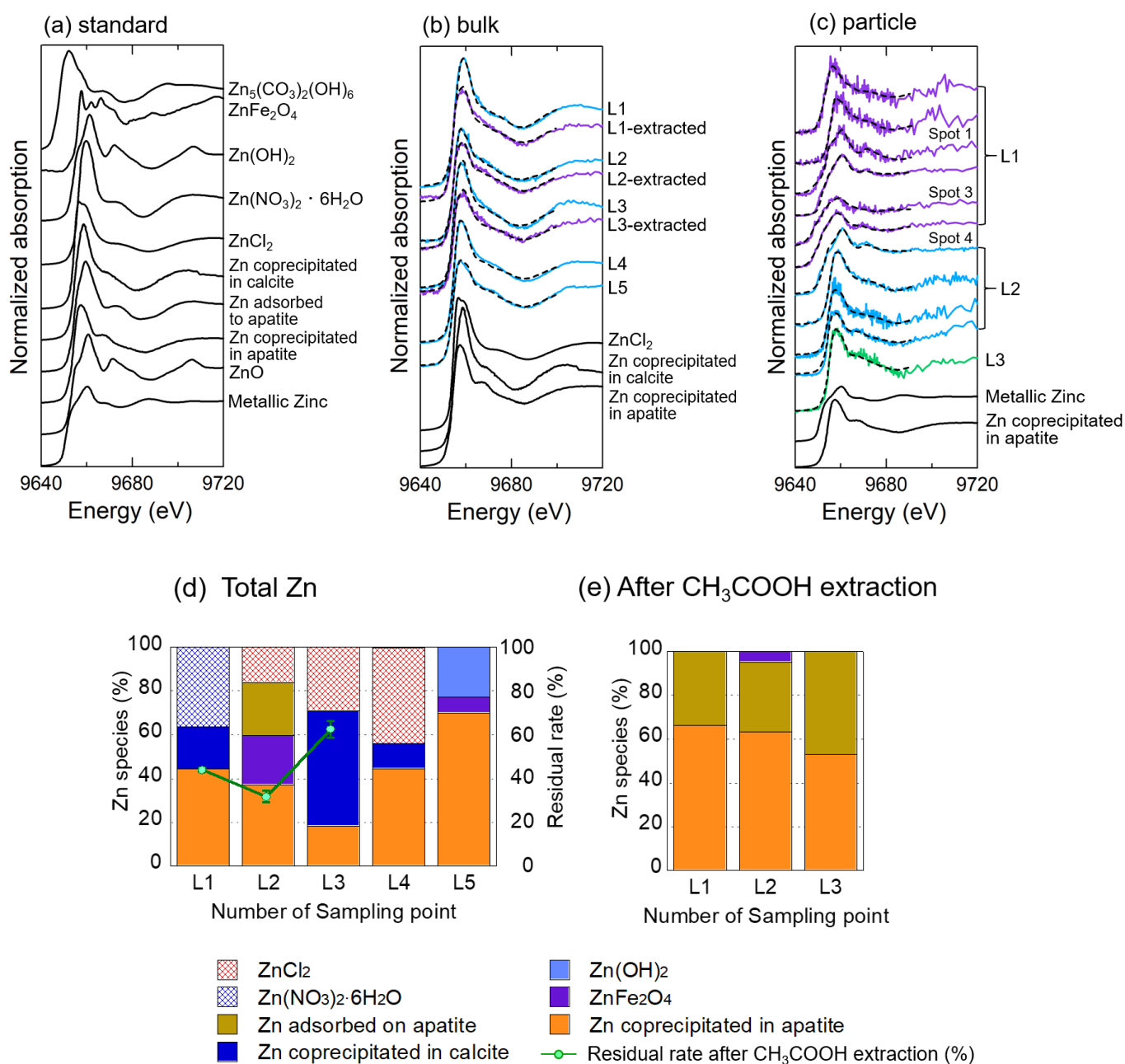


Fig. 5-25. Zinc K-edge XANES spectra of Zn in sediments. (a) Reference Zn materials used the analysis. (b) XANES spectra of bulk sediment samples. (c) XANES spectra of Zn-enriched spots. (d), (e) Ratio of Zn species estimated from XANES analysis. (d) Ratio of the chemical species of Zn in the bulk sample. Green lines indicate the residual fraction of Zn after extraction by acetic acid. (e) Ratio of Zn species in the residual sample after extraction with acetic acid.

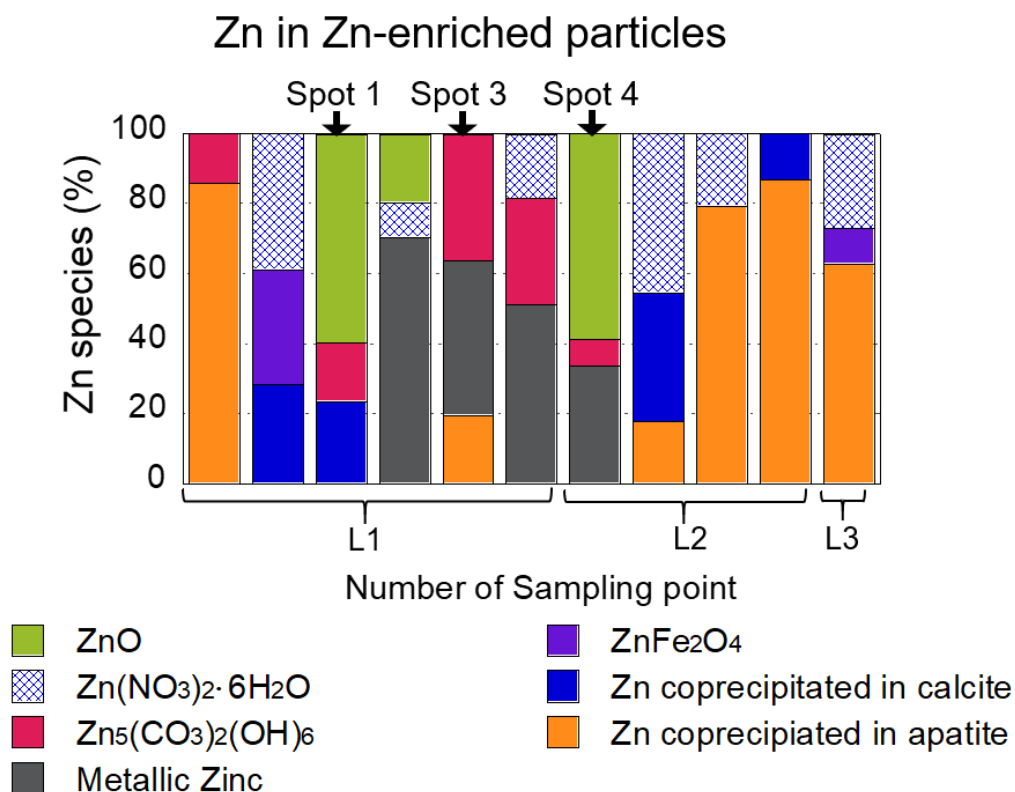


Fig. 5-26. Ratio of Zn species estimated from XANES analysis of Zn-enriched spots. Ratio of Zn species in Zn-enriched particles in L1, L2, and L3. Spots 1, 3, and 4 correspond to the spots shown in Figs. 5-14 and 5-23.

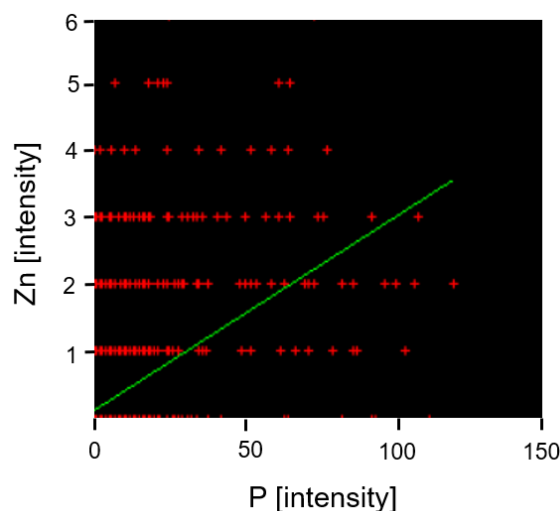


Fig. 5-27. Correlation between P and Zn in micro-XRF mapping in Delap corresponding to Fig. 5-28a, in which the intensity of Zn was stronger. Here, there was weak correlation between P and Zn with correlation coefficient (R) about 0.4.

Although coprecipitated Zn existed with P, correlations between P and Zn in micro-XRF mapping were not always high (Fig. 5-27). This is possibly caused by several reasons as follows: (i) P was distributed in all the areas of foraminifera and showed high concentration where a large apatite grain was observed; (ii) the distribution of Zn was not always similar to that of P due to the presence of metallic Zn particles with high intensities in the mapping; (iii) these metallic Zn particles were often trapped in small voids in foraminifera, where P was not observed.

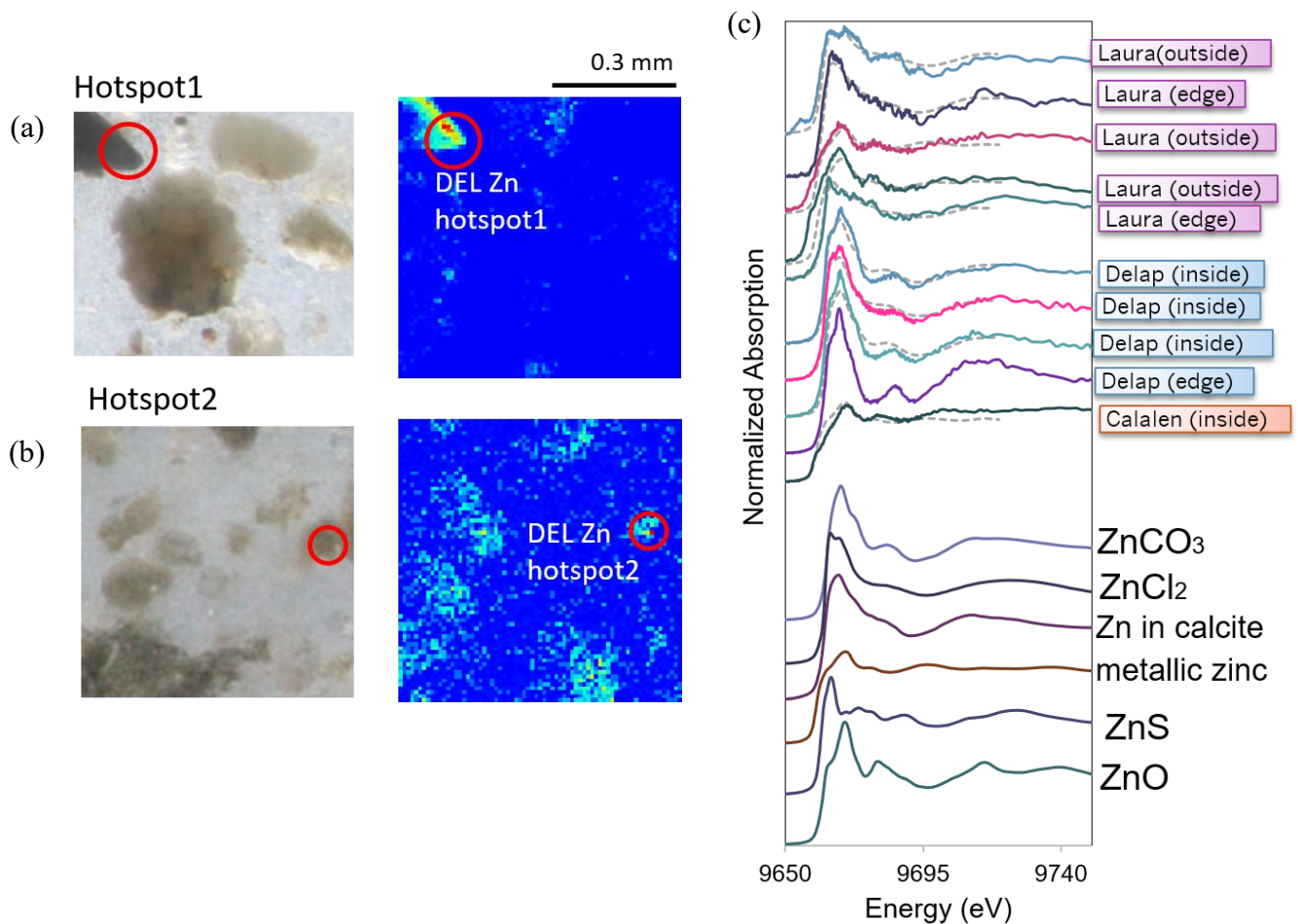


Fig. 5-28. (a), (b) Microscopic images (left) and μ -XRF mapping (right) of Zn in Delap. (c) Comparison of Zn K-edge XANES spectra of particles from three islands, Laura, Delap, and Calalen. Parentheses are the points of foraminifera where Zn particles were found.

Micro XAFS analyses (Figs. 5-25c, 5-26, 5-28) were carried out to identify the Zn species present in Zn hotspots (Figs. 5-14, 5-23, 5-24, 5-26, 5-28a,b). Metallic Zn, ZnO, and $\text{Zn}_5(\text{CO}_3)_2(\text{OH})_6$ were found in the hotspots (Fig. 5-26) in addition to the Zn species found through bulk analyses, such as Zn coprecipitated with apatite. Anthropogenic sources, such as metallic Zn and franklinite (ZnFe_2O_4) (in L2 and L3 layers) may have exclusively supplied the various Zn species to the sediments (Figs. 5-26, 5-30). Metallic Zn was found through the μ -XRF-XAFS analysis of some particles in the L1 and L2 layers (Spots 3 and 4 in Fig. 5-23 with XANES spectra in Fig. 5-25c). Franklinite was found through the μ -XRF-XAFS analysis of some particles in the L1 and L3 layers (Figs. 5-26 and 5-30) and also found through the bulk XANES analysis of the L2 and L5 layers (Fig. 5-25d). Given that ZnO found in L1 and L2 as a particle (Fig. 5-26), which is unlikely to form in a wetland system, its environmental occurrence should be attributable to contamination from an anthropogenic source, such as smelted metal (Sobanska et al., 1999).

Copper K-edge XANES analysis was also applied to determination of Cu species (Fig. 5-29). The spectra of various spots including spots 1, 3, and 4 (Figs. 5-14, 5-23) suggested that metallic Cu was mainly present in the hotspots and that Zn and Cu were present as Zn–Cu alloy.

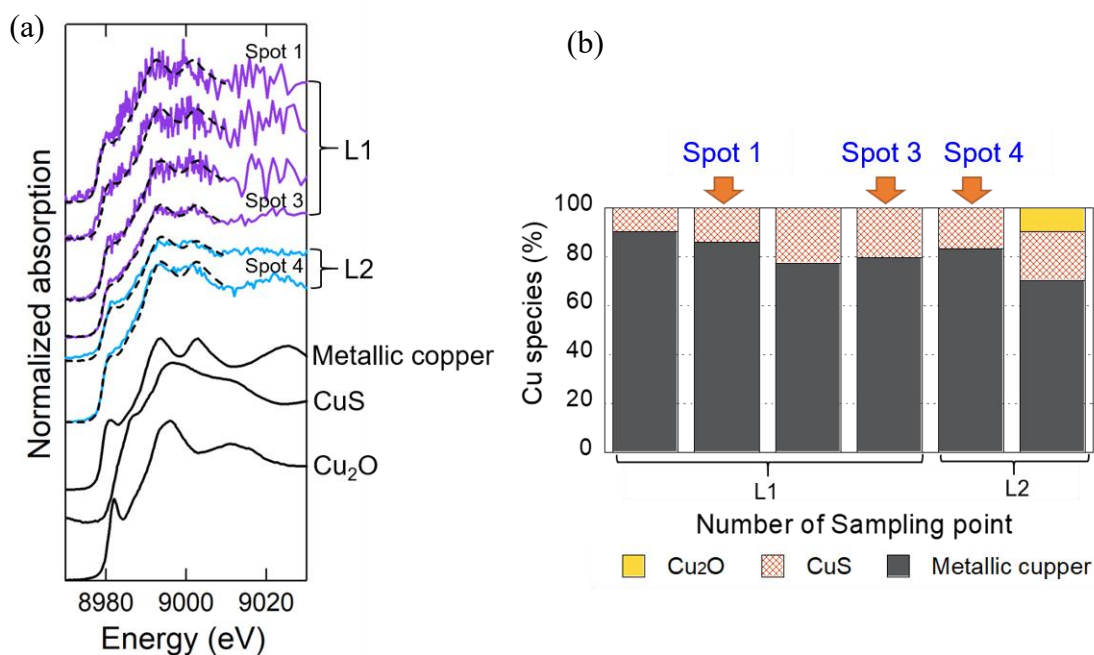


Fig. 5-29. (a) Copper K-edge XANES spectra of Cu-enriched spots in foraminifera or aggregates. Spots 1, 3, and 4 correspond to the spots shown in Figs. 5-14 and 5-23. (b) Ratio of Cu species estimated from XANES analysis.

5.4.10. Sources of Zn

Various industrial products are possible sources of the Zn–Cu alloy and franklinite in the sediment samples. Zn–Cu alloy is used in industrial products and everyday items which are routinely used in Majuro, such as outlets, fluorescent lamp pins, gas stove burner heads, hooks, fasteners, screws, bolts, water faucets, meter frames and radiators of automobiles. Zn–Cu alloy is the main source of Zn pollution in other countries (e.g., Amsterdam, Netherlands; Gouman, 2004). However, there were also Zn particles which did not coexist with Cu (the particles except for Spots 1, 3, and 4 did not exist with Cu in

Fig. 5-26.). For chemical species of those Zn were mainly metallic Zn or Zn coprecipitated with apatite.

Franklinite which was found in both bulk and micro XAFS analyses is a representative spinel ferrite with excellent electrochemical characteristics and has been used in various products such as high density magnetic recording, radar absorption, etc. (e.g., Hashim et al., 2015; Yang et al., 2013; Bresser et al., 2013; Hirosawa et al., 2016). It is also known as a main contaminant species of Zn in soil (Manceau et al., 2002). This chemical species was found in L1 and L3 sedimentary layers as particles and was also identified in the sedimentary layers, L2 and L5. In the particle, Zn coexisted with Fe, which was found in the edge of foraminifera fragment (Fig. 5-30).

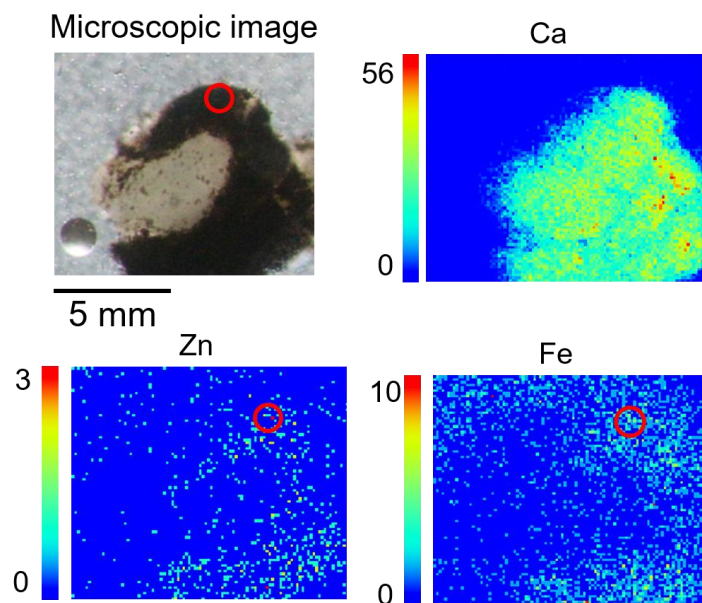


Fig. 5-30. Microscopic images and μ -XRF mapping of Ca, Zn, and Fe of the foraminifera fragment. ZnFe_2O_4 was detected from the point of red circle.

Arimoto et al. (1985) and Duce et al. (1983) reported that EF_{Zn} values normalized to Al for wet and dry depositions in Enewetak Atoll, Marshall Islands, which exceeded

190 and 3.6 during the dry season, respectively, whereas those during wet season are 45 and 33, respectively. The reason of lower EF at Enewetak Atoll (3.1-3.4) was likely due to the seasonal variation of Al concentrations, despite that the atmospheric Zn concentrations was rather stable (Duce et al., 1983). In dry season, dust storm activity in China is greatest because of the combined effects of low rainfall, the increased occurrence of high surface winds associated with cold fronts, and soil freshly plowed for planting (Duce et al., 1980). Moreover, this site is located within the easterly (trade) wind regime, though there is very strong westerly flow north of about 20°N that transport materials from Asia to the central North Pacific during the dry season (Fig. 5-31). Therefore, the dust from China could be readily transported by the mean winds to the region of north of Enewetak. (Duce et al., 1980)

インターネット公表に関する使用承認申請中
につき、本図については、非公開。

Fig. 5-31. Wind trajectory around Majuro Atoll (Modified from Merrill et al. 1989).

The EF values of surface sediments in this study (Fig. 5-7a, Table 5-4) were generally larger than average EF values reported for aerosols (= supplied by the long range transport) in Duce et al. (1983), which suggests that most of the elements with EF values larger than 10 in this study should be more or less originated from local sources (except for Se and Pb). Based on the comparison of EF values in Duce et al. (1983) and this study, about 70% and 60% of Zn and Cu should be derived from aerosols, respectively, but the rest of Zn and Cu were locally supplied, respectively (Table 5-4). For example, Zn-Cu

alloy is likely to be originated from this Atoll due to several reasons as follows. First, the settling velocity increases with the density of the particle and with the square of its diameter as the formula below (Finlayson-Pitts and Pitts, 1999):

$$v = D^2 \rho g / 18 \eta \quad (\text{for } D > 1.5 \mu\text{m}) \quad (47)$$

which suggests that the particles $>10 \mu\text{m}$ settle down rapidly and removed from the atmosphere. The particle size of Zn-Cu alloy found in this atoll was 5-50 μm (Fig. 5-32), while the density of standard Zn-Cu alloy is around 8.5. This fact suggested that even if the particle size was 5 μm , the Zn-Cu alloy particles settle down rapidly after their release into the atmosphere. Thus, we consider that most of Zn-Cu alloy is locally derived.

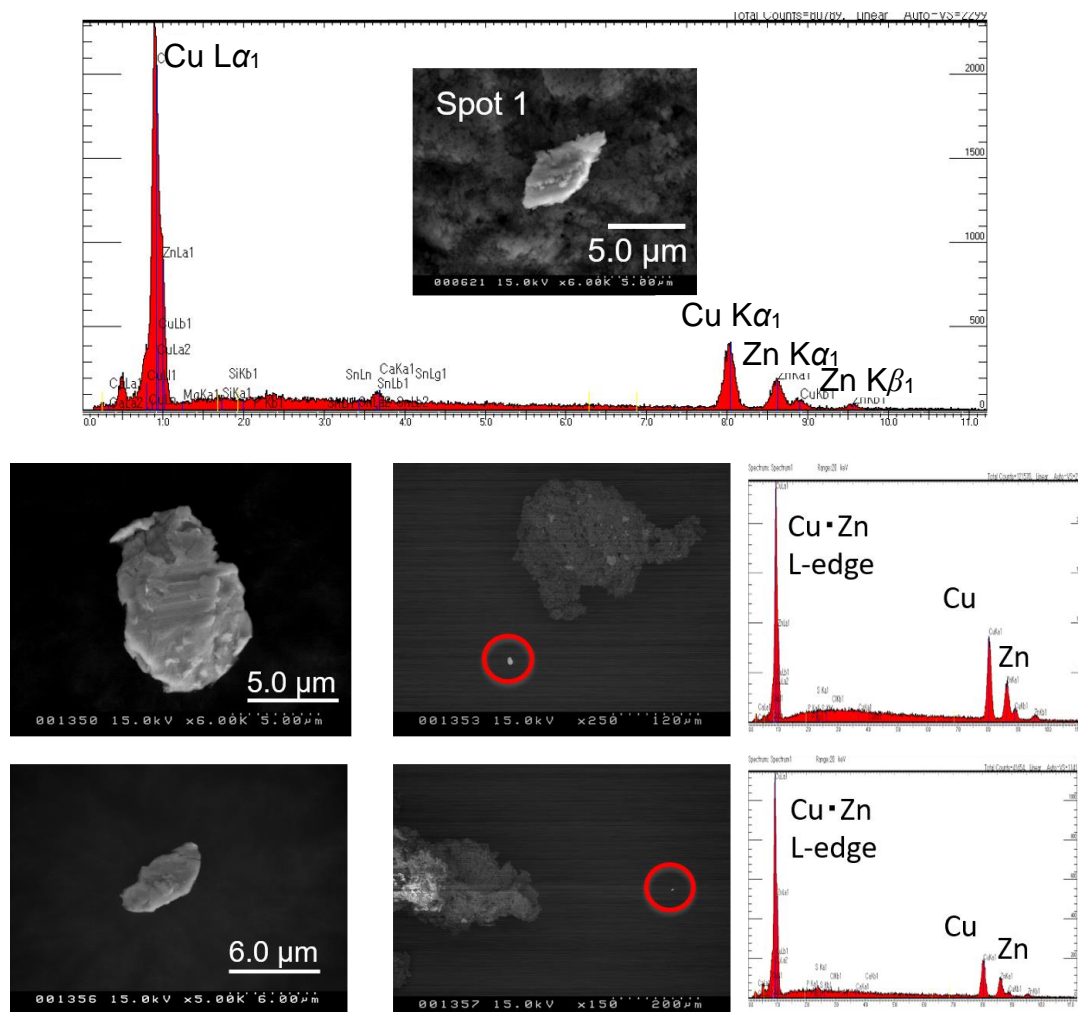


Fig. 5-32. SEM images of the particles which contained Zn and Cu and their spectra obtained by SEM-EDS. The particle of the top figure corresponded to spot 1 (Fig. 5-14).

As a result of the concentration of Zn and Cu in the sediments (Fig. 5-6a), that of Zn was higher than that of Cu. Based on the discussion above, the following reasons are considered for this result. First, it is most likely that Zn amounts are larger than Cu in aerosol. Second, Cu particles are almost found together with Zn in the island. However, since Zn forms its phase, Zn has been supplied from various origins compared to Cu. Therefore, the total amounts of Zn should be larger.

5.4.11. Conservation of groundwater by the fixation of Zn at the surface

The mobilities of the investigated elements in the sediment column are discussed in this section. Results showed that Al^{3+} is fixed at the surface given its immobile nature. By contrast, soluble elements, such as As and Se (presumably present as Se (VI) under oxic condition), from anthropogenic sources ($\text{EF}_{\text{Se}}=1170$ and 666 at the surface in Laura and Calalen, respectively) have migrated to deeper layers compared with Zn reflected in their concentration of the sediments above 50 cm depth in Fig. 5-6a. Given its lower charge, Zn^{2+} is more mobile than Al^{3+} . However, bulk speciation data coupled with acetic acid leaching experiments suggested that Zn is also fixed at the surface as a result of the formation of immobile Zn species, such as Zn coprecipitated with calcite or apatite.

I found that Zn is not readily released to the aquatic environment (groundwater and coastal water) of Majuro Atoll due to the coprecipitation of Zn with carbonate and the secondary production of phosphate in the sediment column. Thus, speciation analysis of such elements is important to predict their mobility and subsequent influence on the ecosystem.

Inhibition of migration of Zn and other heavy metals from surface to deeper depth is highly important in terms of their exposure to aquatic organisms and even to the

residents on Majuro Atoll. Although rain catchment storages are developing on the islands as water resources for the residents at present, fresh groundwater is still an important natural water resource (Presley, 2005; Koda et al., 2013; Bailey and Jenson, 2014) (Fig. 5-33). Thus, the present results showed that coprecipitation and adsorption reactions of calcite and apatite are essential factors on the preservation of freshwater aquifers in Mauro Atoll.



Fig. 5-33. Private house of Laura. Residents make use of both tank for catching the rain water and well for their drinking water.

To support this speculation, concentrations of Zn and Cu in soil water and groundwater were compared. The concentrations of Zn and Cu in groundwater noted as ([Zn], [Cu]) were (0.050 ppb, 0.61 ppb) and (0.15 ppb, 0.87 ppb) in Laura and Calalen, respectively (Table 5-3). On the other hand, concentrations of Zn and Cu in surface soil water, which was not available due to very rapid infiltration of rain water into the

sediments, may be estimated by their concentrations in water in the leaching experiments. As a result, concentrations of Zn and Cu leached in the water were (3.11 ppb, 2.66 ppb), (2.08 ppb, 2.44 ppb), and (0.90 ppb, 1.26 ppb) when soil to water ratios were 1:1, 1:2, and 1:5, respectively. These concentrations are much higher than those in the groundwater, suggesting that Zn and Cu with relatively higher concentrations in the surface water were removed, which results in their lower concentrations in the sediments at deeper depth and also in the groundwater (freshwater lens). These facts suggested that natural attenuation mechanism by the sediment layer has been functioning in Majuro Atoll for heavy metals such as Zn and Cu.

5.5. Conclusions

Aluminum, P, Cu, Zn, and REE concentrations increased in the upper sedimentary layer of Majuro Atoll. The ^{14}C dates of surface sediments in Laura (L1) and Calalen (C1) were 2100–1874 cal BP and 662–542 cal BP, respectively, which revealed that the sedimentation of both islands had been completed well before urbanization.

It is suggested that the origin of Al and REE was continental crust carried by dust. XANES analysis revealed that Zn coprecipitated with calcite in foraminifera tests and apatite from sea bird feces was the dominant Zn species, which hinders the release of Zn into groundwater and coastal water. Consequently, Zn was fixed in the upper layer of the sediment, which can conserve fresh groundwater resources for local residents on Majuro Atoll.

Chapter 6.

General conclusions

6. General conclusions

Reef island in atoll is an island where biological remains such as foraminifera and coral gravels composed of calcium carbonate (CaCO_3) are deposited on the coral reef. Most of them are isolated from the continents. Therefore, all mechanisms concerning material circulation should be different. For example, about the soil formation, clay minerals were readily supplied from nearby continents in many cases of lands. However, since the atoll is far from the major continents, I have to clarify the following points: i) characterization of materials that have been supplied, ii) sources of the materials, and iii) the amount of the materials. There have been no researches that solve all these questions except for this study.

Moreover, behaviors of elements included in the materials after the deposition of these materials were largely unknown. Firstly, I succeeded to identify the factors controlling soil acidification and found out the subsequent processes such as selective dissolution of Mg-calcite and promotion of soil formation processes. Secondly, I quantified the materials added to atolls and evaluated the anthropogenic influence. Followings are summary of this study.

6.1. Soil acidification in atoll

Generally, Soil acidification proceeds with various factors such as NO_x and SO_x concentrations that are mainly emitted by anthropogenic combustion of fossil fuels. Weathering of rock and nitrification are also important factors for soil acidification. Since acidified soil in industrial countries contains all these factors, it is difficult to evaluate each factor separately. On the other hand, sediments of atoll are unconsolidated bioclastic sand such as foraminifera, coral, and calcareous algae that are simply composed of calcium carbonate (CaCO_3). Therefore, it is relatively easy to discuss anthropogenic impacts and natural effects, separately. Here, I investigated the degrees of acidity in Majuro Atoll, one of the atolls of Marshall Islands, where human residence has lasted for about 2000 years, which is the longest history in atolls around the world (Yamaguchi et al., 2005, 2009). However, the traditional life style in the island has changed, and the residents started to use more industrial products such as motor vehicles only after 1900s. I focused on factors that may influence the change of the surface environment of reef islands from both artificial and natural factors. In particular, calcium (Ca) and magnesium (Mg) concentrations, inorganic ions (NO_3^- , SO_4^{2-} , and NH_4^+), pH of sediment, mineral composition, porosity of foraminifera coupled with synchrotron-based X-ray μ -CT, TOC, and stable isotope of nitrogen (N) and triple oxygen isotope (O) in nitrate in sediment at different depths were examined. I found that Mg concentration decreased near the surface layer, especially Mg-calcite fraction to total CaCO_3 (calcite + magnesian calcite (Mg-calcite)) of foraminifera decreased. In contrast, the NO_3^- concentration increased near the surface layer. From the analysis of the stable isotopes of N and O, I found that NO_3^- was originated from the nitrification by bacteria, which transform NH_4^+ whose origin is considered both anthropogenic and natural one. Organic acid concentration also had

correlation with pH of sediment. From the range of soil pH 7.5-8.2, the value of correlation coefficient between NO_3^- and soil pH was especially higher than that between organic acid and pH. On the other hand, soil pH 7.5-9.2, the value of correlation coefficient between organic and soil pH was generally high. This soil acidification accelerated the dissolution and weathering of the foraminifera. Weathered foraminifera become finer with increased degree of water retention. Sediment with pH under circumneutral pH condition contributes to the development of vegetation, since more plants are suitable for neutral soil pH. Subsequently, humus increased and promoted soil formation. Concentrated NO_3^- also becomes nutrition for plants. In this way, this chapter concluded that H^+ derived from (i) release by the process of nitrification and (ii) production of organic acids by plants worked together as a trigger to make the sediments acidified on Majuro Atoll, which promoted the chemical weathering and formation of soil (Fig. 6-1).

本図については、5年以内に雑誌等で刊行予定のため、非公開。

Fig. 6-1. Dominant factor of soil acidification in atoll.

6.2. Origin of the materials in atoll

Identifying the anthropogenic sources of sediments in an urbanized area, such as Tokyo, Japan, is difficult. However, the anthropogenic sources of sediments in Majuro Atoll can be readily evaluated given its isolation from other land masses. In this study, I focused on the sources of the trace elements Al, P, Cu, Zn, Se, and REE. Aluminum, P, Cu, Zn, and REE concentrations in the upper sedimentary layer increased toward the surface above 50 cm depth. Ca concentration was stable, whereas Mg concentration decreased toward the upper sedimentary layer. The ^{14}C dates of surface sediments in Laura and Calalen were 2100–1874 and 662–542 cal BP, respectively. These results revealed that the sedimentation of the surface layer at depths above 12 and 24 cm in Laura and Calalen, respectively, had been completed well before urbanization.

The sources of the trace elements based on their high concentrations in the upper sedimentary layer into anthropogenic, natural, and seabirds can be classified by this study. The inventory of Al deposited for ca. 2000 years was similar to the Al inventory calculated from (i) annual wet and dry depositions and (ii) accumulated amount in sediments per 1000 year reported in the central Pacific. REE with EF_{REE} of approximately 1 was shown as a representative of trace elements supplied by continental crust. This interpretation was also supported by the variation in the REE pattern. Phosphorus had the highest EF (> 976) among the investigated trace elements. Phosphorus hotspots existed in the edges and interiors of foraminifera and aggregates in the sediments, respectively. Given that seabird feces contain a large amount of P (e.g., Mulder and Ellis, 2010), and the XANES spectrum of each sample was similar to that of seabird feces, seabird feces may be a source of P. This conclusion is in accordance with other studies on the origins of P in various isolated islands.

EF_{Zn} and EF_{Cu} were nearly or more than 10, indicating that those elements were derived from anthropogenic sources. XANES analysis revealed that some Zn and Cu hotspots were located at the same position as Zn–Cu alloy derived from anthropogenic materials such as brass used in roofs and rain gutters (Gouman, 2004). Bulk analysis also revealed that Zn coprecipitated with calcite and apatite was the dominant Zn species, which hinders the release of Zn into groundwater and coastal water. Consequently, Zn was fixed in the upper layer of the sediment, which can protect the heavy metal contamination from aquatic organisms (Fig. 6-2, Ito et al., 2018b).

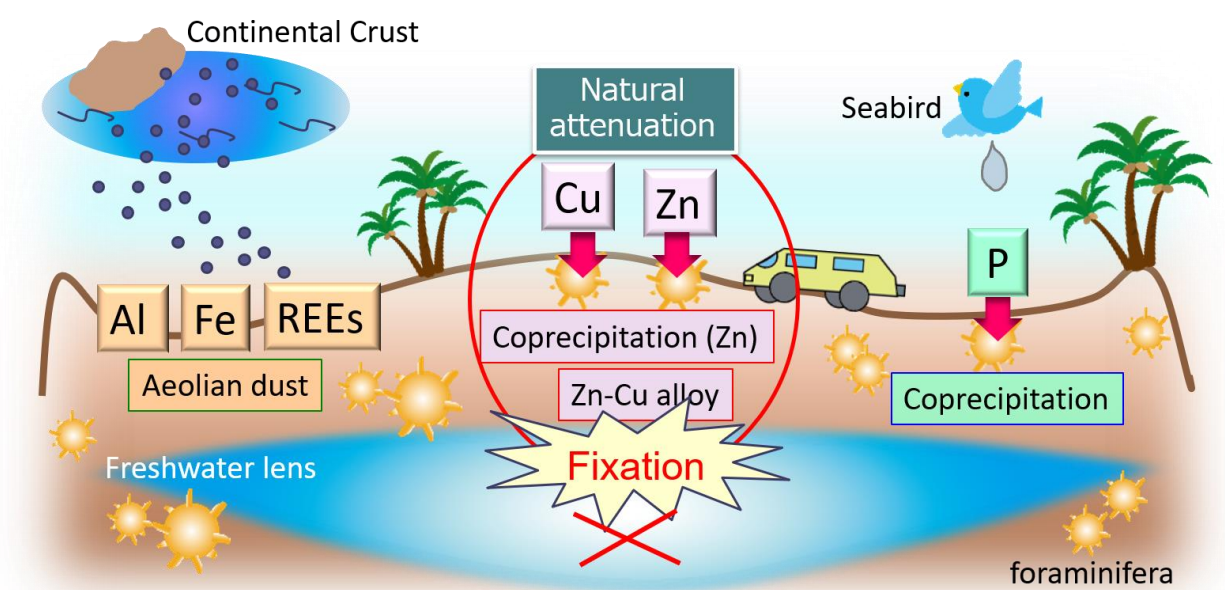
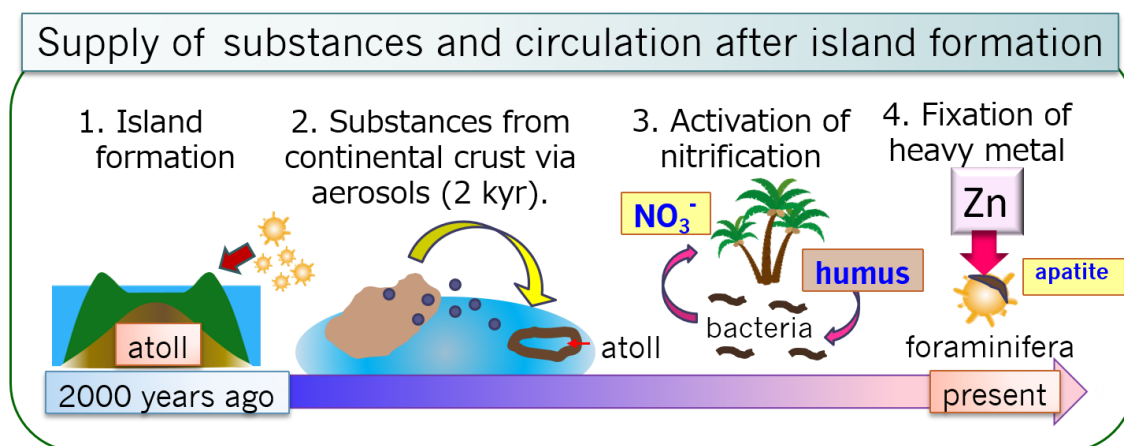


Fig. 6-2. Fixation mechanism of heavy metals in atoll.

6.3. Novelties and significant points of this study

To summarize this study, following points were revealed (Fig. 6-3).

1. In the case of coral reef islands studied in this study, deposition rate was very fast, and formation of the islands was completed within 2000 to 700 years.
2. After the formation of the island, the surface layer was exposed for a long time, and materials derived from the continental crust were added via the atmosphere for 2000 years.
3. Humic substances (black layer) were produced by plants. These organic matter, organic acid, and NO_3^- lower the soil pH. On the other hand, neutralization by CaCO_3 occurred and the optimum pH was maintained for nitrate bacteria. This condition is considered as an ideal environment for that bacteria, which activates nitrification on the island. As a result, soil was produced in a short period right after the island was formed.
4. Heavy metals have been released by urbanization of the island. However, heavy metals such as zinc were coprecipitated with calcite and apatite and fixed in the surface of the sediment. This hinders the migration of heavy metals to groundwater. This mechanism would be functioned as a natural attenuation for heavy metals in these atolls.



Ito et al. (2018a, b)

Fig. 6-3. Novelties and significant points of this study.

Acknowledgments

I greatly appreciated Prof. Yoshio Takahashi from bottom of my heart for everything on my research and study environment. His innumerable valuable advices were very helpful to writing papers and thesis and encouraged and stimulated my mind and motivation for my study and geochemistry. I also really thankful for him to give me a chance to study about Majuro again, and furthermore kindly gave me an opportunity to do fieldwork in Majuro Atoll again and newly in Arno Atoll. In fieldwork, his supporting was greatly helpful that this fieldwork would not have been succeeded without his help. I also appreciated Prof. Takaaki Itai for thoughtful advices and encouragement. Furthermore, I am grateful to all the members of Takahashi laboratory including graduated members. They always encouraged me and gave me great advice, and sometimes assisted me on the study. Their each study also gave me nice hint to improve my study and experiments. I would like to thank Prof. Ryuji Tada for great advices and supporting for best condition of study environment. I am grateful to Prof. Toru Yamaguchi for giving me a trigger to have interests on atolls and a lot of important advice. I also appreciated Ryuta Kobayashi, Dr. Kentaro Shimoda in Keio University, Shun Muto in the University of Tokyo for sampling and useful advices on the fieldwork. I am grateful to Hideto Yoshida (XRF and SEM), Koji Ichimura (XRD and SEM), Ryosuke Kikuchi (thin section and XRD), and Yuki Saito (^{13}C -NMR) in the University of Tokyo, Dr. Takayuki Omori (^{14}C dating) and Dr. Hiromasa Ozaki (^{14}C dating), and Kohei Yamazaki (^{14}C dating) in the University of Tokyo, the University Museum, Dr. Shohei Hattori (Isotope analysis) in Tokyo Institute of Technology, Hiroki Suga in Hiroshima University (μ -CT), Dr. Oki Sekizawa (μ -CT), Dr. Yusuke Tamemori (XAFS analysis for P), Dr. Kiyofumi Nitta (μ -CT), and Dr. Yasuko Terada (μ -CT) in SPring-8, and Dr. Katsunori

Kimoto (μ -CT) in JAMSTEC for assistant and helpful advices for analysis. I am thankful to Aiko Sakamoto in Microanalytical Laboratory in the University of Tokyo for TOC (solid) measurements. I appreciated Prof. Minoru Yoneda for using CHRONOSHPERE compact accelerator mass spectrometry. I thank Marshall Islands Visitors Authority (MIVA) for permission of sampling in Majuro Atoll and Arno Atoll. I also thank for Emelyn Simon (MIVA), Nawaia Arobatitrandolph (Majuro Police), Makji Lokboj, Colette Reimers (Hotel Robert Reimers), Prof. K. Fellenius in University of Hawaii, Cary Evarts in Wasabi, Risi Graham, Toshiya Sawai in Kamiichi-machi Tourist Association of Toyama, Hiroshi Adachi in Geoact. Co., Ltd. and many volunteers in Majuro Atoll and Arno Atoll who gave me great help on the fieldwork. I am also grateful to Prof. Asuka Yamaguchi in Atmosphere and Ocean Research Institute, the University of Tokyo and Dr. Kazumi Ozaki in Georgia Institute of Technology, NASA for giving me many useful advices on the studies. I appreciate Prof. Masahiro Hoshino in the University of Tokyo for supporting for the study environment. I am also thankful to my family. Finally, I am grateful for all the examiners, Profs. Akihiro Kano, Yoshio Takahashi, Toshihiro Kogure, Yohei Suzuki, and Takaaki Itai.

This study was supported by Grants-in-Aid for scientific research from the Ministry of Education, Culture, Sports, Science and Technology of Japan (17H04582, 16K13911, 17H06458, 15H02149, 16H04073, and 16K12627). This work has been performed with the approval of KEK (Proposal Nos. 2014G058, No. 2016G632) and SPring-8 (Proposal Nos. 2015A0126, 2015B0126, 2015A1809, 2015A0118, 2015B0118, 2016A0118, and 2016A1642).

References

- Aharon, P., & Veeh, H. H. (1984). Isotope studies of insular phosphates explain atoll phosphatization. *Nature*, 309 (5969), 614-617.
- Adachi, H., Yamano, H., Miyajima, T., & Nakaoka, M. (2010). A simple and robust procedure for coring unconsolidated sediment in shallow water. *Journal of oceanography*, 66 (6), 865-872.
- Akagi, T., Hashimoto, Y., Fu, F. F., Tsuno, H., Tao, H., & Nakano, Y. (2004). Variation of the distribution coefficients of rare earth elements in modern coral-lattices: species and site dependencies. *Geochimica et Cosmochimica Acta*, 68 (10), 2265-2273.
- Alcamo, J., Amann, M., Hettelingh, J. P., Holmberg, M., Hordijk, L., Kämäri, J., Kauppi, L., Kauppi, P., Kamai, G., & Mäkelä, A. (1987). Acidification in Europe: a simulation model for evaluating control strategies. *Ambio*, 232-245.
- Andersson, A. J., Mackenzie, F. T., & Bates, N. R. (2008). Life on the margin: implications of ocean acidification on Mg-calcite, high latitude and cold-water marine calcifiers. *Marine Ecology Progress Series*, 373, 265-273.
- Anthony, S. S., Peterson, F. L., MacKenzie, F. T., & Hamlin, S. N. (1989) Geohydrology of the Laura fresh water lens, Majuro atoll: A hydrogeochemical approach. *Geological Society of America Bulletin.*, 101, 1066-1075.
- Antoniou, P., Hamilton, J., Koopman, B., Jain, R., Holloway, B., Lyberatos, G., & Svoronos, S. A. (1990). Effect of temperature and pH on the effective maximum specific growth rate of nitrifying bacteria. *Water research*, 24 (1), 97-101.

- Arimoto, R., Duce, R. A., Ray, B. J., & Unniel, C. K. (1985). Atmospheric trace elements at Enewetak Atoll: 2. Transport to the ocean by wet and dry deposition. *Journal of Geophysical Research: Atmospheres*, 90 (D1), 2391-2408.
- Bae, W., Baek, S., Chung, J., & Lee, Y. (2001). Optimal operational factors for nitrite accumulation in batch reactors. *Biodegradation*, 12 (5), 359-366.
- Bailey, J. E., & Ollis, D. F. (1986). *Fundamentals of Biochemical engineering*. McGraw-Hill, New York.
- Bailey, R. T., & Jenson, J. W. (2014). Effects of marine overwash for atoll aquifers: environmental and human factors. *Groundwater*, 52 (5), 694-704.
- Bergkvist, B. O., & Folkeson, L. (1992). Soil acidification and element fluxes of a *Fagus sylvatica* forest as influenced by simulated nitrogen deposition. *Water, Air, and Soil Pollution*, 65(1-2), 111-133.
- Bresser, D., Paillard, E., Kloepsch, R., Krueger, S., Fiedler, M., Schmitz, R., Baither, D., Winter, M., & Passerini, S. (2013). Carbon Coated ZnFe₂O₄ Nanoparticles for Advanced Lithium-Ion Anodes. *Advanced Energy Materials*, 3 (4), 513-523.
- Busenberg, E., & Plummer, L. N. (1989). Thermodynamics of magnesian calcite solid-solutions at 25°C and 1 atm total pressure. *Geochimica et Cosmochimica Acta*, 53(6), 1189-1208.
- Carlson, A.R. & Roush, T.H. (1985). *Site-specific water quality studies of the Straight River, Minnesota: Complex effluent toxicity, Zn toxicity, and biological survey relationships*. PB85-160703. U.S. Environmental Research Laboratory, Duluth, USA.
- Cheng, R. J., Hwu, J. R., Kim, J. T., & Leu, S. M. (1987). Deterioration of Marble Structures. The Role of Acid Rain. *Analytical Chemistry*, 59(2), 104A-106A.

- Chikamori, T. (1995). Palm trees planted by Hiku -Development of topography and prehistoric sites in the Northern Cook Islands. *Shigaku (in Japanese)*, 64 (2), 117-135.
- Chikamori, T. (1996). Pit cultivation in atolls. In. Ryu, M. (Ed.), *Dr. Kokubu Naoichi Bei-jyu commemorative papers: Anthropology of human beings, materials, and words* (pp. 331-345) (*in Japanese*), Keiyusya, Tokyo.
- Christensen, S., & Tiedje, J. M. (1988). Sub-parts-per-billion nitrate method: Use of an N_2O^- producing denitrifier to convert NO_3^- or $^{15}\text{NO}_3^-$ to N_2O . *Applied and environmental microbiology*, 54(6), 1409-1413.
- Clements, W. H., & Kiffney, P. M. (1995). The influence of elevation on benthic community responses to heavy metals in Rocky Mountain streams. *Canadian Journal of Fisheries and Aquatic Sciences*, 52 (9), 1966-1977.
- Collen, J. D., & Garton, D. W. (2004). Larger foraminifera and sedimentation around Fongafale Island, Funafuti atoll, Tuvalu. *Coral Reefs*, 23(3), 445-454.
- Cook, R. L., & Langford, C. H. (1998). Structural characterization of a fulvic acid and a humic acid using solid-state ramp-CP-MAS ^{13}C nuclear magnetic resonance. *Environmental science & technology*, 32(5), 719-725.
- Darwin, C., (1842). The structure and distribution of coral reefs: London, Royal Society.
- Davis, D. D., Grodzinsky, G., Kasibhatla, P., Crawford, J., Chen, G., Liu, S., Bandy, A., Thornton, D., Guan, H., & Sandholm, S. (2001). Impact of ship emissions on marine boundary layer NO_x and SO_2 distributions over the Pacific Basin. *Geophysical Research Letters*, 28(2), 235-238.
- Deenik, J. L., & Yost, R. S. (2006). Chemical properties of atoll soils in the Marshall Islands and constraints to crop production. *Geoderma*, 136(3), 666-681.

- Dias, B. B., Hart, M. B., Smart, C. W., & Hall-Spencer, J. M. (2010). Modern seawater acidification: the response of foraminifera to high-CO₂ conditions in the Mediterranean Sea. *Journal of the Geological Society*, 167(5), 843-846.
- Dickinson, W. R. (2003). Impact of mid-Holocene hydro-isostatic highstand in regional sea level on habitability of islands in Pacific Oceania. *Journal of Coastal Research*, 489-502.
- Dickinson, W. R. (2004). Impacts of eustasy and hydro-isostasy on the evolution and landforms of Pacific atolls. *Palaeogeography, Palaeoclimatology, Palaeoecology*, 213(3-4), 251-269.
- Dickinson, W. R. (2009). Pacific atoll living: How long already and until when. *GSA today*, 19(3), 4-10.
- Dignon, J. (1992). NO_x and SO_x emissions from fossil fuels: A global distribution. *Atmospheric Environment. Part A. General Topics*, 26(6), 1157-1163.
- Dittrich, M., Müller, B., Mavrocordatos, D., & Wehrli, B. (2003). Induced calcite precipitation by cyanobacterium *Synechococcus*. *Clean (Weinh)*, 31 (2), 162-169.
- Donnegan, J. A., Trimble, S. T., Kusto, K., Kuegler, O., & Hiserote, B. A. (2011). *Republic of the Marshall Islands' forest resources, 2008*, Washington, D.C., U.S.A., p. 28
- Downing, A. L., Painter, H. A., & Knowles, G. (1964). Nitrification in the activated sludge process. *Journal and proceedings - Institute of Sewage Purification*, 63, 130-153.

- Duce, R. A., Unni, C. K., Ray, B. J., Prospero, J. M., & Merrill, J. T. (1980). Long-range atmospheric transport of soil dust from Asia to the tropical North Pacific: Temporal variability. *Science*, 209 (4464), 1522-1524.
- Duce, R. A., Arimoto, R., Ray, B. J., Unni, C. K., & Harder, P. J. (1983). Atmospheric trace elements at Enewetak Atoll: 1. Concentrations, sources, and temporal variability. *Journal of Geophysical Research: Oceans*, 88 (C9), 5321-5342.
- Engel, M. S., & Alexander, M. (1958). Growth and autotrophic metabolism of *Nitrosomonas europaea*. *Journal of Bacteriology*, 76 (2), 217.
- Feely, R. A., Doney, S. C., & Cooley, S. R. (2009). Ocean acidification: present conditions and future changes in a high-CO₂ world. *Oceanography*, 22 (4), 36-47.
- Finlayson-Pitts, B.J., & Pitts, J.N. (1999). *Chemistry of the Upper and Lower Atmosphere*. Academic Press, San Diego, USA.
- Flemming, C. A., & Trevors, J. T. (1989). Copper toxicity and chemistry in the environment: a review. *Water, Air, and Soil Pollution*, 44(1-2), 143-158.
- Fujita, K., Osawa, Y., Kayanne, H., Ide, Y., & Yamano, H. (2009). Distribution and sediment production of large benthic foraminifers on reef flats of the Majuro Atoll, Marshall Islands. *Coral Reefs*, 28(1), 29-45.
- Fujita, M., Suzuki, J., Sato, D., Kuwahara, Y., Yokoki, H., & Kayanne, H. (2013). Anthropogenic impacts on water quality of the lagoonal coast of Fongafale Islet, Funafuti Atoll, Tuvalu. *Sustainability Science*, 8(3), 381-390.
- Fujita, M., Ide, Y., Sato, D., Kench, P. S., Kuwahara, Y., Yokoki, & Kayanne, H. (2014). Heavy metal contamination of coastal lagoon sediments: Fongafale Islet, Funafuti Atoll, Tuvalu. *Chemosphere*, 95, 628-634.

- Gaillard, J. F., Webb, S. M., & Quintana, J. P. (2001). Quick X-ray absorption spectroscopy for determining metal speciation in environmental samples. *Journal of Synchrotron Radiation*, 8 (2), 928-930.
- Galloway, J. N. (2001). Acidification of the world: natural and anthropogenic. *Water, Air, and Soil Pollution*, 130(1-4), 17-24.
- Gauthier, D., Diem, H. G., & Dommergues, Y. (1981). In vitro nitrogen fixation by two actinomycete strains isolated from *Casuarina* nodules. *Applied and Environmental Microbiology*, 41 (1), 306-308.
- Gouman, E. (2004). Reduction of zinc emissions from buildings; the policy of Amsterdam. *Water Science and Technology*, 49 (3), 189-196.
- Greene, J. C., Miller, W. E., Shiroyama, T., & Merwin, E. (1975). *Toxicity of zinc to the green alga Selenastrum capricornutum as a function of phosphorus or ionic strength. Ecological research series*. In Proceedings, Biostimulation and Nutrient Assessment Workshop 16-17 October 1973 EPA-660/3-75-034, 284-43. U.S. Environmental Protection Agency, Corvallis, Oregon.
- Hallock, P. (2000). Symbiont-bearing foraminifera: harbingers of global change?. *Micropaleontology*, 95-104.
- Hameed, S., & Dignon, J. (1988). Changes in the geographical distributions of global emissions of NO_x and SO_x from fossil-fuel combustion between 1966 and 1980. *Atmospheric Environment (1967)*, 22(3), 441-449.
- Hamlin, S. N., & Anthony, S. S. (1987). *Water-Resources Investigations Report*, USGS, Honolulu, Hawaii, p. 69.

- Hashim, M., Shirsath, S. E., Meena, S. S., Mane, M. L., Kumar, S., Bhatt, P., Kumar, R., Prasad, N. K., Alla, S. K., Shah, J., Kotnala, R. K., Mohammed, K. A., Şentürk, E., & Alimuddina. (2015). Manganese ferrite prepared using reverse micelle process: structural and magnetic properties characterization. *Journal of Alloys and Compounds*, 642, 70-77.
- Hatheway, W. H. (1953). Land vegetation of Arno Atoll, Marshall Islands. *Atoll Research Bulletin*, 16, 1-68.
- Hattori, S., Savarino, J., Kamezaki, K., Ishino, S., Dyckmans, J., Fujinawa, T., Caillon, N., Barbero, A., Mukotaka, A., Toyoda, S., Well, R., & Yoshida, N. (2016). Automated system measuring triple oxygen and nitrogen isotope ratios in nitrate using the bacterial method and N₂O decomposition by microwave discharge. *rapid communications in mass spectrometry*, 30(24), 2635-2644.
- He, S., & Morse, J. W. (1993). The carbonic acid system and calcite solubility in aqueous Na-K-Ca-Mg-Cl-SO₄ solutions from 0 to 90 °C. *Geochimica et Cosmochimica Acta*, 57(15), 3533-3554.
- Helyar, K. R., & Porter, W. M. (1989). Soil acidification, its measurement and the processes involved. *Soil acidity and plant growth*, 61-101.
- Higgins, S. M., Broecker, W., Anderson, R., McCorkle, D. C., & Timothy, D. (1999). Enhanced sedimentation along the equator in the western Pacific. *Geophysical Research Letters*, 26 (23), 3489-3492.
- Hinsinger, P., Plassard, C., Tang, C., & Jaillard, B. (2003). Origins of root-mediated pH changes in the rhizosphere and their responses to environmental constraints: a review. *Plant and soil*, 248(1-2), 43-59.

- Hirosawa, F., Iwasaki, T., Hayashi, K., & Watano, S. (2016). Kinetic analysis of mechanochemical reaction for synthesis of zinc ferrite nanoparticles. *Journal of the Society of Powder Technology, Japan*, 53, 768-773.
- Hodson, R V., Borgmann, U. and Shear, H. (1979) in J. O. Nriagu (ed.), *Copper in the Environment. Part II: Health Effects*, John Wiley and Sons. Toronto. pp.307-372.
- Hoegh-Guldberg, O., Mumby, P. J., Hooten, A. J., Steneck, R. S., Greenfield, P., Gomez, E., Harvell, C. D., Sale, P. F., Edwards, A. J., Caldeira, K., Knowlton, N., Eakin, C. M., Iglesias-Prieto, R., Muthiga, N., Bradbury, R. H., Dubi, A., & Hatziolos, (2007). Coral reefs under rapid climate change and ocean acidification. *science*, 318(5857), 1737-1742.
- Hua, Q., Barbetti, M., & Rakowski, A. Z. (2013). Atmospheric radiocarbon for the period 1950–2010. *Radiocarbon*, 55(4), 2059-2072.
- Huesman, R. H. (1977). The effects of a finite number of projection angles and finite lateral sampling of projections on the propagation of statistical errors in transverse section reconstruction. *Physics in Medicine & Biology*, 22(3), 511.
- Imai, N., Terashima, S., Itoh, S., & Ando, A. (1996). 1996 compilation of analytical data on nine GSJ geochemical reference samples, “Sedimentary rock series”. *Geostandards and Geoanalytical Research*, 20(2), 165-216.
- Islam, K. R., & Weil, R. R. (2000). Land use effects on soil quality in a tropical forest ecosystem of Bangladesh. *Agriculture, Ecosystems & Environment*, 79(1), 9-16.
- Ito, L. (2010). Relationship between geomorphic development and early stage of human settlement in Majuro Atoll. Graduation thesis of Keio University.

- Ito, L., Yamaguchi, T., Kobayashi, R., Terada, Y., & Takahashi, Y. (2018a). Influence of Acidification on Carbonate Sediments of Majuro Atoll, Marshall Islands. *Chemistry Letters*, 47(4), 566-569.
- Ito, L., Omori, T., Yoneda, M., Yamaguchi, T., Kobayashi, R., & Takahashi, Y. (2018b). Origin and migration of trace elements in the surface sediments of Majuro Atoll, Marshall Islands. *Chemosphere*, 202, 65-75.
- Kayanne, H., Yamano, H., & Randall, R. H. (2002). Holocene sea-level changes and barrier reef formation on an oceanic island, Palau Islands, western Pacific. *Sedimentary Geology*, 150(1), 47-60.
- Kayanne, H., Yasukochi, T., Yamaguchi, T., Yamano, H., & Yoneda, M. (2011). Rapid settlement of Majuro Atoll, central Pacific, following its emergence at 2000 years CalBP. *Geophysical Research Letters*, 38 (20), L20405.
- Kemp, A. L. W., Thomas, R. L., Dell, C. I., & Jaquet, J. M. (1976). Cultural impact on the geochemistry of sediments in Lake Erie. *Journal of the Fisheries Research Board of Canada*, 33 (3), 440-462.
- Kendall, C. (1998). Tracing nitrogen sources and cycling in catchments. *Isotope tracers in catchment hydrology*, 519-576.
- Kendall, C., & Doctor, D. H. (2003). *Stable isotope applications in hydrologic studies. Treatise on geochemistry*, 5, 605.
- Kitagawa, H., Masuzawa, T., Makamura, T., & Matsumoto, E. (1993). A batch preparation method for graphite targets with low background for AMS ^{14}C measurements. *Radiocarbon*, 35 (2), 295-300.

- Koda, K., Manpuku, Y., Kobayashi, T., Ishida, S., Yoshimoto, S., & Okubo, M. (2013). A study of the sealing effect in the observation well of the freshwater lens at Laura Island, Republic of the Marshall Islands. *Japan Agricultural Research Quarterly*, 47 (3), 257-272.
- Kunhikrishnan, A., Thangarajan, R., Bolan, N. S., Xu, Y., Mandal, S., Gleeson, D. B., Seshadri, B., Zaman, M., Barton, L., Tang, C., Luo, J., Dalal, R., Ding, W., Kirkham, M. B., & Naidu, R. (2016). Functional relationships of soil acidification, liming, and greenhouse gas flux. *Advances in Agronomy*, 139, 1-71.
- Kurusu, M., Sakata, K., Miyamoto, C., Takaku, Y., Iizuka, T., & Takahashi, Y. (2016). Variation of iron isotope ratios in anthropogenic materials emitted through combustion processes. *Chemistry Letters*, 45 (8), 970-972.
- Laird, W. E. (1989) *Soil survey of the islands of Airik, Arno, Majuro, Mili, and Taroa, Republic of the Marshall Islands*, Washington, D.C., U.S.A., p.47.
- Laudelout, H. (1978). Mathematical modeling of biological ammonium oxidation. *Microbiology*, 384-386.
- Li, C., Aber, J., Stange, F., Butterbach - Bahl, K., & Papen, H. (2000). A process - oriented model of N₂O and NO emissions from forest soils: 1. Model development. *Journal of Geophysical Research: Atmospheres*, 105(D4), 4369-4384.
- Likens, G. E., & Butler, T. J. (1981). Recent acidification of precipitation in North America. *Atmospheric Environment* (1967), 15(7), 1103-1109.
- Likens, G. E., Driscoll, C. T., & Buso, D. C. (1996). Long-term effects of acid rain: response and recovery of a forest ecosystem. *Science*, 272(5259), 244.

- Liu, J., Ye, X., Wang, H., Zhu, M., Wang, B., & Yan, H. (2003). The influence of pH and temperature on the morphology of hydroxyapatite synthesized by hydrothermal method. *Ceramics international*, 29 (6), 629-633.
- Liu, X. D., Sun, L. G., Cheng, Z. Q., Zhao, S. P., Liu, K. X., Wu, X. H., Xie, Z. Q., Yin, X. B., Luo, H. H., Ding, X. F., Fu, D. B. & Wang, Y. H. (2008). Paleoenviromental implications of the guano phosphatic cementation on Dongdao Island in the South China Sea. *Marine Geology*, 247 (1), 1-16.
- Liu, D., Zhu, W., Wang, X., Pan, Y., Wang, C., Xi, D., Bai, E., Wang, Y., Han, X. & Fang, Y. (2017). Abiotic versus biotic controls on soil nitrogen cycling in drylands along a 3200km transect. *Biogeosciences*, 14(4), 989.
- Loder III, T. C., Ganning, B., & Love, J. A. (1996). Ammonia nitrogen dynamics in coastal rockpools affected by gull guano. *Journal of Experimental Marine Biology and Ecology*, 196 (1-2), 113-129.
- Luo, Y., Durenkamp, M., De Nobili, M., Lin, Q., & Brookes, P. C. (2011). Short term soil priming effects and the mineralisation of biochar following its incorporation to soils of different pH. *Soil Biology and Biochemistry*, 43(11), 2304-2314.
- Maejima, Y., & Nagatsuka, S. (2011). Age of soils on the coral limestone in Nansei Islands, Japan. *Chikyu Kankyo*, 16 (2), 169-177
- Maejima, Y., Nagatsuka, S., & Higashi, T. (2002). Application of the crystallinity ratio of free iron oxides for dating soils developed on the raised coral reef terraces of Kikai and Minami-Daito Islands, Southwest Japan. *The Quaternary Research*, 41 (6), 485-493.
- Malcolm, R. L. (1990). The uniqueness of humic substances in each of soil, stream and marine environments. *Analytica Chimica Acta*, 232, 19-30.

- Manceau, A., Marcus, M. A., & Tamura, N. (2002). Quantitative speciation of heavy metals in soils and sediments by synchrotron X-ray techniques. *Reviews in Mineralogy and Geochemistry*, 49 (1), 341-428.
- Merrill, J. T., Uematsu, M., & Bleck, R. (1989). Meteorological analysis of long range transport of mineral aerosols over the North Pacific. *Journal of Geophysical Research: Atmospheres*, 94 (D6), 8584-8598.
- Michalski, G., Scott, Z., Kabling, M., & Thiemens, M. H. (2003). First measurements and modeling of $\Delta^{17}\text{O}$ in atmospheric nitrate. *Geophysical Research Letters*, 30(16).
- Michalski, G., Meixner, T., Fenn, M., Hernandez, L., Sirulnik, A., Allen, E., & Thiemens, M. (2004). Tracing atmospheric nitrate deposition in a complex semiarid ecosystem using $\Delta^{17}\text{O}$. *Environmental science & technology*, 38(7), 2175-2181.
- Miller, M. F. (2002). Isotopic fractionation and the quantification of ^{17}O anomalies in the oxygen three-isotope system: an appraisal and geochemical significance. *Geochimica et Cosmochimica Acta*, 66(11), 1881-1889.
- Minagawa, M., Winter, D. A., & Kaplan, I. R. (1984). Comparison of Kjeldahl and combustion methods for measurement of nitrogen isotope ratios in organic matter. *Analytical Chemistry*, 56 (11), 1859-1861.
- Ministry of the Environment, Japan, (2012), *Sediment Monitoring Methods*, 78-79.
- Morin, S., Savarino, J., Frey, M. M., Domine, F., Jacobi, H. W., Kaleschke, L., & Martins, J. M. (2009). Comprehensive isotopic composition of atmospheric nitrate in the Atlantic Ocean boundary layer from 65°S to 79°N. *Journal of Geophysical Research: Atmospheres*, 114 (D5).

- Morse, J. W., Arvidson, R. S., & Lüttge, A. (2007). Calcium carbonate formation and dissolution. *Chemical reviews*, 107(2), 342-381.
- Mucci, A. (1983). The solubility of calcite and aragonite in seawater at various salinities, temperatures, and one atmosphere total pressure. *American Journal of Science*, 283(7), 780-799.
- Mulder, C. P., & Ellis, J. C. (2010). *Seabird Island Ecology*. In: eLS. John Wiley & Sons, Ltd: Chichester.
- Nakanishi, J., Naito, W., & Kamo, M. (2008). *Risk Assessment Document Series 20: Zinc (in Japanese)*. Maruzen, Tokyo, Japan.
- Nriagu, J. O. (1979). Global inventory of natural and anthropogenic emissions of trace metals to the atmosphere. *Nature*. 279 (5712), 409-411.
- Nriagu, J. O. (1989). A global assessment of natural sources of atmospheric trace metals. *Nature*. 338 (6210), 47-49.
- Ohashi, H., Ishiguro, E., Tamenori, Y., Okumura, H., Hiraya, A., Yoshida, H., Senba, Y., Okada, K., Saito, N., Suzuki, I. H., Ueda, K., Ibuki, T., Nagaoka, S., Koyano, I., & Ishikawa, T. (2001). Monochromator for a soft X-ray photochemistry beamline BL27SU of SPring-8. *Nuclear Instruments and Methods in Physics Research Section A: Accelerators, Spectrometers, Detectors and Associated Equipment*, 467, 533-536.
- Okazaki, K., & Ando, T. (1997). NO_x reduction mechanism in coal combustion with recycled CO₂. *Energy*, 22(2-3), 207-215.
- OPS (Office of Planning and Statistics). (1989). *Census of Population and Housing 1988: Final Report*. Majuro, Marshall Islands.

- Osawa, Y., Fujita, K., Umezawa, Y., Kayanne, H., Ide, Y., Nagaoka, T., Miyajima, T., & Yamano, H. (2010). Human impacts on large benthic foraminifers near a densely populated area of Majuro Atoll, Marshall Islands. *Marine pollution bulletin*, 60(8), 1279-1287.
- Paces, T. (1985). Sources of acidification in Central Europe estimated from elemental budgets in small basins. *Nature*, 315(6014), 31.
- Painter, H. A., & Loveless, J. E. (1983). Effect of temperature and pH value on the growth-rate constants of nitrifying bacteria in the activated-sludge process. *Water research*, 17 (3), 237-248.
- Patton, C. J., & Crouch, S. R. (1977). Spectrophotometric and kinetics investigation of the Berthelot reaction for the determination of ammonia. *Analytical chemistry*, 49 (3), 464-469.
- Perry, C. T., Kench, P. S., Smithers, S. G., Riegl, B., Yamano, H., & O'Leary, M. J. (2011). Implications of reef ecosystem change for the stability and maintenance of coral reef islands. *Global Change Biology*, 17(12), 3679-3696.
- Piper, D.Z., Loebner, B., & Aharon, P. (1990). *Physical and chemical properties of the phosphate deposit on Nauru, western equatorial Pacific Ocean*, in: Cook, P.J., and Shergold, J.H. (Eds.), *Phosphate Deposits of the World: Neogene to modern phosphorates*. Cambridge University Press, Cambridge, pp. 177–194.
- Presley, T. K. (2005). *Effects of the 1998 drought on the freshwater lens in the Laura area, Majuro Atoll, Republic of the Marshall Islands: U.S. Geological Survey Scientific Investigations Report 2005-5098*, Reston, USA.

- Raja, R., Saraswati, P. K., & Iwao, K. (2007). A field-based study on variation in Mg/Ca and Sr/Ca in larger benthic foraminifera. *Geochemistry, Geophysics, Geosystems*, 8(10), Q10012.
- Ramsey, C.B., (2013). *OxCal Program ver.4.3 Oxford Radiocarbon Accelerator Unit Research Lab for Archaeology*: University of Oxford, Oxford (<https://c14.arch.ox.ac.uk/oxcal.html>).
- Rasband, W.S., ImageJ, U. S. National Institutes of Health, Bethesda, Maryland, USA, <http://rsb.info.nih.gov/ij/>, 1997-2012.
- Reimer, P. J., Bard, E., Bayliss, A., Beck, J. W., Blackwell, P. G., Ramsey, C. B., Buck, C. E., Cheng, H., Edwards, R. L., Friedrich, M., Grootes, P. M., Guilderson, T. P., Hafliðason, H., Hajdas, I., Hatte, C., Heaton, T. J., Hoffmann, D. L., Hogg, A. G., Hughen, K. A., Kaiser, K. F., Kromer, B., Manning, S. W., Niu, M., Reimer, R. W., Richards, D. A., Scott, E. M., Southon, J. R., Staff, R. A., Turney, C. S. M., & van der Plicht, J. (2013). IntCal13 and Marine13 radiocarbon age calibration curves 0–50,000 years cal BP. *Radiocarbon*, 55 (4), 1869-1887.
- Reis, V. M., Baldani, J. I., Baldani, V. L. D., & Dobereiner, J. (2000). Biological dinitrogen fixation in gramineae and palm trees. *Critical Reviews in Plant Science*, 19 (3), 227-247.
- Rietveld, H. (1969). A profile refinement method for nuclear and magnetic structures. *Journal of applied Crystallography*, 2(2), 65-71.
- Roettger, R., Krueger, R., & de Rijk, S. (1990). Larger Foraminifera; variation in outer morphology and prolocular size in *Calcarina gaudichaudii*. *The Journal of Foraminiferal Research*, 20(2), 170-174.

- Roggy, J. C., Prévost, M. F., Gourbiere, F., Casabianca, H., Garbaye, J., & Domenach, A. M. (1999). Leaf natural ^{15}N abundance and total N concentration as potential indicators of plant N nutrition in legumes and pioneer species in a rain forest of French Guiana. *Oecologia*, 120 (2), 171-182.
- Sabath, M. D. (1977). Vegetation and urbanization on Majuro atoll, Marshall Islands. *Pacific Science*, 31 (4), 321-333.
- Sakata, K., Sakaguchi, A., Tanimizu, M., Takaku, Y., Yokoyama, Y., & Takahashi, Y. (2014). Identification of sources of lead in the atmosphere by chemical speciation using X-ray absorption near-edge structure (XANES) spectroscopy. *Journal of Environmental Sciences*, 26(2), 343-352.
- Sannigrahi, P., Sullivan, A. P., Weber, R. J., & Ingall, E. D. (2006). Characterization of water-soluble organic carbon in urban atmospheric aerosols using solid-state ^{13}C NMR spectroscopy. *Environmental science & technology*, 40(3), 666-672.
- Schumacher, B. A. (2002). Methods for the determination of total organic carbon (TOC) in soils and sediments. *Ecological Risk Assessment Support Center*, 2002, 1-23.
- Sobanska, S., Ricq, N., Laboudigue, A., Guillermo, R., Brémard, C., Laureyns, J., Merlin, J. C., & Wignacourt, J. P. (1999). Microchemical investigations of dust emitted by a lead smelter. *Environmental Science & Technology*, 33 (9), 1334-1339.
- Spennemann, D. H. R. (1992). Historic demography of Majuro Atoll, Republic of the Marshall Islands. *Journal of the Pacific Society*, 15(1), 152-131.
- Spennemann, D. R. (1993). *Ennaanin Etto: a collection of essays on the Marshallese past* (No. 1). Republic of the Marshall Islands, Ministry of Internal Affairs, Historic Preservation Office.

- Spennemann, D. H. R., & Franke, B. (1995). Decomposition of buried human bodies and associated death scene materials on coral atolls in the tropical Pacific. *Journal of Forensic Science*, 40(3), 356-367.
- Stevenson, F. J. (1994). *Humus chemistry : genesis, composition, reactions -2nd ed.*, John Wiley & Sons, Inc., New York.
- Stoddart, D. R. (1992). Biogeography of the tropical Pacific. *Pacific Science*, 44 (2), 276-293.
- Strong, D. T., Sale, P. W. G., & Helyar, K. R. (1997). Initial soil pH affects the pH at which nitrification ceases due to self-induced acidification of microbial microsites. *Soil Research*, 35 (3), 565-570.
- Stumm, W., & Morgan, J. J. (1996). *Aquatic chemistry: chemical equilibria and rates in natural waters -3rd ed.*, John Wiley & Sons, Inc., New York.
- Sugiura, Y., Onuma, K., & Yamazaki, A. (2014). Solution chemical synthesis of hollow vaterite particles for advanced biomaterial applications. *Chemistry Letters*, 44 (1), 20-22.
- Takahashi, Y., Yoshida, H., Sato, N., Hama, K., Yusa, Y., & Shimizu, H. (2002). W-and M-type tetrad effects in REE patterns for water–rock systems in the Tono uranium deposit, central Japan. *Chemical Geology*, 184 (3), 311-335.
- Takahashi, Y., Manceau, A., Geoffroy, N., Marcus, M. A., & Usui, A. (2007). Chemical and structural control of the partitioning of Co, Ce, and Pb in marine ferromanganese oxides. *Geochimica et Cosmochimica Acta*, 71 (4), 984-1008.

- Takahashi, Y., Higashi, M., Furukawa, T., & Mitsunobu, S. (2011). Change of iron species and iron solubility in Asian dust during the long-range transport from western China to Japan. *Atmospheric Chemistry and Physics*, 11 (21), 11237–11252.
- Taylor, S. R., & McLennan, S. (1985). *The continental crust: its composition and evolution*. Blackwell, Oxford.
- Terada, Y., Suzuki, Y., Uesugi, K., & Miura, K. (2016, January). Progress of projection computed tomography by upgrading of the beamline 37XU of SPring-8. In *XRM 2014: Proceedings of the 12th International Conference on X-Ray Microscopy* (Vol. 1696, p. 020023). AIP Publishing.
- Tetard, M., Beaufort, L., & Licari, L. (2017). A new optical method for automated pore analysis on benthic foraminifera. *Marine Micropaleontology*, 136, 30-36.
- The Committee on Soil Reaction Measurements Second International Commission, (1930). Berlin, Germany, July 8-11, 1930.
- Underwood, M. R., Peterson, F. L., & Voss, C. I. (1992). Groundwater lens dynamics of atoll islands. *Water Resources Research*, 28(11), 2889-2902.
- Van Breemen, N., Burrough, P. A., Velthorst, E. V., Van Dobben, H. F., de Wit, T., Ridder, T. D., & Reijnders, H. F. R. (1982). Soil acidification from atmospheric ammonium sulphate in forest canopy throughfall. *Nature*, 299(5883), 548.
- Wakamura, M., Kandori, K., & Ishikawa, T. (1997). Influence of chromium (III) on the formation of calcium hydroxyapatite. *Polyhedron*, 16 (12), 2047-2053.
- Wallace, A. (1994). Soil acidification from use of too much fertilizer. *Communications in Soil Science and Plant Analysis*, 25(1-2), 87-92.

- Walter, L. M., & Morse, J. W. (1985). The dissolution kinetics of shallow marine carbonates in seawater: A laboratory study. *Geochimica et Cosmochimica Acta*, 49(7), 1503-1513.
- Warby, R. A., Johnson, C. E., & Driscoll, C. T. (2009). Continuing acidification of organic soils across the northeastern USA: 1984–2001. *Soil Science Society of America Journal*, 73(1), 274-284.
- Webb, S. M., Leppard, G. G., & Gaillard, J. F. (2000). Zinc speciation in a contaminated aquatic environment: characterization of environmental particles by analytical electron microscopy. *Environmental Science & Technology*, 34 (10), 1926-1933.
- Werner, A. D., Sharp, H. K., Galvis, S. C., Post, V. E., & Sinclair, P. (2017). Hydrogeology and management of freshwater lenses on atoll islands: Review of current knowledge and research needs. *Journal of Hydrology*, 551, 819-844.
- Wollast, R., & Reinhard-Derie, D. (1977). Equilibrium and mechanism of dissolution of Mg-calcites. In: Andersen, N.R., Malahoff, A. (Eds.), *The Fate of Fossil Fuel CO₂ in the Oceans*. Plenum Press, New York.
- Woodroffe, C. D., McLean, R. F., Smithers, S. G., & Lawson, E. M. (1999). Atoll reef-island formation and response to sea-level change: West Island, Cocos (Keeling) Islands. *Marine Geology*, 160(1), 85-104.
- Xu, L. Q., Liu, X. D., Sun, L. G., Yan, H., Liu, Y., Luo, Y. H., Huang, J., & Wang, Y. H. (2010). Distribution of radionuclides in the guano sediments of Xisha Islands, South China Sea and its implication. *Journal of Environmental Radioactivity*, 101 (5), 362-368.
- Xue, C. (2001). Coastal erosion and management of Majuro atoll, Marshall Islands. *Journal of Coastal Research*, 909-918.

- Yamaguchi, T., Kayanne, H., Yamano, H., Najima, Y., Chikamori, M., & Yokoki, H. (2005). Excavation of pit-agriculture landscape on Majuro Atoll, Marshall Islands, and its implications. *Global Environmental Research -English Edition-*, 9(1), 27-36.
- Yamaguchi, T., Kayanne, H., & Yamano, H. (2009). Archaeological Investigation of the Landscape History of an Oceanic Atoll: Majuro, Marshall Islands 1. *Pacific Science*, 63(4), 537-565.
- Yamamoto, S., Kayanne, H., Terai, M., Watanabe, A., Kato, K., Negishi, A., & Nozaki, K. (2012). Threshold of carbonate saturation state determined by CO₂ control experiment. *Biogeosciences*, 9(4), 1441-1450.
- Yamano, H., Miyajima, T., & Koike, I. (2000). Importance of foraminifera for the formation and maintenance of a coral sand cay: Green Island, Australia. *Coral Reefs*, 19(1), 51-58.
- Yamanouchi, H. (1988) The distribution of sandy sediments around coral reefs and the effect of reef topography Proc. 6th Int. Coral Reef Symp., Townsville, Australia, vol. 3, pp. 497-502
- Yanagi, Y. and Shindo, H. (2016). Assessment of Long-Term Compost Application on Physical, Chemical, and Biological Properties, as Well as Fertility, of Soil in a Field Subjected to Double Cropping. *Agricultural Sciences*, 7 (01), 30.
- Yang, Y., Liu, X., Yang, Y., Xiao, W., Li, Z., Xue, D., Fahsen, L., & Ding, J. (2013). Synthesis of nonstoichiometric zinc ferrite nanoparticles with extraordinary room temperature magnetism and their diverse applications. *Journal of Materials Chemistry C*, 1 (16), 2875-2885.

- Yasukochi, T. (2008). Ecological and physical factors of Holocene atoll-island formation in the Pacific. PhD. thesis of the University of Tokyo.
- Yasukochi, T., Kayanne, H., Yamaguchi, T., & Yamano, H. (2014). Sedimentary facies and Holocene depositional processes of Laura Island, Majuro Atoll. *Geomorphology*, 222, 59-67.
- Young, E. D., Galy, A., & Nagahara, H. (2002). Kinetic and equilibrium mass-dependent isotope fractionation laws in nature and their geochemical and cosmochemical significance. *Geochimica et Cosmochimica Acta*, 66(6), 1095-1104.
- Zhang, J., & Nozaki, Y. (1996). Rare earth elements and yttrium in seawater: ICP-MS determinations in the East Caroline, Coral Sea, and South Fiji basins of the western South Pacific Ocean. *Geochimica et Cosmochimica Acta*, 60 (23), 4631-4644.